



Structural and biochemical study of the proteins AmiC, NlpD and FtsW involved in the bacterial cell division

By

Mathieu Rocaboy

Thesis Supervisors: Paulette CHARLIER & Mohammed TERRAK

Thesis Committee: Bernard JORIS

Paulette CHARLIER

Meriem EL GHACHI

Mohammed TERRAK

Georges FELLER

Erik GOORMAGHTIGH (Université libre de Bruxelles)

Johan WOUTERS (Université de Namur)

Waldemar VOLLMER (Newcastle University)

December 2013

Abstract

Cell division in the Gram negative bacterium *Escherichia coli* is a highly coordinated mechanism involving various physiological functions such as chromosome segregation, cell envelope invagination, peptidoglycan synthesis at the division site and separation of the daughter cells. All these functions require a high level of spatio-temporal regulation in order to preserve the physical integrity of the cell. At least 20 proteins required for a proper cell division are recruited to the division site to form a supramolecular complex called the divisome. This thesis work focused on three major components of the *E. coli* division machinery: the N-acetylmuramyl L-alanine amidase AmiC, the LytM factor NlpD and the lipid II flippase FtsW. These proteins are recruited at midcell at a late stage of cell division. FtsW is an integral membrane protein crucial for the translocation of the peptidoglycan precursor from the cytoplasm to the periplasm where it will be processed to produce septal peptidoglycan. AmiC acts as a septal peptidoglycan hydrolase that allow the separation of the daughter cells. This enzyme has been shown to be activated by the LytM factor NlpD.

The crystal structure of AmiC from *E. coli* presented in this work confirms the presence of an inhibitory helix in the active site. The AmiC variant lacking this helix exhibits by itself an activity comparable to that of the wild type AmiC activated by NlpD. Furthermore, the direct interaction between AmiC and NlpD has been detected by microscale thermophoresis with an apparent K_d of about 13 μM . The crystal structure of AmiC also reveals the β -sandwich fold of the AMIN domain, responsible for the septal targeting of AmiC to the division site. The two symmetrical four-stranded β -sheets exhibit highly conserved motifs on the two outer faces. Along with the peptidoglycan binding capacity of the AMIN domain, results obtained so far suggest that the AMIN domain could be involved in the recognition of a specific peptidoglycan architecture or a composition different than the lateral peptidoglycan.

Production screenings of FtsW from different strains were realized and FstW from *E. coli* was purified. This challenging project will require additional efforts to obtain sufficient amount of protein for structural investigation.

Information gathered in this work confirms the high level of regulation of the hydrolytic activity at the septum and gives a structural basis for a more precise molecular characterization of the division site targeting. Disruption or over-activation of these regulation mechanisms could represent a new strategy in the development of antibacterial compounds.

Résumé

La division cellulaire chez la bactérie à Gram négatif *Escherichia coli* est un processus cellulaire regroupant de nombreuses fonctions physiologiques telles que la ségrégation chromosomique, l'invagination de la paroi cellulaire, la synthèse de peptidoglycane au site de division et la séparation des cellules filles. Toutes ces fonctions nécessitent un haut niveau de régulation spatio-temporelle afin de préserver l'intégrité physique de la cellule. Au moins 20 protéines impliquées dans la division cellulaire sont recrutées au site de division pour former un complexe multi-protéique appelé divisome. Ce travail de thèse porte sur trois membres de la machinerie de division d'*E. coli* : la N-acetylmuramyl L-alanine amidase AmiC, le facteur LytM NlpD et FtsW, la flipase du lipide II. Ces protéines sont recrutées au milieu de la cellule à un stade avancé de la division. FtsW est une protéine intégralement membranaire indispensable à la translocation du précurseur du peptidoglycane du cytoplasme vers le périplasme où il sera pris en charge pour produire le peptidoglycane septal. AmiC est une hydrolase du peptidoglycane septal qui permet la séparation des cellules filles. Il a été montré que cette enzyme est activée par NlpD (facteur LytM).

La structure cristallographique d'AmiC d'*E. coli* présentée dans ce travail confirme la présence d'une hélice inhibitrice dans le site actif. Le variant d'AmiC dépourvu de cette hélice possède une activité comparable à celle d'AmiC sauvage activé par NlpD. De plus, l'interaction directe entre AmiC et NlpD a été détectée par thermophorèse avec un Kd apparent d'environ 13 μ M. La structure cristallographique d'AmiC révèle également pour la première fois l'architecture du domaine AMIN avec un repliement de type β -sandwich. Ce domaine, responsable de la localisation au site de division, est composé de deux feuillets symétriques comportant chacun quatre brins β et exposant des motifs conservés sur leurs faces externes. En prenant en compte la capacité du domaine AMIN à lier le peptidoglycane, les résultats obtenus suggèrent que le domaine AMIN pourrait être impliqué dans la reconnaissance d'une architecture ou composition spécifique du peptidoglycane au site de division.

Des criblages de production de protéines FtsW provenant de différentes souches ont été réalisés et la protéine FtsW d'*E. coli* a été purifiée. Cette partie du projet nécessitera davantage d'efforts pour obtenir des quantités suffisantes de protéines en vue d'une étude structurale.

Les informations récoltées au terme de ce travail confirment le haut niveau de régulation de l'activité hydrolytique au niveau du septum et fournissent une base structurale pour une caractérisation plus précise des déterminants de l'adressage au site de division. La suppression ou la sur-activation de ces systèmes de régulation pourraient représenter une nouvelle stratégie dans le développement de composés antibactériens.

Remerciements

Je souhaite d'abord remercier le Professeur Bernard Joris de m'avoir accueilli au Centre d'Ingénierie des Protéines de l'Université de Liège. Je remercie également le Professeur Moreno Galleni qui lui a succédé au poste de directeur.

Je remercie les Fonds pour la formation à la Recherche dans l'Industrie et dans l'Agriculture (FRIA) pour avoir financé ces années de thèse.

Je tiens à remercier tout particulièrement Paulette Charlier pour m'avoir permis de terminer mon stage de fin de Master au sein de l'équipe de cristallographie. Je la remercie également de m'avoir donné l'opportunité de réaliser ces quatre années de thèse et d'avoir été une promotrice toujours à l'écoute. Merci pour cet encadrement, ce soutien (et ces manons lors des voyages au Synchrotron...) pendant ces quatre années qui resteront une très belle expérience.

Merci Eric et Fred, j'ai énormément appris à vos côtés. Merci pour vos conseils et votre soutien tout au long de cette thèse. Travailler avec vous aura été un vrai plaisir. Merci à Raphael pour m'avoir initié à l'art délicat de la cristallogénèse et pour tous les conseils qu'il m'a donnés.

Un grand merci à Mohammed Terrak pour m'avoir accueilli au labo 1.28 et accepté de m'accompagner en tant que promoteur pendant cette thèse. Merci pour tes innombrables conseils, ta disponibilité et ton écoute qui m'ont grandement facilité la tâche.

Je tiens particulièrement à remercier André Piette et Nicolas Dony avec lesquels j'ai appris énormément de choses durant cette thèse. J'ai vraiment apprécié de travailler avec vous et le fait que cette thèse se soit si bien passée tient beaucoup à votre présence et à votre aide. Merci à Sébastien de Boel pour tous ses conseils et sa disponibilité au début de ma thèse. Merci Adeline pour tes précieux conseils au labo et aussi pendant la phase de rédaction. Isma et Sophie, je vous souhaite le meilleur, bon courage pour la suite ! Samir, j'espère que tu passeras d'aussi bons moments que moi au CIP à condition que tu te fasses aux rudesses du climat... Thank you Badrish, it was a pleasure to work with you (and Mobinius...). Thanks for the invitation in India, it was incredible and I will not forget this amazing trip. शुक्रिया मेरी दोस्त !

Merci à Jean-Marie Frère pour la relecture de mon article et à Martine Nguyen-Distèche pour ses conseils et sa précieuse aide bibliographique.

Merci aux réguliers de la salle de pause en biochimie où les leçons de vocabulaire se mêlaient aux concours de chant et aux résumés des aventures de Victor Newman : Fabienne, Florence, Caroline S., Linda, Amandine, Isma, Sophie, Samir, Nicolas, Caroline M., Bryan et Georges.

Merci aux membres des Enzymes Volants, Alain, Philippe, Jean-Marie, Marc, Fred, Dave, Julien et Patrick (a.k.a Michel P.) pour ces quelques années de mini-foot, cette qualification en 8^{ème} de finale restera dans les mémoires.

Un grand merci aux membres du CIP qui m'ont soutenu, aidé et avec qui j'ai énormément appris scientifiquement, le tout dans une excellente ambiance rythmée par les barbecues, trappistes et autres festivités.

Merci à Fred et Mohammed pour leurs patientes relectures de ce manuscrit. Un grand merci à Roya et Marie pour leur précieuse aide et leur soutien dans les derniers moments de rédaction et lors de l'impression de cette thèse.

Enfin, merci à mes parents de m'avoir fait confiance.

Abbreviations

<i>A. aeolicus</i>	<i>Aquifex aeolicus</i>
ADP	Adenosine di-phosphate
Ala	Alanine
AMIN	Amidase N-terminal domain
ATP	Adenosine tri-phosphate
<i>B. henselae</i>	<i>Bartonella henselae</i>
<i>B. subtilis</i>	<i>Bacillus subtilis</i>
C ₅₅ -P	Undecaprenyl-phosphate
<i>C. crescentus</i>	<i>Caulobacter crescentus</i>
CABS	N-cyclohexyl-3-aminobutanesulfonic acid
CAPS	N-cyclohexyl-3-aminopropanesulfonic acid
CCP4	Collaborative Computational Project No. 4
CSI-Blast	Context-Specific Blast
CSS	Complexation Significance Score
DAP	Diamino-pimelic acid
<i>dcw</i>	<i>division cell wall</i>
DDM	n-Dodecyl-β-D-maltopyranoside
DNA	Deoxyribonucleic acid
DTT	Dithiothréitol
<i>E. coli</i>	<i>Escherichia coli</i>
EDTA	Ethylenediaminetetraacetic acid
EM	Electron microscopy
ESRF	European Synchrotron Radiation Source Facility
GFP	Green fluorescent protein
GlcNAc	N-acetyl glucosamine
D-iGlu	Iso-glutamate
FIP	French beamline for Investigation of Proteins
<i>fts</i>	filament-forming temperature-sensitive
<i>G.thermodenitrificans</i>	<i>Geobacillus thermodenitrificans</i>
GTP	Guanosine triphosphate
IPTG	Isopropyl-β-D-1-thiogalactopyranoside

LB	Luria-Bertani broth
<i>L. lactis</i>	<i>Lactococcus lactis</i>
LPS	Lipopolysaccharides
LTA	Lipoteichoic acid
Lys	Lysine
MurNAc	N-acetyl muramic acid
NADPH	Nicotinamide adenine dinucleotide phosphate
NTA	Nitrilotriacetic acid
OD ₆₀₀	Optical density measured at a wavelength of 600 nm
PAGE	Polyacrylamide gel electrophoresis
PBP	Penicillin-binding protein
PCR	Polymerase chain reaction
PDB	Protein Data Bank
PEG	Polyethylene glycol
PG	Peptidoglycan
PEP	Phosphoenolpyruvate
PTS	Phosphotransferase system
PISA	Proteins, Interfaces, Structures and Assemblies
POTRA	Polypeptide transport associated
RBB	Remazol Brilliant Blue
RMSD	Root-mean-square deviation
<i>S. aureus</i>	<i>Staphylococcus aureus</i>
<i>S. pneumoniae</i>	<i>Streptococcus pneumoniae</i>
<i>S. epidermidis</i>	<i>Staphylococcus epidermidis</i>
SDS	Sodium dodecyl sulfate
SEDS	Shape, elongation, division and sporulation
SPOR	Sporulation-related repeat
TB	Terrific broth
TEV	Tobacco Etch Virus
Tat	Twin-arginine transport
UDP	Uridine diphosphate
WTA	Wall teichoic acid

Contents

INTRODUCTION	1
1. Structure of the bacterial cell wall	3
1.1. General points	3
1.2. Peptidoglycan	5
2. Bacterial division	11
2.1. Divisome presentation	11
2.2. Division triggering	12
2.2.1. Min system	13
2.2.2. Nucleoid occlusion system	14
2.3. Early stage of the divisome assembly	15
2.3.1. Constriction ring formation (FtsZ)	15
2.3.2. Membrane anchoring of the Z ring (ZipA, FtsA)	17
2.3.3. Ring stabilization (ZapA-D)	18
2.3.4. Hypotheses for the FtsZ constriction mechanism	19
2.3.5. FtsE/X	20
2.4. Maturation of the divisome	21
2.4.1. FtsK and DNA segregation	21
2.4.2. FtsQLB: the divisome link between cytoplasm and periplasm	22
2.4.3. Translocation of the PG precursor to the periplasm	24
2.4.4. Biosynthesis of glycan chains and incorporation in pre-existent PG	26
2.4.5. Outer membrane invagination	27
2.4.6. Peptidoglycan hydrolysis and bacterial division	29
2.4.6.1. <i>E. coli</i> periplasmic amidases, key players of cell separation	29
2.4.6.2. Regulation of septal amidases: the LytM factors	31
2.4.6.3. Regulation of murein hydrolysis in the context of septum formation	34
2.4.6.4. Coupling murein hydrolase activity and Z ring positioning	35
2.5. Divisome network	35
OBJECTIVES	37

MATERIAL AND METHODS	41
3. Molecular Biology	43
3.1. Cloning of <i>amiC</i> , <i>nlpD</i> and variants	43
3.2. Cloning of <i>ftsW</i> from different bacteria	44
4. Productions and Purifications	45
4.1. Overexpression and purification of AmiC, NlpD and variants	45
4.2. Overexpression and purification of selenomethionyl-AmiC	45
4.3. Expression tests of FtsW constructs in <i>E. coli</i> C43 (DE3) and membrane preparation	46
4.4. Membrane solubilization and purification of <i>E. coli</i> FtsW	47
4.5. Expression tests of <i>E. coli</i> FtsW in <i>L. lactis</i> NZ9000	47
5. Structural study of AmiC	47
5.1. Crystallization and data collection	47
5.2. Data processing	48
5.3. Structure analysis	48
6. Activity tests	49
6.1. Preparation of peptidoglycan sacculi	49
6.2. SDS detection method (Hayashi)	49
6.3. Labelling of peptidoglycan with Remazol Brilliant Blue	50
6.4. Activity tests with RBB-labelled peptidoglycan	50
6.5. Peptidoglycan-binding assay	50
7. Interaction study	51
RESULTS	53
8. Cloning, Production and Purification	55
8.1. Cloning, production and purification of FtsW	55
8.1.1. <i>ftsW</i> cloning in production vectors	55
8.1.2. Production and purification tests	56
8.1.2.1. Production and purification of <i>E. coli</i> FtsW	56
8.1.2.2. <i>G. thermodenitrificans</i> , <i>A. aeolicus</i> and <i>S. aureus</i> FtsWs	58
8.2. <i>E. coli</i> AmiC & NlpD	60
8.2.1. Cloning of <i>amiC</i> and <i>nlpD</i>	60
8.2.2. Production & Purification of AmiC and NlpD	61

9. Crystallogenes and data collection	66
9.1. Crystallogenes	66
9.2. Diffraction and data collection	69
10. AmiC crystal structure	70
11. Role for the auto-inhibiting α-helix	78
12. AMIN domain interaction with peptidoglycan sacculi	80
13. The AmiC-NlpD interaction	82
DISCUSSION	85
ANNEXES	99
Annexe 1:	
Paper accepted in <i>Molecular Microbiology</i>	101
Annexe 2:	
List of protein sequences related to AmiC used for the amino-acid conservation analysis with ConSurf	113
REFERENCES	121

Introduction

1. Structure of the bacterial cell wall

1.1. General points

The bacterial cell wall is an important structure of the prokaryote cell. This layer lying above the plasma membrane confers to the bacterium its morphology, allows it to resist internal osmotic pressure, represents a physical protection against toxic substances and can also contribute to the pathogenicity of various micro-organisms. Based on the staining assay developed by Gram in 1884, two major types of cell wall architectures were identified and the corresponding bacteria named Gram positive or Gram negative.

- Gram positive bacteria cell wall

The Gram positive cell wall is mainly composed of a layer of peptidoglycan (described in section 1.2) 20 to 80 nanometers thick. Two abundant types of phosphate-rich glycopolymers called teichoic acids, synthesized exclusively by Gram positive bacteria, interact with the peptidoglycan and provide stability to the plasma membrane (Figure 1).

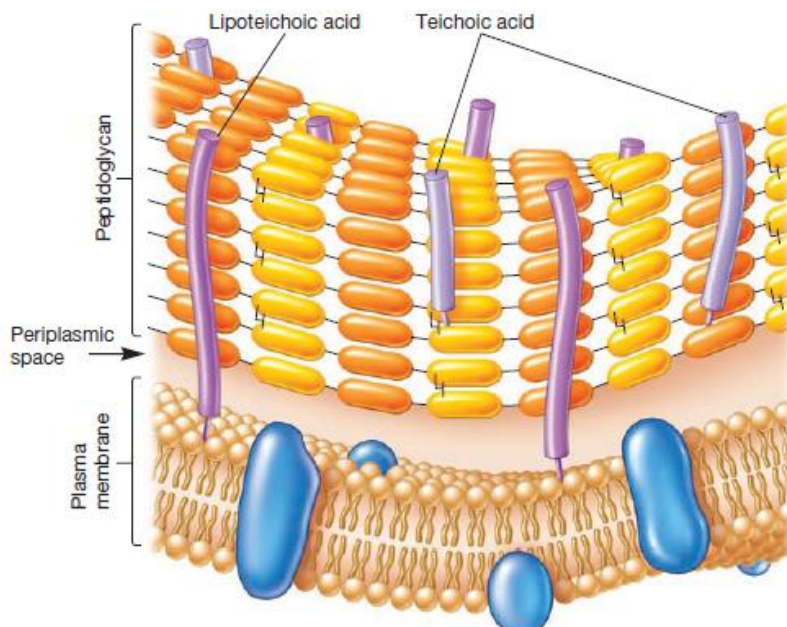


Figure 1. Gram positive envelope (Prescott, 2007)

Wall teichoic acids (WTA) are covalently linked to the peptidoglycan via a linkage unit and extend through and beyond the cell wall. Lipoteichoic acids (LTA) are anchored to the

cytoplasmic membrane via a glycolipid link. Together with peptidoglycan, lipoteichoic acids influence the elasticity and porosity of the cell wall. They are also involved in pathogenic mechanisms such as resistance against antibiotics and horizontal gene transfer. The existence of a periplasmic space has been suggested by cryo-TEM experiments on *Bacillus subtilis* (Matias & Beveridge, 2005). Two major parts of the cell wall were discriminated: the inner wall zone with low abundance of substance and designated as the periplasm and the outer wall zone, which contains mature peptidoglycan associated with WTA and cell surface proteins.

- Gram negative bacteria cell wall

The cell wall of Gram negative bacteria is characterized by the presence of an outer membrane that determines with the plasma membrane, the limits of the periplasmic space (Figure 2). The latter comprises a thin layer (1 to 3 nm thick) of one or two sheets of peptidoglycan.

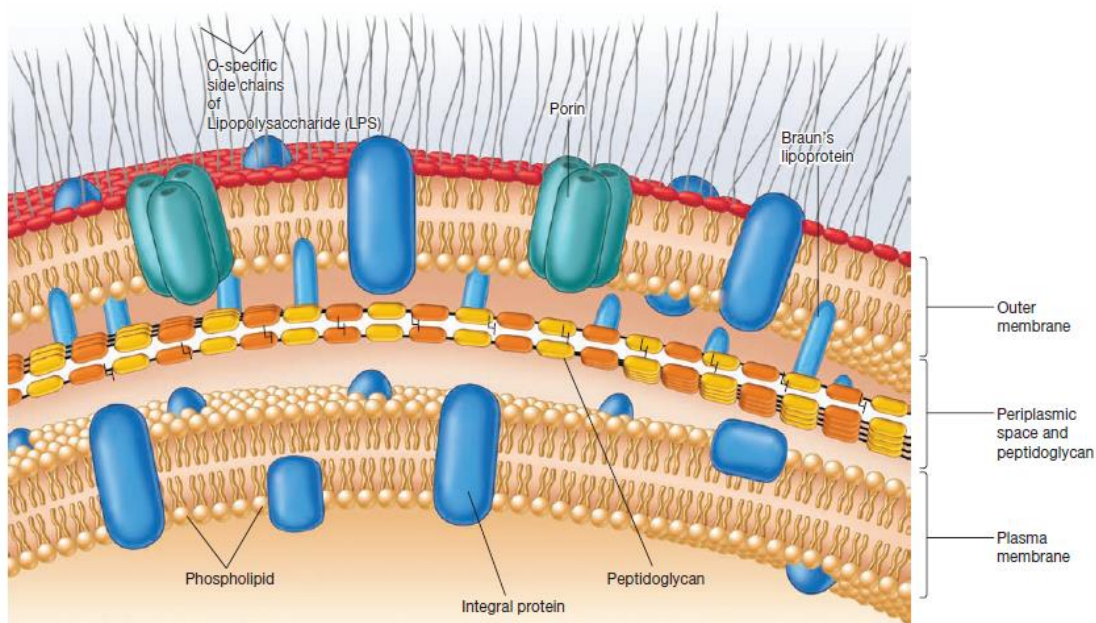


Figure 2. Gram negative envelope (Prescott, 2007)

The most abundant proteins of the outer membrane, Braun's lipoproteins, are covalently linked to the peptidoglycan. The outer membrane is a lipid bilayer but unlike the plasma membrane, phospholipids are only present in the inner leaflet. The outer leaflet is composed of glycolipids, essentially lipopolysaccharides (LPSs) which are known to induce strong inflammatory reactions. The LPS also constitutes a permeability barrier. The high density of LPS molecules

at the bacterial surface and the interactions between them restrict the entry of hazardous molecules such as bile salts or antibiotics. However, the outer membrane is not totally hermetic to the external medium. General porins allow a passive transport of compounds not exceeding 700 daltons across the outer membrane. Intake of larger molecules requires specific transporters such as the Phosphotransferase system (PTS) for carbohydrates transport. Export of molecules is also carried out by Gram negative bacteria in various physiological contexts: antibiotics resistance with efflux pumps, synthesis of cell surface organelles with secretion systems or predation with export of bacteriocin in the medium.

1.2. Peptidoglycan

- Introduction

The peptidoglycan (or murein) is a net-like macromolecule that dictates the shape of the bacteria. It is made of glycan chains cross-linked via peptide stems linked to the sugar moieties. This type of linkage confers strength and elasticity to the peptidoglycan and preserves the integrity of the bacterium. The following points will describe the chemical composition, high order structure and biosynthesis of this important bacterial polymer.

- General chemical composition and diversity

General composition

The glycan chains of peptidoglycan are made of a repeated basic unit composed of alternating N-acetyl glucosamine (GlcNAc) and N-acetyl muramic acid (MurNAc) linked by a β ,1-4 bond (Figure 3). The lactyl group at position 3 on the MurNAc is substituted by a pentapeptide stem of varied amino-acids of L and D series depending on the bacterial species. Most often this peptide stem is made of L-Ala-D-iGlu (iso-glutamate)-meso-DAP (diamino-pimelic acid)-D-Ala-D-Ala in Gram negative bacteria. The meso-DAP is replaced by a L-Lys in some Gram positive bacteria like *Staphylococcus aureus*. In mature peptidoglycan, the last alanine is lost in cross-linking and maturation reactions catalyzed by transpeptidases and carboxypeptidases respectively (see below).

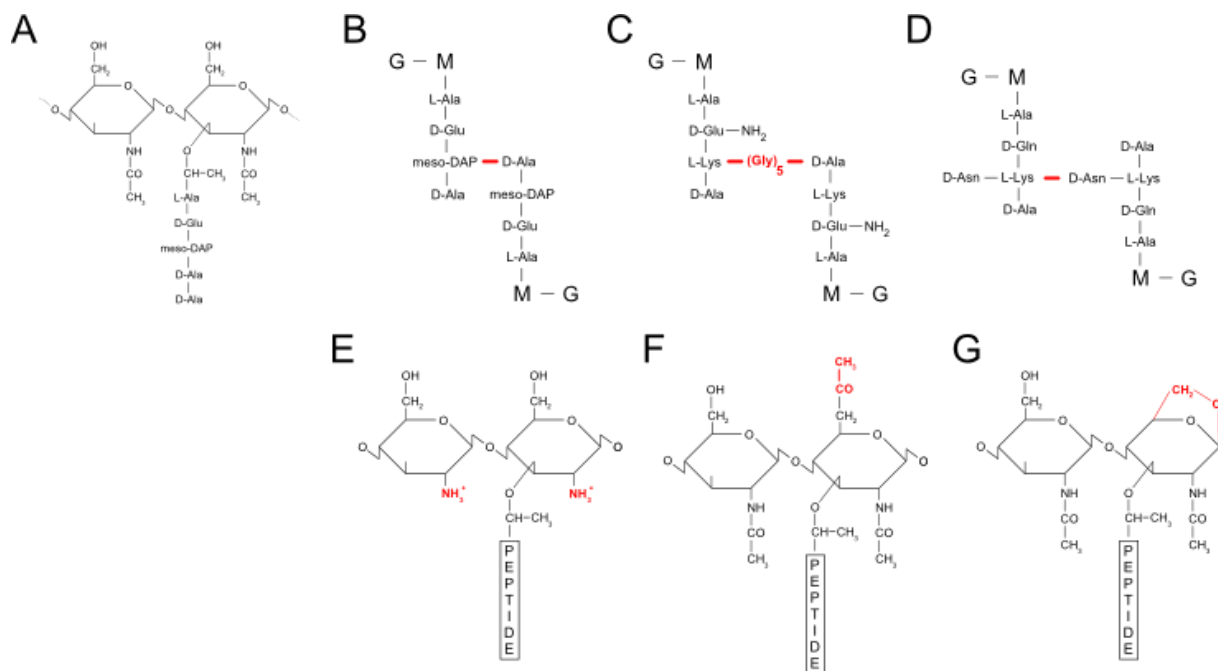


Figure 3. Diversity in peptidoglycan composition. A. Basic unit of *E. coli* peptidoglycan. B. 4-3 cross-link present in *E. coli*. C. 4-3 cross-link with peptide bridge (*S. aureus*). D. Indirect 3-3 cross-link (*E. Faecium*). E. Deacetylated disaccharide. F. O-acetylation of muramic acid. G. 1,6 anhydroMurNAc disaccharide.

Diversity of peptidoglycan composition among bacteria

The most common cross link (called 4-3) is formed between the D-Alanine at position 4 and the amine function of a DAP (or L-Lysin) at position 3 belonging to an adjacent glycan chain (Schleifer & Kandler, 1972). A 4-2 cross-link has been observed in coryneform bacteria between the α -carboxylic function of D-Glu at position 2 and the carboxylic function of D-Ala at position 4. In both cases, the catalytic reaction linking the two peptide stems is performed by D-D-transpeptidases, members of the penicillin-binding protein family (Sauvage *et al.*, 2008). A third kind of cross-link was observed in *Enterococcus faecium* (Mainardi *et al.*, 2000): a 3-3 bond connecting two L-Lys at position 3. Interestingly, the formation of this link requires the catalytic action of the L-D transpeptidase Ldt_{fm}, which is insensitive to most β -lactams antibiotics (Mainardi *et al.*, 2005). L-D transpeptidases have also been found in *Escherichia coli* (Magnet *et al.*, 2008) and *Mycobacterium tuberculosis* (Lavollay *et al.*, 2008). The wide presence of L-D transpeptidases in the bacterial kingdom along with the potential to bypass the β -lactam sensitive synthesis of peptidoglycan could constitute a threat in the fight against multi-drug resistant bacteria.

The cross-link between peptide stems is a direct link in Gram negative bacteria but can be indirect in Gram positive bacteria. In the latter case, the bridge between the lysine of one stem peptide and the D-alanine of the other stem peptide is composed of one to seven residues. For example the *S. aureus* peptide bridge is composed of five glycine residues (Figure 3C).

Substitutions on the peptidoglycan sugar moieties represent another source of variability in the composition of mature peptidoglycan (Vollmer, 2008). Some of these modifications have important physiological impacts on peptidoglycan integrity and bacterial cell cycle. N-deacetylation of glycan chain and O-acetylation of MurNAc sugar alter the conformation of peptidoglycan and restrict the action of muramidases like lysozyme (Amano *et al.*, 1977, Brumfitt *et al.*, 1958). Recently O-acetylation of both MurNAc and GlcNAc were observed in *Lactobacillus plantarum* (Bernard *et al.*, 2011). While the O-acetylation of GlcNAc inhibits the activity of the major *L. plantarum* autolysin, the O-acetylation of MurNAc was shown to activate autolysis via the activity of a putative amidase. Thus, the ratio and localization of these glycan chain modifications modulate the peptidoglycan degradation of the bacterium.

The MurNAc moiety can also be modified into 1,6-anhydroMurNAc by lytic transglycosylases. This modification is found at glycan chains termination in Gram negative bacteria like *E.coli* (Holtje *et al.*, 1975). In the presence of β -lactam antibiotics the peptidoglycan synthesis machinery is inhibited and leads to an uncontrolled hydrolytic activity. Degradation products containing 1,6-anhydroMurNAc are transported to the cytoplasm by the peptidoglycan recycling system. In some Gram negative bacteria like *Citrobacter freundii* and *Enterobacter cloacae* (Holtje *et al.*, 1994, Jacobs *et al.*, 1994), the 1,6 anhydroMurNAc-tripeptide acts as a signaling molecule to induce the expression of the β -lactam hydrolyzing enzyme AmpC via the transcription factor AmpR.

- High order structure

Although the chemical composition of peptidoglycan has been studied for decades, models of its supramolecular arrangement have only been experimentally supported in the last few years. Two main architecture models were proposed: The layered model considers glycan chains running parallel to the cell surface (Ghuysen, 1968) whereas in the scaffold model, they are arranged radially to the cell, perpendicular to the cytoplasmic membrane (Dmitriev *et al.*, 2003) (Figure 4A-B).

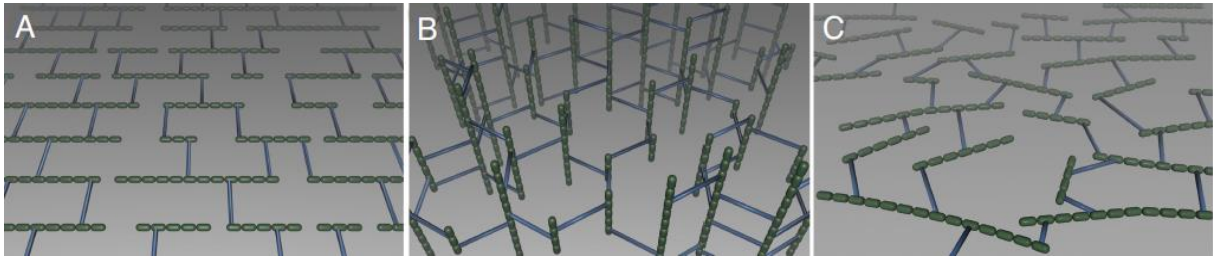


Figure 4. Peptidoglycan architecture models for Gram negative bacteria. A. Layered model. B. Scaffold model. C. Disorganized layers. Glycan chains and peptide cross links are depicted in green and blue respectively (Gan *et al.*, 2008).

For Gram negative bacteria, experimental data argue in favor of the layered model. Indeed, the observation by fluorescence microscopy of labeled proteins involved in peptidoglycan synthesis reveal a spiral motion (van Teeffelen *et al.*, 2011) in agreement with the proposed mechanism of circumferential insertion of newly synthesized glycan chains (Holtje, 1998). Moreover, direct observation by cryotomography of purified murein from *E. coli* and *Caulobacter crescentus* confirmed that glycan strands are oriented parallel to the cell surface and in a disorganized hoop-like fashion (Gan *et al.*, 2008) (Figure 4C).

From Gram positive bacteria, which possess a 5- to 10-fold thicker peptidoglycan, three architectural models were proposed, all supported with experimental evidences: Aside from the two aforementioned “layered” and “scaffold” models, a third alternative consists in 50 nm coiled cables of peptidoglycan strands arranged circumferentially around the cell (Hayhurst *et al.*, 2008) (Figure 5). Recent experiments combining electron tomography on *Bacillus subtilis* peptidoglycan and molecular dynamics simulations strongly argue for the layered model and dismiss the two other ones (Beeby *et al.*, 2013). The capacity of *B. subtilis* to synthesize Gram negative like peptidoglycan during sporulation also argue for a similar synthesis machinery in the bacterial kingdom, leading to a layered murein (Tocheva *et al.*, 2013).

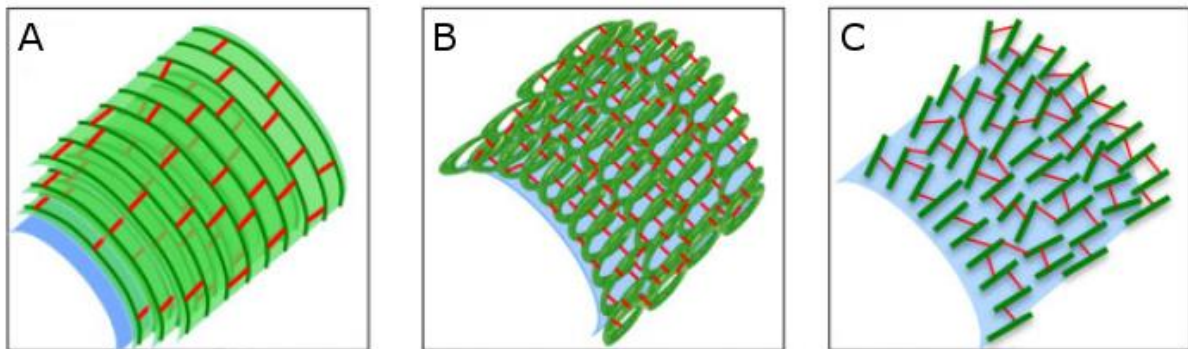


Figure 5. Peptidoglycan architecture models for Gram positive bacteria. A. Layered model. B. Coil-coiled model. C. Scaffold model. The cytoplasmic membrane is depicted in blue. Glycan strands and peptide cross links are shown in green and red respectively (Popham, 2013).

- Peptidoglycan synthesis

Before being integrated in the nascent glycan chains, disaccharide-pentapeptides precursors have to be synthesized in the cytoplasm and coupled to a lipidic carrier in order to be translocated to the periplasm (Figure 6).

In *E.coli*, the first cytoplasmic step is the transfer of the enolpyruvyl moiety of phosphoenolpyruvate (PEP) to uridine diphosphate (UDP); catalyzed by the essential MurA enzyme (Brown *et al.*, 1995, Zemell & Anwar, 1975). The resulting enolpyruvyl UDP-GlcNAc undergo a NADPH-dependant reduction by the MurB enzyme to produce the UDP-MurNac (Taku *et al.*, 1970). The next steps are the stepwise addition of amino-acids to the UDP-MurNac to obtain the final pentapeptide. The ATP-dependent amino-acid ligases responsible for this sequential synthesis are the following: MurC for the first L-Ala, MurD for D-Glu, MurE for meso DAP and MurF for the terminal dipeptide D-Ala-D-Ala (Bouhss *et al.*, 1999, Bouhss *et al.*, 1997, Bouhss *et al.*, 2008, Eveland *et al.*, 1997). The MurNac-pentapeptide is then attached to the lipidic carrier undecaprenyl-phosphate (or C₅₅-P) by the MraY tranferase to form the lipid I. This reaction is followed with the conversion by the enzyme MurG of lipid I into lipid II by the addition of GlcNAc. The lipid II is therefore made of a disaccharide composed of GlcNAc and MurNac, the latter being substituted at position 3 by a pentapeptide and at position 1 by a C₅₅ isoprenyl diphosphate.

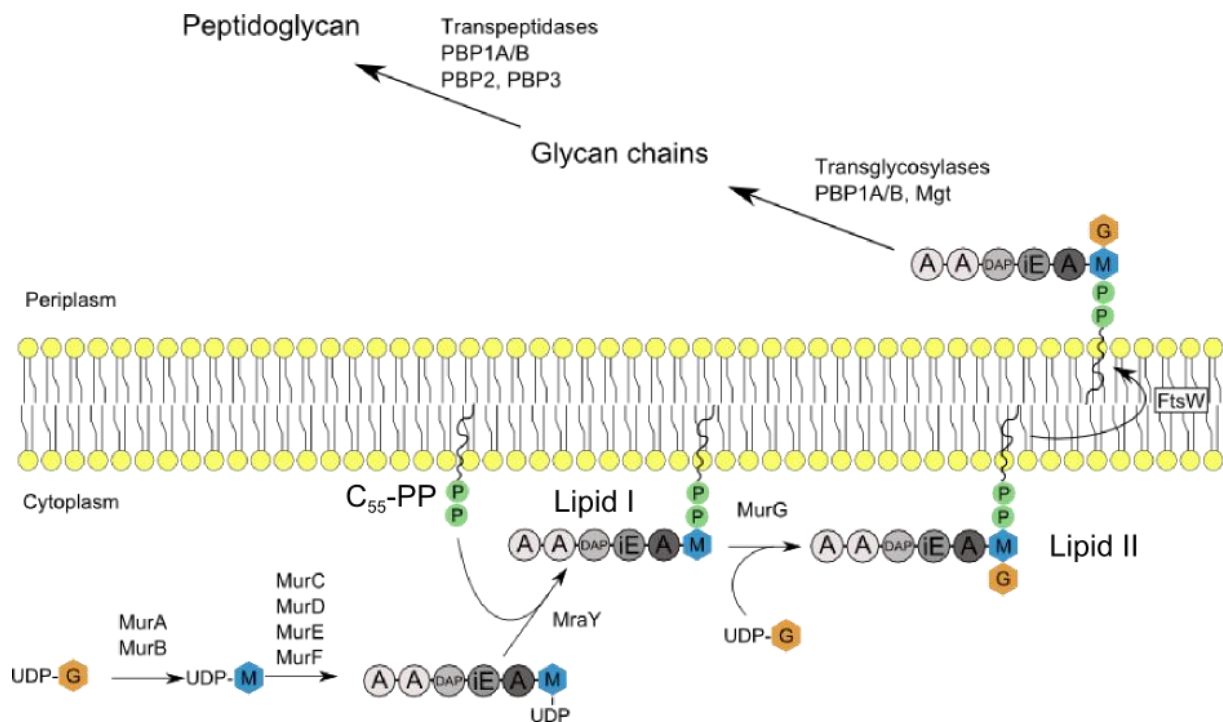


Figure 6. Peptidoglycan synthesis. G: GlcNAc, M: MurNac. Aminoacids are represented as circles. A (grey circle): L-Ala, iE: iso-glutamate, DAP: diaminopimelic acid, A (white circle): D-Ala.

The translocation of lipid II to the periplasm is performed by the flippases FtsW and RodA. The lipid II is then processed by glycosyltransferases that catalyze the β ,1-4 bond formation between the GlcNAc of the lipid II precursor and the MurNAc of the growing glycan chain. Peptides protruding on the synthesized glycan strands are cross-linked by transpeptidase reactions to form the peptidoglycan network. During this reaction, the last D-Alanine residue of the donor peptide is lost. Critical proteins involved in these reactions have been identified and belong to the penicillin binding proteins (PBPs) family. PBP1A and PBP1B are bifunctional PBPs that possess both transglycosylase and transpeptidase activities (Egan & Vollmer, 2013). PBP2 and PBP3 are monofunctional transpeptidases required for elongation and cell division respectively (den Blaauwen *et al.*, 2003, Weiss *et al.*, 1997).

2. Bacterial division

2.1. Divisome presentation

The process responsible for the binary fission of one mother cell into two daughter cells implies the participation of a supramolecular complex called the divisome (Figure 7). This division machinery is composed of, at least, 20 proteins involved in various physiological functions such as chromosome segregation, cell envelope invagination, peptidoglycan synthesis at the division site (called septum) and separation of daughter cells. All these functions require a high level of spatio-temporal regulation in order to preserve the physical integrity of the cell. Mutational experiments have highlighted several genes playing a role in the synthesis of peptidoglycan and division. In *E. coli*, several are located in the same 2 minutes region of the genome, the *dcw* cluster (division cell wall) (Ayala *et al.*, 1994). This cluster is conserved in a broad range of bacterial genomes with mainly the same organization, showing its importance in the bacterial kingdom. In the following description, we will focus on the *E. coli* divisome with few comparisons with known specificities of other bacteria.

The first step of the divisome formation is the polymerization of FtsZ proteins to form a contractile ring (called Z ring). Its stabilization and anchoring to the cytoplasmic membrane is mainly assured by the ZipA, ZapA-D and FtsA proteins. The formation of the Z ring is regulated in time and space by the nucleoid occlusion and the MinCDE systems.

The second step is the maturation of the divisome by the sequential and interdependent recruitment of proteins or protein sub complexes (FtsK, FtQ, FtsL, FtsB, FtsW, PBP3, PBP1B, FtsN, AmiC, etc.) involved in the stabilization of the divisome, septal peptidoglycan synthesis and eventually, separation of the daughter cells.

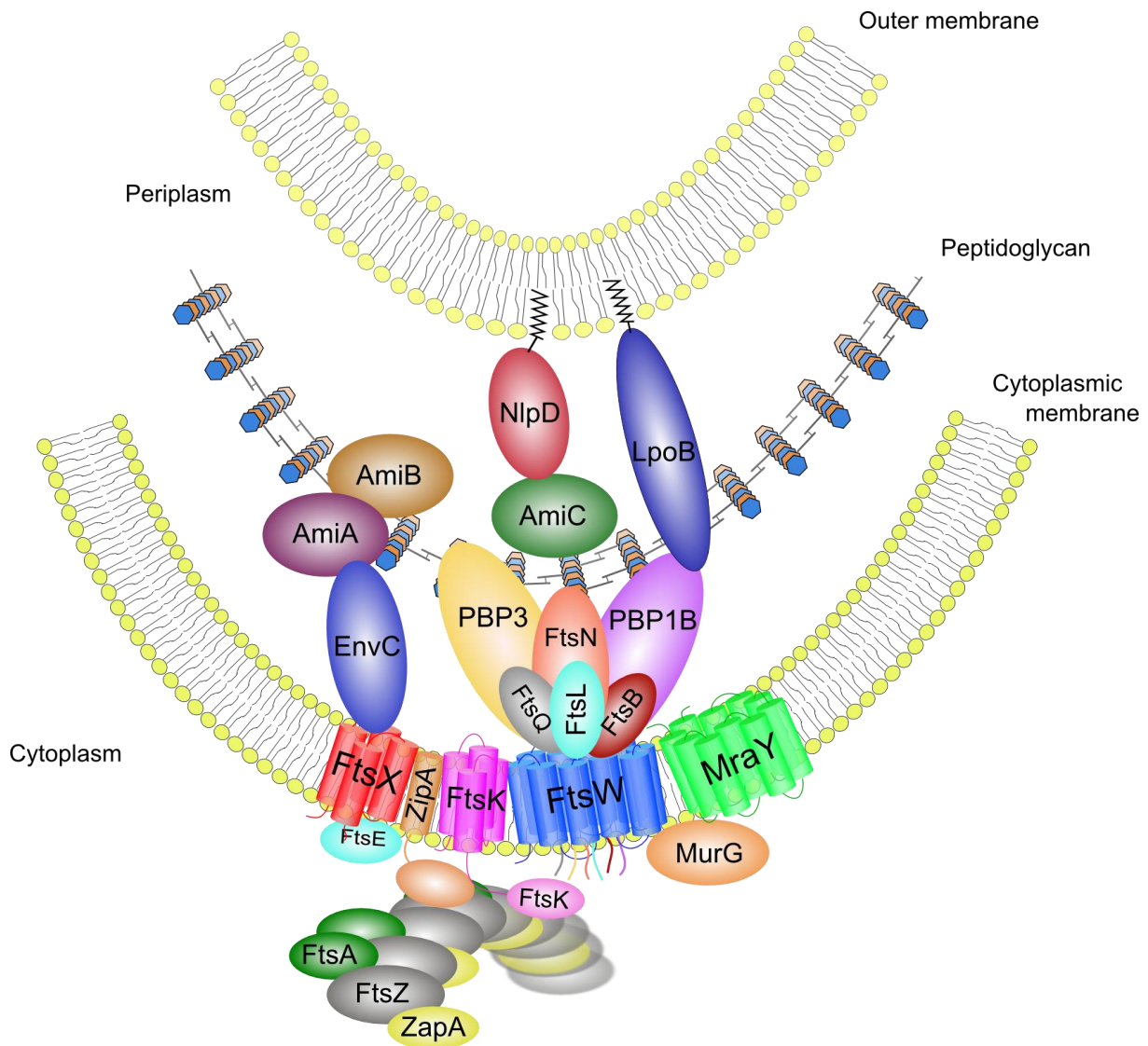


Figure 7. Schematic view of the bacterial divisome of *E. coli*

2.2. Division triggering

The polymerization of the Z ring is a key step of the bacterial division that provides the driving force for the cell constriction. Two specialized systems control this event in time and space. The Min system restricts the FtsZ ring polymerization in protofilaments at mid-cell and the Nucleoid Occlusion system allow a proper segregation of the chromosomes between daughter cells (Figure 8). Both mechanisms result in a precise positioning of the contractile ring, with less than 3% relative deviation (den Blaauwen, 2013, Trueba, 1982, Yu & Margolin, 1999).

2.2.1. Min system

In rod-shaped bacteria, the Min system allows the positioning at midcell of the Z ring by the creation of a concentration gradient of FtsZ-polymerization inhibitors through the long axis of the cell, the concentration being maximal at the cell poles. In *E.coli*, in order to achieve this gradient, a pole-to-pole oscillating system carries the FtsZ-polymerization antagonist MinC. This protein is composed of two domains, both interacting with FtsZ. The N-terminal domain inhibits the polymerization of FtsZ and the C-terminal interrupts lateral interactions between FtsZ protofilaments and also interacts with MinD (Hu & Lutkenhaus, 2000, Shiomi & Margolin, 2007). The oscillation is generated by the protein couple MinD/MinE. The MinD is a ParA-like ATPase which binds to the membrane as a symmetrical dimer in an ATP-bound form (Hu *et al.*, 2002). Upon binding of MinE, the ATPase activity of MinD is stimulated. The ADP-form of MinD undergoes conformational changes, disassembling the dimer and provoking its release from the membrane. The iteration of membrane anchoring-release events generates the oscillation phenomenon. MinC also interacts with MinD and thus acts as a passenger of this oscillating system. GFP fusions have revealed this particular pattern for the three proteins involved (Fu *et al.*, 2001, Hu & Lutkenhaus, 1999, Raskin & de Boer, 1999). The concentration gradient of MinD is also proposed to be involved in the segregation of chromosomes. Indeed, MinD possesses a DNA binding capacity that could create a DNA tethering gradient to move duplicated chromosomes from the division site to the cell poles (Di Ventura *et al.*, 2013).

In *B. subtilis*, the MinE equivalent is absent. The MinCD complex is recruited by DivIVA containing an amphipathic helix. This protein preferentially assembles in negatively curved membranes such as cell poles and division sites (Lenarcic *et al.*, 2009). The most recent model proposes that the membrane curvature at mid-cell allows the recruitment of DivIVA which sequesters the MinCD complex close to the FtsZ ring and regulates the MinC activity to prevent formation of an aberrantly positioned division septum (Eswaramoorthy *et al.*, 2011).

In the vibrioid rod *Caulobacter crescentus*, the positioning of the FtsZ ring is dictated by the bipolar gradient of the antagonist MipZ ATPase with the low point at midcell. The latter is recruited at the cell poles by ParB which binds to DNA sequences near the segregated chromosome origins (Davis & Austin, 1988, Viollier *et al.*, 2004). ParB and chromosomal DNA are thought to be involved in release-capture events that concentrate MipZ at the cell poles and generate an ATP dependent gradient of this FtsZ antagonist (Kiekebusch *et al.*, 2012).

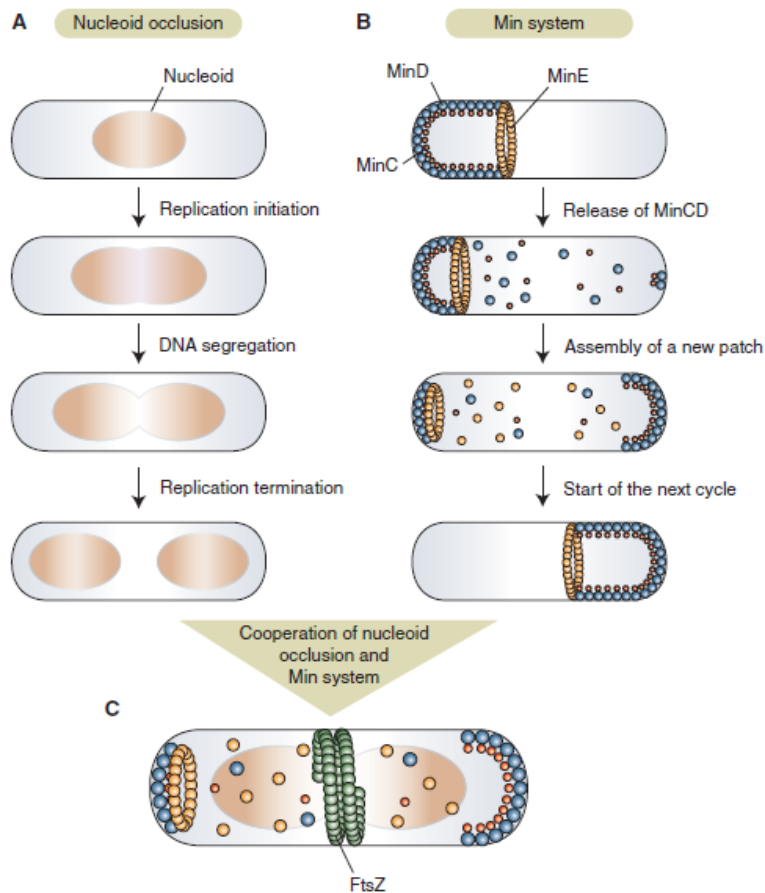


Figure 8. Positioning of the Z-ring with the MinCDE and Nuclear occlusion systems in *E. coli* (Thanbichler, 2010)

2.2.2. Nucleoid occlusion system

The absence of the Min system leads to improper localization of the contractile ring and generate anucleated minicells (Bi & Lutkenhaus, 1993). However, the Z ring is formed only in DNA-free regions so the nucleoid appears to be involved in a second mechanism to prevent the assembly of the divisome machinery.

In *E. coli*, screening of mutants lacking the Min system highlighted the SlmA (Synthetically lethal with a defective Min system) antagonist of the FtsZ ring (Bernhardt & de Boer, 2005). This protein binds to specific DNA sites evenly distributed on the chromosome but not in the Ter region known to be the last to partition during the division process (Niki *et al.*, 2000). Upon this required DNA-binding, the SlmA protein oligomerizes to form high order structures able to prevent the polymerization and bundling of FtsZ protofilaments (Tonthat *et al.*, 2011, Tonthat *et al.*, 2013).

Noc, the SlmA equivalent in *B. subtilis*, has been shown to target 70 regions of the chromosome also absent in the replication terminus. This protein is a potent division inhibitor involved in the spatial regulation of chromosome segregation but the detailed mechanism is not yet known (Wu & Errington, 2004, Wu *et al.*, 2009).

The existence of the Min system and the nucleoid occlusion mechanism stresses the importance of a properly located polymerization of the FtsZ ring. This step, tightly regulated in time and space, is the starting point for the formation of the macromolecular complex responsible for the bacterial division.

2.3. Early stage of the divisome assembly

2.3.1. Constriction ring formation (FtsZ)

FtsZ is a protein homologous to tubulin and its GTP-dependant polymerization at midcell is considered as the first step of bacterial division. FtsZ monomers associate in a head to tail manner to form protofilaments with an observed exchange rate of a few seconds between FtsZ molecules present in the protofilaments and the FtsZ monomers or short oligomers. This protein is conserved in most bacteria, all chloroplasts and primitive mitochondria (Beech *et al.*, 2000, Takahara *et al.*, 2000).

FtsZ crystal structures from different organisms (*Aquifex aeolicus*, *B. subtilis*, *Methanococcus jannaschi*, *M. tuberculosis*, *P. aeruginosa*, *Thermotoga maritima*) show a similar conformation with two globular domains connected by a central α -helix (Lowe & Amos, 1998, Matsui *et al.*, 2012, Oliva *et al.*, 2007, Szwedziak *et al.*, 2012) (Figure 9A). The N-terminal domain adopts a Rossmann fold which binds GTP. The C-terminal domain possesses a chorismate mutase-like fold and a synergy loop that interacts with the N-terminal domain of an adjacent monomer to induce GTP hydrolysis (Lowe & Amos, 1998, Romberg & Levin, 2003) (Figure 9B-C).

The ring ultrastructure of the FtsZ polymer was first observed by immunoelectron microscopy in *E. coli* (Bi & Lutkenhaus, 1991). Its structural arrangement is not fully understood but it has been suggested that this highly dynamic structure is made of overlapping and laterally

interacting FtsZ protofilaments of approximately 30 subunits (Chen & Erickson, 2005, Fu *et al.*, 2010) (Figure 9D). Cryo-EM experiments in *Caulobacter* support this hypothesis (Li *et al.*, 2007). Association of protofilaments would not consist in physical and regular interactions expected for protein-protein contacts but Lennard-Jones type interactions involving ions between protofilaments (Horger *et al.*, 2008). An alternative model proposes that FtsZ protofilaments could anneal into much longer filaments exceeding the circumference of the cell. This model is supported by the observation of protofilament annealing in bulk solvent (Chen & Erickson, 2009) and by fluorescence microscopy of the separation of a Z ring into a two turn helix (Erickson *et al.*, 2010). However, this model is not consistent with the high turn-over of subunits in the Z ring that would imply frequent breakage and reannealing events, incompatible with a long and continuous contractile ring.

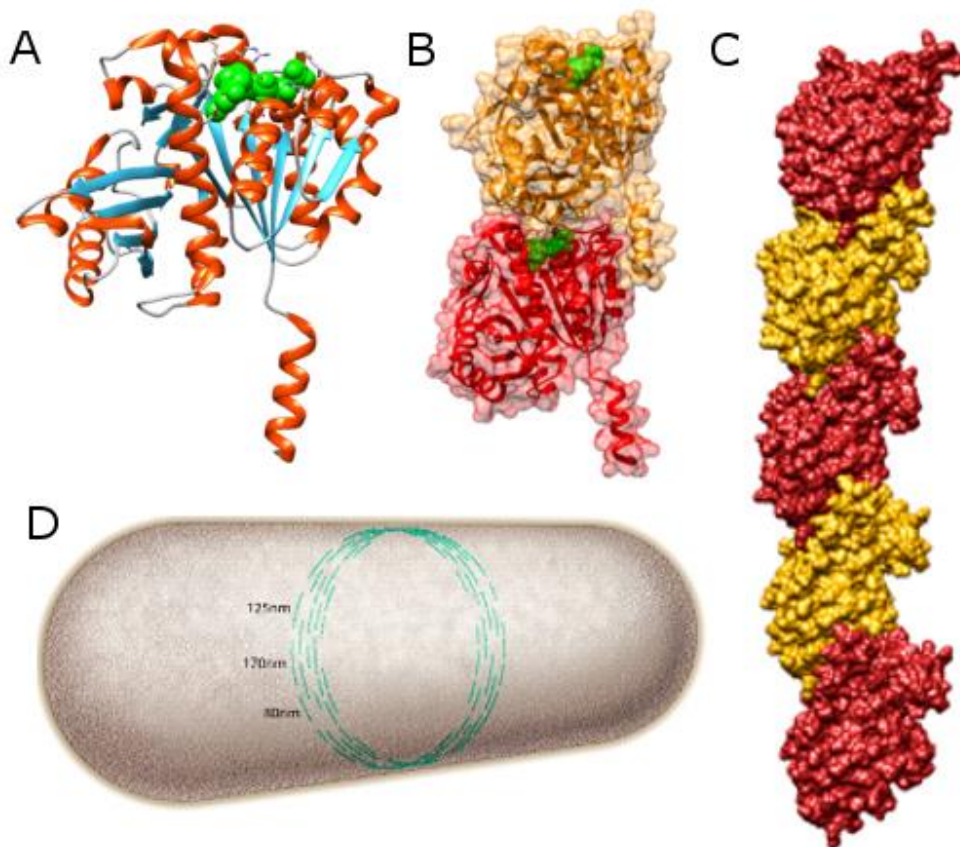


Figure 9. FtsZ and the Zring. A. FtsZ from *M. jannaschii*. B. FtsZ dimer. C. Model of a straight FtsZ filament. D. Proposed model for the organization of the Z ring involving short protofilaments (from 80 to 125nm) interacting laterally. Adapted from (Erickson *et al.*, 2010)

2.3.2. Membrane anchoring of the Z ring (ZipA, FtsA)

The formation of the Z ring depends on the polymerization of FtsZ but also on its tethering to the membrane by two proteins: FtsA and ZipA (Figure 10). FtsZ can assemble into a ring in the presence of either FtsA or ZipA alone but not in the absence of both (Hale & de Boer, 1999, Pichoff & Lutkenhaus, 2002).

FtsA is a widely conserved ATP binding protein of the actin/Hsp70/hexokinase superfamily that localizes at midcell in a FtsZ-dependent manner (Pichoff & Lutkenhaus, 2002). Tethering of the Z ring to the membrane is mediated by the direct interaction of FtsA with the C-terminal peptide of FtsZ and the presence at the opposite side of FtsA of an amphipathic helix that allows its membrane anchoring (Din *et al.*, 1998, Ma & Margolin, 1999). The FtsZ/FtsA ratio has been demonstrated to be important for a proper division. The cell division is blocked by the overexpression of FtsZ. This effect can be reversed when FtsA is also overexpressed. The normal FtsZ to FtsA ratio is of the order of 100:1 (Dewar *et al.*, 1992). Crystal structure of the *Thermotoga maritima* FtsA showed that this protein has an actin-like fold. Moreover, overexpression in *E. coli* of FtsAs from *T. maritima*, *E. coli* and *B. subtilis* form filaments. The authors suggest that the Z ring could be tethered to the membrane by an “A-ring” made of FtsA polymers (Szwedziak *et al.*, 2012). FtsA is also involved in the recruitment of the downstream proteins PBP3 and FtsN and a direct interaction with the latter has been demonstrated (Busiek *et al.*, 2012, Corbin *et al.*, 2004, Rico *et al.*, 2004).

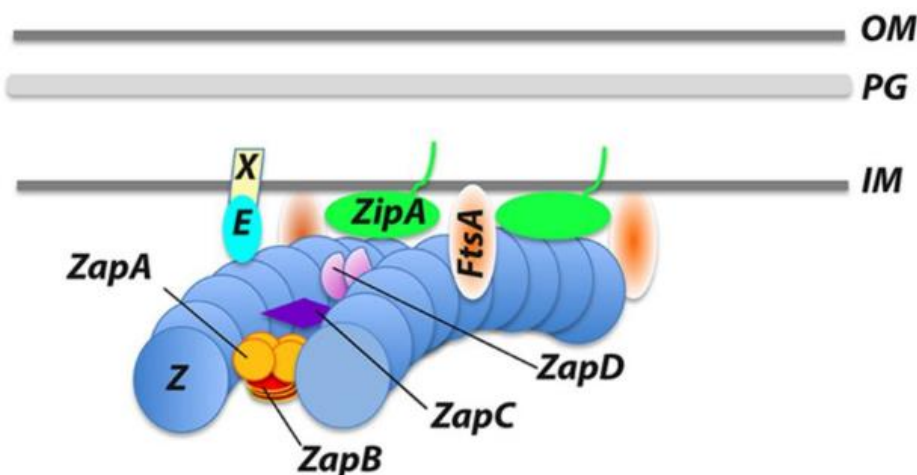


Figure 10. Z-ring positive regulators present in *E. coli* (Huang *et al.*, 2013).

ZipA is an essential bitopic membrane protein only present in gammaproteobacteria (de Boer, 2010). This protein bundles FtsZ protofilaments *in vitro* and modulates their oligomeric state and shape (RayChaudhuri, 1999). Indeed, ZipA binds directly to FtsZ by its C-terminal domain. This interaction has been further characterized by NMR and crystal structures of ZipA in complex with a C-terminal peptide of FtsZ which forms a helix and a beta strand along a hydrophobic groove present in ZipA (Mosyak *et al.*, 2000, Moy *et al.*, 2000). Finally, ZipA is required for the recruitment of downstream proteins such as FtsK, FtsQ, FtsL and FtsN (Hale & de Boer, 2002).

2.3.3. Ring stabilization (ZapA-D)

Stabilization of the Z ring at the early stage is mediated by the four non-essential FtsZ associated proteins ZapA, ZapB, ZapC and ZapD which directly interact with FtsZ (Huang *et al.*, 2013). These four proteins are not present in the whole bacterial kingdom: the gammaproteobacteria possess all the Zap proteins whereas only ZapD is present in betaproteobacteria and ZapA and ZapD in the firmicutes (Natale *et al.*, 2013).

ZapA promotes the Z ring stability by bundling FtsZ protofilaments and *in vitro* experiments suggest that ZapA is in competition with the FtsZ inhibitor MinC in *E. coli* (Dajkovic *et al.*, 2008, Gueiros-Filho & Losick, 2002). Besides the direct binding to FtsZ, ZapA also interacts with ZapB, through its coiled-coil domain (Galli & Gerdes, 2012). ZapB is a Z ring stabilizer that localizes at the division site in a ZapA-dependant manner. *In vitro* experiments have shown that ZapB copellets with FtsZ only in the presence of ZapA, suggesting that ZapA bridges the interaction between ZapB and FtsZ (Galli & Gerdes, 2010). The two other Zap proteins, ZapC and ZapD, also interact with FtsZ but via two different sites, suggesting different molecular mechanisms in the stabilization of the Z ring (Durand-Heredia *et al.*, 2012). As for the FtsA-FtsZ couple, experimental data available so far suggest that a proper stoichiometry of the Zap proteins to FtsZ is required for the formation of the Z ring.

In Gram positive bacteria, the *ylmF* gene located in a broadly conserved gene cluster codes for the SepF protein that promotes assembly and bundling of FtsZ filaments in *B. subtilis* (Hamoen *et al.*, 2006). Unlike Zap proteins alteration, *sepF* mutants have a cell division defect displaying septa with abnormal morphology. Electron microscopy experiments revealed a ring-like

organization of SepF able to bundle FtsZ protofilaments into tubular structures, suggesting a microtubule-like organization (Gundogdu *et al.*, 2011).

In *C. crescentus*, FzlA is a critical protein for cell division that was found to mediate the FtsZ polymerization *in vitro* (Goley *et al.*, 2010). Depletion of FzlA leads to filamentation and cells without constriction. Moreover, FzlA alters the structure of FtsZ filaments into helical bundles and could be involved in the constriction process. The stabilization role of FzlA is consistent with its antagonism towards the FtsZ inhibitor MipZ, involved in the Z ring positioning (cf section 2.2.1). Another FtsZ binding protein, FlzC, is not essential for viability of *C. crescentus* (Goley *et al.*, 2010).

2.3.4. Hypotheses for the FtsZ constriction mechanism

The FtsZ ring is thought to be the main division component able to provide the driving force leading to membrane constriction. This hypothesis is supported by reconstitution of membrane targeted FtsZ into liposomes where constriction is observed (Osawa *et al.*, 2008). Two main models are proposed to explain the contractile ability of the Z ring (Erickson, 2009).

The sliding model is based on FtsZ protofilaments that can span the circumference of the cell, the two ends interacting via lateral bonds. The increase of lateral bonds is thermodynamically favored and thus induces a condensation of the protofilament providing a constriction force. The proteins involved in the formation and stabilization of the Z ring (FtsA, ZipA, Zap proteins) could also modulate the local environment of the protofilaments and generate a variety of contractile forces. Computational modeling supports the hypothesis that the sliding movement between protofilaments is sufficient to generate a contractile force able to achieve cell division (Lan *et al.*, 2009). GTP hydrolysis would not directly generate contractile force but facilitate the monomer turnover during the condensation events.

The bending model proposes that FtsZ protofilaments can switch from a straight to curved conformation in a GTP hydrolysis-dependent fashion and thus, when tethered to the membrane, impose a bending force to the membrane. Electronic microscopy experiments showed curvature of the Z ring *in vitro* in *E. coli*, *M. jannaschii* and *P. aeruginosa* (Chen *et al.*, 2012, Huecas & Andreu, 2004, Lu *et al.*, 2000). The recently solved crystal structure of *M. tuberculosis* FtsZ (MtbFtsZ) in a GTP-bound form gives more insight on the molecular mechanisms involved.

Compared to the crystal structure of a FtsZ dimer of *S. aureus*, a major conformational bend of almost 50° is observed between two adjacent molecules of MtbFtsZ. This observation gives rise to a “hinge opening” mechanism where two consecutive GTP bound-FtsZ molecules in a straight conformation undergo a GTP hydrolysis that induces an opening motion pivoted around a highly conserved interface region. The authors suggest that this mechanism along with the FtsZ tethering by FtsA would constitute a structural scaffold able to provide the driving force for membrane constriction (Li *et al.*, 2013) (Figure 11).

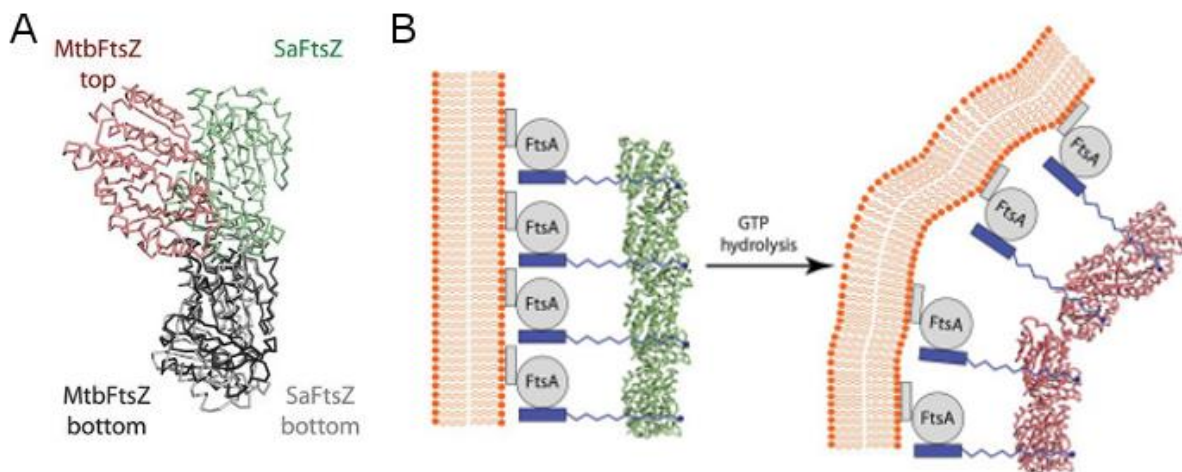


Figure 11. FtsZ is proposed to provide the driving force for cell constriction. A. Superposition of the GDP-bound form of the *M. tuberculosis* FtsZ dimer (MtbFtsZ) with the GDP-bound *S. aureus* FtsZ dimer. B. Proposed mechanism for the cell constriction with the participation of the membrane anchored FtsA. Adapted from (Li *et al.*, 2013)

2.3.5. FtsE/X

FtsE is an ATPase which forms with the membrane protein FtsX an ATP binding transporter-like complex strongly suggested to be involved in the FtsZ assembly and stability at the division site. In *E. coli*, GFP-fusion with FtsX showed that the localization of the protein at the division site is dependent on FtsZ, FtsA or ZipA but independent of downstream proteins (Schmidt *et al.*, 2004). FtsE interaction with FtsZ was assessed by coimmuno-precipitation experiments (Corbin *et al.*, 2007). In *C. crescentus*, FtsE was also found to localize at midcell in dividing cells (Goley *et al.*, 2010).

Recently, another role of FtsEX has been established in *E. coli*. FtsX interacts with the LytM factor EnvC which activates the amidases AmiA and AmiB involved in the cleavage of peptidoglycan during the daughter cells separation (Uehara *et al.*, 2010, Yang *et al.*, 2011). A

similar activation pathway is also present in the Gram positive *Streptococcus pneumoniae* where FtsEX interacts with the putative peptidoglycan hydrolase PcsB (Sham *et al.*, 2011). Mutational studies suggest that the FtsEX-PcsB complex could be involved in the activation of the LytA amidase, known as the major *S. pneumoniae* autolysin (Sham *et al.*, 2013).

The FtsEX complex in *B. subtilis* was also found to be required for the hydrolase activity of the endopeptidase CwlO. However, the latter is not involved in the division but in the elongation process (Bisicchia *et al.*, 2007, Hashimoto *et al.*, 2012). Indeed, in a mutant lacking FtsEX, division is not impaired (Garti-Levi *et al.*, 2008).

These results suggest that the FtsEX complex is a broadly conserved hydrolase activator involved in peptidoglycan metabolism in different physiological contexts depending on the bacterial species.

2.4. Maturation of the divisome

Once the Z ring is formed, a delay is observed in *E. coli*, *B. subtilis* and *C. crescentus* until the complete assembly of the divisome and the beginning of division (Aarsman *et al.*, 2005, Gamba *et al.*, 2009, Goley *et al.*, 2011). During this period, a set of proteins responsible for the synthesis of the septal peptidoglycan (at the division site) and eventually the daughter cell separation will be sequentially recruited at midcell in an inter-dependent manner. This second step, termed maturation of the divisome, will lead to a functional division machinery. The transition between the two modes of peptidoglycan synthesis (lateral for the elongation and septal for the division) is progressive and recent results propose that the two machineries interact with each other to promote cell division (van der Ploeg *et al.*, 2013). The proteins part of the maturation phase of the divisome will be described in their recruitment order.

2.4.1. FtsK and DNA segregation

FtsK is a multidomain protein involved in chromosome decatenation and segregation which is essential for cell division (Yu *et al.*, 1998). Its architecture is highly conserved in bacteria. In *E. coli*, the N-terminal domain consists of four transmembrane segments critical for cell division

and septal localization, followed by a long proline-glutamine linker (Dorazi & Dewar, 2000). The C-terminal domain is a RecA-type ATPase which acts as a DNA translocation machine involved in the chromosome segregation (Dubarry & Barre, 2010). Crystal structure of FtsK from *Pseudomonas aeruginosa* shows a ring-like hexameric form of FtsK in which the DNA would be translocated in an ATP-dependant manner (Massey *et al.*, 2006). Ftsk also interacts with XerC and XerD that recognize the *dif* sites (DNA recombination sites) and deconcatenate the chromosomes (Aussel *et al.*, 2002).

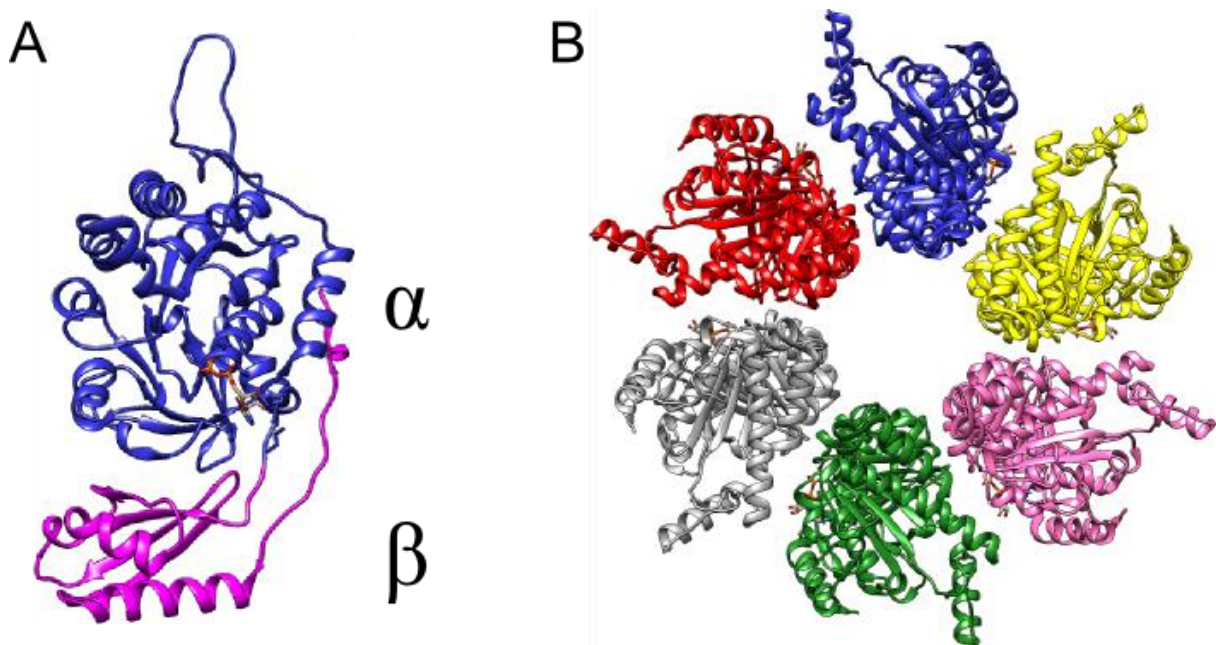


Figure 12. Crystal structure of FtsK from *P. aeruginosa*. A. Monomer of the C-terminal domain (304-811) of FtsK. Two domains are shown: the α domain (blue) is unique to FtsK and the β domain (purple) is RecA related. B. Crystal structure of hexameric FtsK, viewed from the top.

2.4.2. FtsQLB: the divisome link between cytoplasm and periplasm

FtsQ, FtsL and FtsB assemble in a complex (FtsQLB) that is formed independently of the other members of the divisome (Buddelmeijer & Beckwith, 2004). Each of these inner-membrane proteins is bitopic with their major part in the periplasm. Two hybrid experiments have shown that FtsQ interacts with itself, FtsA, FtsX, FtsK, FtsL, FtsB, the recently discovered septal component YmgF (Karimova *et al.*, 2009) and proteins involved in the peptidoglycan synthesis (FtsW, FtsI, FtsN). FtsB also interacts with YmgF whereas FtsL interacts with FtsK, FtsW and

YmgF (Akerlund *et al.*, 2002, Di Lallo *et al.*, 2003, Dubarry *et al.*, 2010, D'Ulisse *et al.*, 2007, Grenga *et al.*, 2010, Grenga *et al.*, 2008, Karimova *et al.*, 2005, Karimova *et al.*, 2009).

The crystal structure of the periplasmic part of FtsQ reveals two distinct domains termed α and β (van den Ent *et al.*, 2008). The α domain, adjacent to the cytoplasmic membrane, exhibits a POTRA (polypeptide transport associated) motif in which the second β -strand is essential for midcell localization. The β domain in C-terminal position is essential to the recruitment of FtsL, FtsB and FtsW (Chen *et al.*, 2002, van den Ent *et al.*, 2008).

FtsB and FtsL are involved in the recruitment of late division proteins and are suggested to participate in the Z-ring stabilization (Geissler & Margolin, 2005, Gonzalez & Beckwith, 2009). They are thought to interact with each other through leucine zippers-like motifs located on their periplasmic part (Robichon *et al.*, 2011).

The stoichiometry of the complex is not fully understood. Computational modeling suggest two models: the hexameric 2:2:2 or trimeric 1:1:1, both stable and in agreement with experimental evidences even if the crystal structure of FtsQ as a dimer favors the hexameric model (van den Ent *et al.*, 2008, Villanelo *et al.*, 2011).

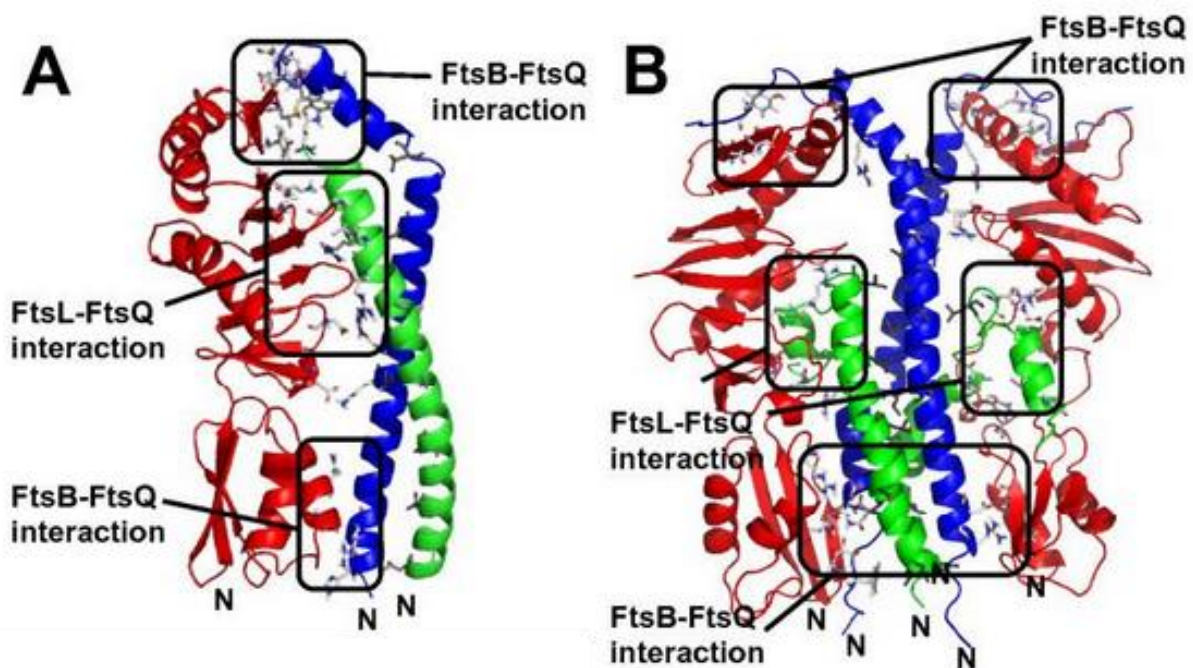


Figure 13. FtsQ/FtsL/FtsB complex models produced by dynamics simulation. A. Trimeric 1:1:1 model. FtsB is depicted in blue, FtsL in green and FtsQ in red. Residues involved in interaction regions are represented as sticks B. Hexameric 2:2:2 model. Adapted from (Villanelo *et al.*, 2011)

The multiple interactions shared by the FtsQLB complex with components of the divisome along with its requirement for the recruitment of downstream proteins make these three proteins important for the connection between cytoplasmic and periplasmic events of the bacterial division.

2.4.3. Translocation of the PG precursor to the periplasm

Once synthesized by the Mur proteins and MraY, the lipidic precursor of the peptidoglycan (lipid II) has to be translocated into the periplasm in order to provide the disaccharide pentapeptide to the peptidoglycan synthesis machinery. A first candidate for this crucial role, MviN, was identified in *E.coli* by a bioinformatics approach (Ruiz, 2008). However, the *B. subtilis* homologs were found to be not essential for growth, thus discarding a potential lipid II flippase role in this organism (Fay & Dworkin, 2009). The FtsW protein was identified two years later as the cell division flippase *E.coli* (Mohammadi *et al.*, 2011). The gene coding for FtsW is located in the *dcw* cluster including the genes coding for MraY and MurG (Ayala *et al.*, 1994). FtsW shares interactions with multiple actors of the cell division (FtsQ, FtsL, FtsN, PBP3 and PBP1B) and is required for the recruitment of the peptidoglycan synthetase PBP3 (Alexeeva *et al.*, 2010, Di Lallo *et al.*, 2003, Fraipont *et al.*, 2011, Karimova *et al.*, 2005). The latter forms a sub-complex with FtsW independently of the other division proteins (Fraipont *et al.*, 2011).

The topology of FtsW from *E. coli* shows ten transmembrane (TM) segments linked by cytoplasmic and periplasmic loops (Lara & Ayala, 2002). The large loop between TM 7 and 8 appears to be important in the functioning of FtsW (Pastoret *et al.*, 2004). The loop between TM 9 and 10 is involved in the interaction with PBP3 and PBP1B and could mediate the positioning of the peptidoglycan synthetases (Fraipont *et al.*, 2011). Two other FtsW topologies from *S. pneumoniae* and *M. tuberculosis* have been determined so far (Datta *et al.*, 2006, Gérard *et al.*, 2002). FtsW from *M. tuberculosis* shows a shorter loop between the TM segments 7-8 and a longer C-terminal periplasmic tail which has been shown to interact with FtsZ and required for a proper cell division in *M. smegmatis* (Rajagopalan *et al.*, 2005).

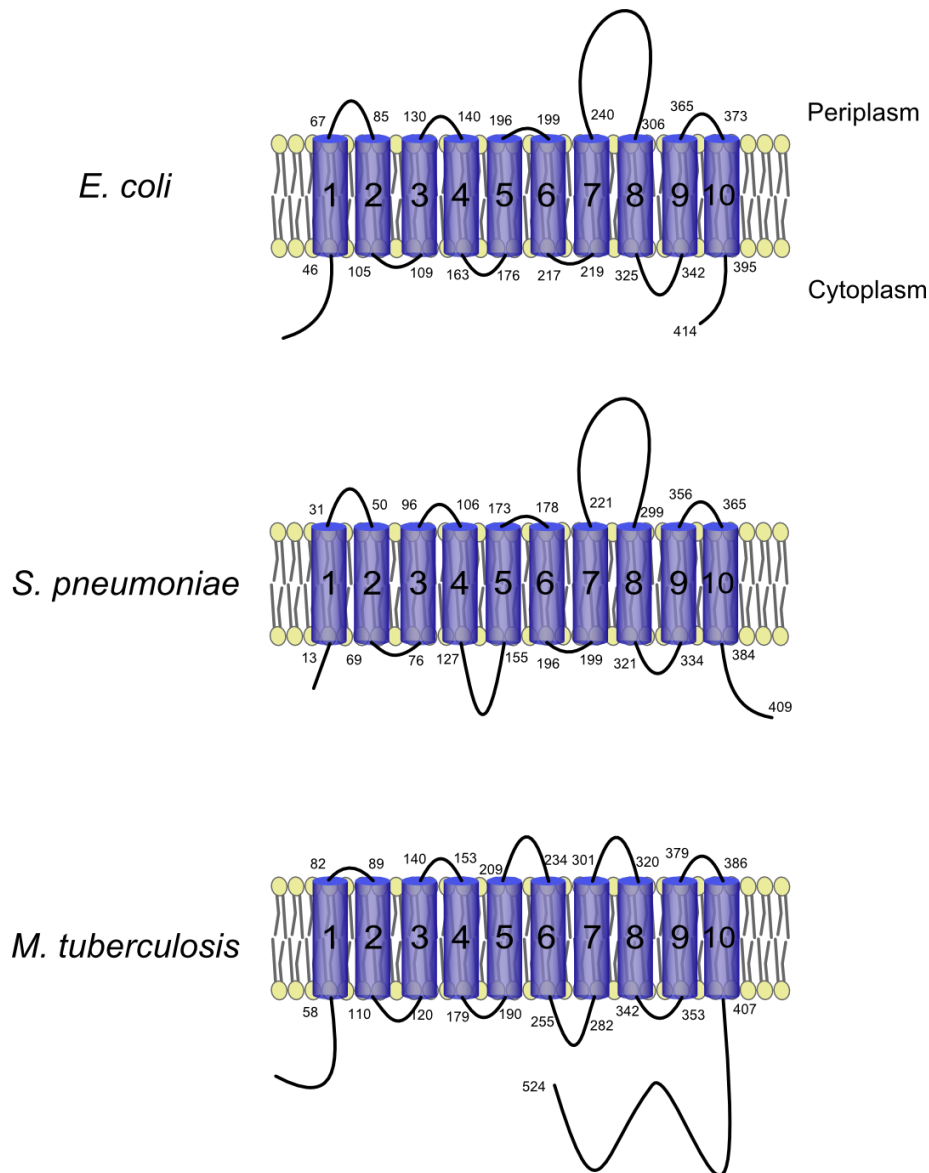


Figure 14. Membrane topologies of FtsW from *E. coli* (Lara & Ayala, 2002), *S. pneumoniae* (Gérard et al., 2002) and *M. tuberculosis* (Datta et al., 2006). The numbers indicate residues surrounding transmembrane segments and the C-terminus of each protein.

FtsW is a member of the SEDS (shape, elongation, division and sporulation) which includes RodA and SpoVE involved in elongation in *E. coli* and sporulation in *B. subtilis* respectively (Ikeda *et al.*, 1989). Thus, RodA and SpoVE are candidates for the role of flippase in their respective physiological context. SEDS proteins are typically located in the same operon than their cognate PBP (PBP3 for FtsW, PBP2 for RodA and SpoVD for SpoVE).

2.4.4. Biosynthesis of glycan chains and incorporation in pre-existent PG

As mentioned above, the lipid II flippase FtsW interacts with PBP3 and PBP1B in *E. coli*. These two proteins are responsible for the polymerization of the glycan chains and their incorporation into pre-existent peptidoglycan at the division site (Figure 15).

PBP3 is an essential bitopic protein with a large cytoplasmic part. The latter includes two domains: a N-terminal non-penicillin binding domain suggested to be involved in the correct folding of the protein (Goffin *et al.*, 1996) and a C-terminal which possesses the DD-transpeptidase activity (Pares *et al.*, 1996) allowing peptidoglycan cross-linking. In *E. coli*, the transmembrane segment is required for the localization of PBP3 at midcell, its dimerization and the interaction with FtsW (Fraipont *et al.*, 2011, Piette *et al.*, 2004, Weiss *et al.*, 1999, Wissel & Weiss, 2004).

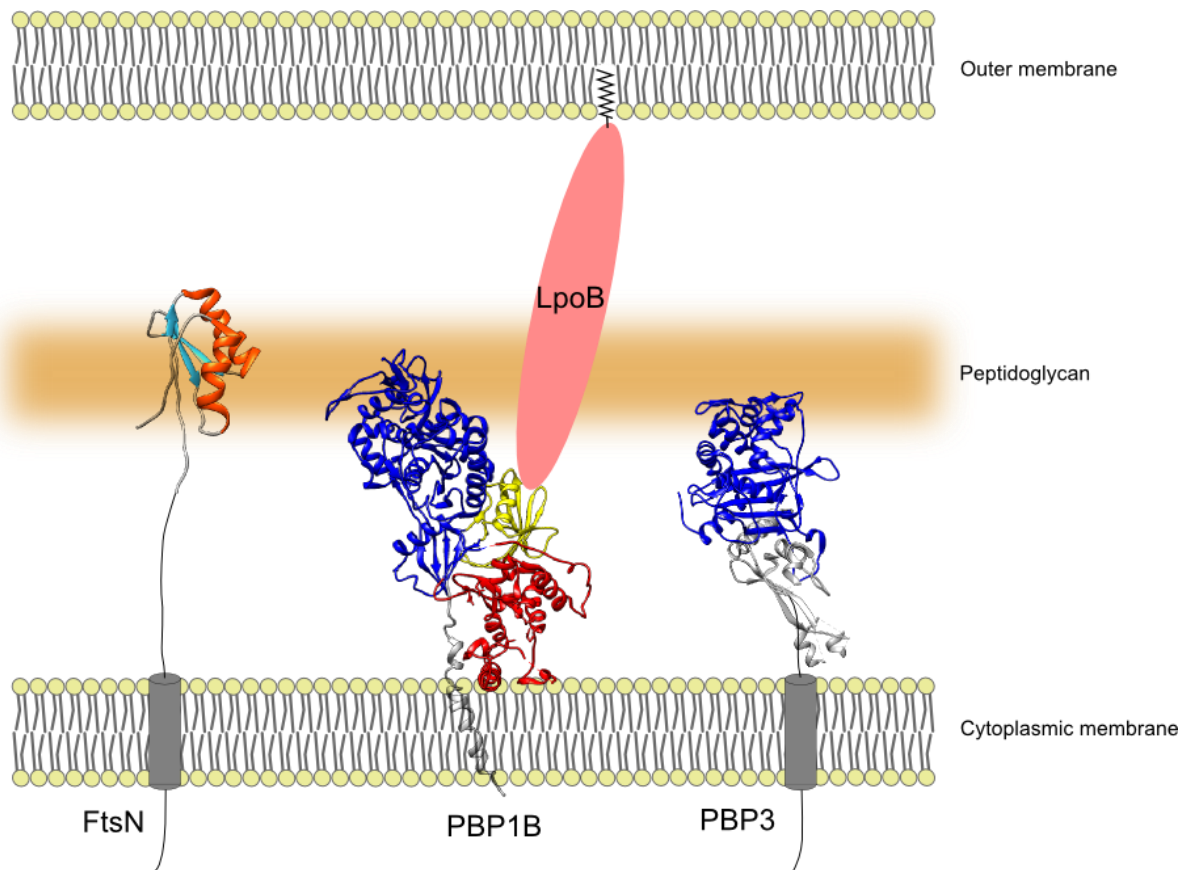


Figure 15. Septal peptidoglycan synthesis actors in *E. coli*. For FtsN, helix and strands are depicted in orange and cyan respectively. For PBP1B, the transglycosylase domain is colored in red, the UB2H domain in yellow, the transpeptidase domain in blue and the transmembrane segment in grey. For PBP3 the transpeptidase domain is colored in blue and the non-penicillin binding domain in grey. Grey cylinders represent transmembrane segments.

PBP1B possesses both DD-transpeptidase and transglycosylase domains. *In vitro*, PBP1B was shown to be more active in conditions favoring its dimerization (Bertsche *et al.*, 2005). The crystal structure of PBP1B suggests that the glycan chain polymerized by the transglycosylase domain could serve as substrate for the transpeptidase domain (Sung *et al.*, 2009). An additional third domain of around 100 residues called UB2H is located between the transpeptidase and transglycosylase domains. Upon interaction with the outer membrane-anchored lipoprotein LpoB, this domain mediates an increase of the transpeptidase activity of PBP1B (Typas *et al.*, 2010) (Figure 15). A model suggests that the porosity and density of peptidoglycan could regulate the activation of PBP1B by LpoB (Paradis-Bleau *et al.*, 2010, Tullman-Ercek *et al.*, 2007, Typas *et al.*, 2010).

FtsN is one of the last proteins recruited at the division site (Figure 15). This essential bitopic membrane protein is thought to improve the assembly and stability of the divisome (Rico *et al.*, 2010). FtsN was shown to interact with PBP1B, PBP3, FtsA and FtsQ (Bertsche *et al.*, 2006, Di Lallo *et al.*, 2003, Karimova *et al.*, 2005, Müller *et al.*, 2007). The periplasmic part of FtsN contains three short α -helices followed by a long linker connected to a C-terminal non-essential SPOR domain (Ursinus *et al.*, 2004, Yang *et al.*, 2004). The latter usually contains around 70 residues with a β -sheet of 4 β -strands flanked by two α -helices on one face. In *E. coli*, this domain is present in four proteins (FtsN, DamX, DedD and RlpA) that localize at the division site. The SPOR domain of FtsN is known to interact with the peptidoglycan suggesting that this domain recognizes a specific septal peptidoglycan architecture (Arends *et al.*, 2010, Gerding *et al.*, 2009, Möll & Thanbichler, 2009). Mutational and structural analysis of DamX and FtsN demonstrate that the β -sheet is involved in the peptidoglycan binding and septal localization of these two proteins (Duncan *et al.*, 2013, Williams *et al.*, 2013). *In vitro*, FtsN was shown to stimulate the polymerase activity of PBP1B and is suggested to modulate the concerted activities of PBP1B and PBP3 (Müller *et al.*, 2007).

2.4.5. Outer membrane invagination

The Tol-Pal system is often cited for its role in the maintenance of the outer membrane and is composed of two sub-complexes. The first one comprises TolQ, TolR and TolA which are inner membrane proteins forming a complex with a stoichiometry of 4-6:2:1 (Cascales *et al.*, 2001, Zhang *et al.*, 2009) (Figure 16). The second complex includes TolB, a periplasmic protein, and

Pal, an outer membrane lipoprotein. Inner and outer membrane can be bridged by specific interactions between the periplasmic part of TolA and Pal or TolB (Carr *et al.*, 2000, Cascales *et al.*, 2002, Cascales *et al.*, 2000, Llobes *et al.*, 2001). *In vivo* cross-linking experiment also showed interactions between the Pal protein and the outer membrane proteins OmpA and Lpp (Cascales *et al.*, 2002).

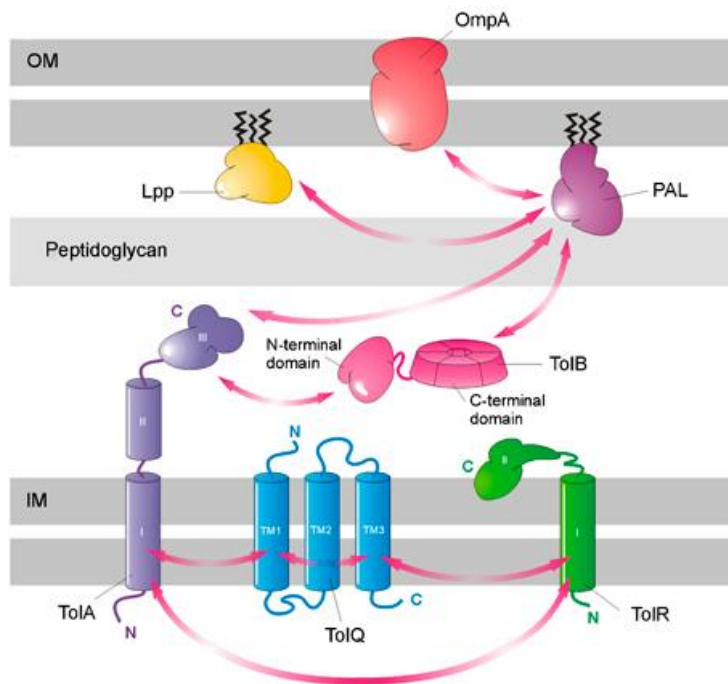


Figure 16. Tol-Pal system of *E. coli* and its interaction network. Interactions are indicated by pink arrows (Godlewska *et al.*, 2009).

Mutational studies showed that the *E. coli* cells lacking the *tolA* gene exhibit a chaining phenotype and division defects (Meury & Devilliers, 1999). Moreover, all five proteins of the Tol-Pal system have been shown to accumulate at constriction sites but failed to localize in cells depleted in FtsN. Tol mutants also show a delay in outer membrane invagination and contain outer membrane blebs at constriction sites and cell poles. The authors propose that the Tol-Pal system is a sub-complex of the divisome drawing the outer membrane in the space generated by the separation of the new cell poles during the division process (Gerding *et al.*, 2007). Recently, FtsN and TolQ were shown to interact through their periplasmic parts by a two-hybrid experiment (Teleha *et al.*, 2013).

2.4.6. Peptidoglycan hydrolysis and bacterial division

Peptidoglycan hydrolases have been shown to be involved in various physiological contexts such as bacterial growth, peptidoglycan turnover, sporulation and germination events, assembly of secretion systems, pili and flagella (Vollmer *et al.*, 2008). The following section will focus on septal peptidoglycan hydrolases and their respective role and known regulations in the division process of *E. coli*.

2.4.6.1. *E. coli* periplasmic amidases, key players of cell separation

The amidases AmiA, AmiB and AmiC belongs to the amidase_3 family and consist of Zn²⁺-metallo-enzymes that cleave the amide bond between the lactyl group of the N-acetylmuramic acid and the L-Alanine of the peptide stem. AmiA and AmiC are translocated to the periplasm via the twin-arginine transport (Tat) pathway whereas AmiB transport is mediated by the Sec machinery. Their involvement in the bacterial division have been demonstrated in mutational studies where a triple amidase mutant shows a chaining phenotype in which 90 to 100% of the cells are not able to achieve binary fission (Heidrich *et al.*, 2001). A similar but less severe phenotype is observed for *amiA* and *amiC* single mutant with 5-10% and 20-30% of chain-forming cells respectively whereas *amiB* mutant showed no such division defects (Heidrich *et al.*, 2001). In the absence of AmiC, deletion of the D,D-endopeptidases PBP4 and PBP7 (two low molecular weight PBP) or lytic transglycosylases (e.g. Slt70) exacerbates the chaining phenotype (Priyadarshini *et al.*, 2006). Moreover, deletion of entire families of peptidoglycan hydrolases showed a preponderant role in cell separation for periplasmic amidases followed by lytic transglycosylases and to a lesser extent, D,D-endopeptidases (Heidrich *et al.*, 2002).

AmiC and AmiB localize to the division site of constricting cells in a FtsN-dependant fashion thanks to their N-terminal AMIN domain (Bernhardt & de Boer, 2003, Peters *et al.*, 2011). The latter, preponderant in Gram negative bacteria, is mostly present at the N-terminus of periplasmic proteins involved in cell wall metabolism or transport structure such as the type IV pilus (de Souza *et al.*, 2008). Consistent with the septal localization of AmiB and AmiC, AmiA, devoid of AMIN domain, exhibits a dispersed localization throughout the periplasm (Bernhardt & de Boer, 2003) (Figure 17).

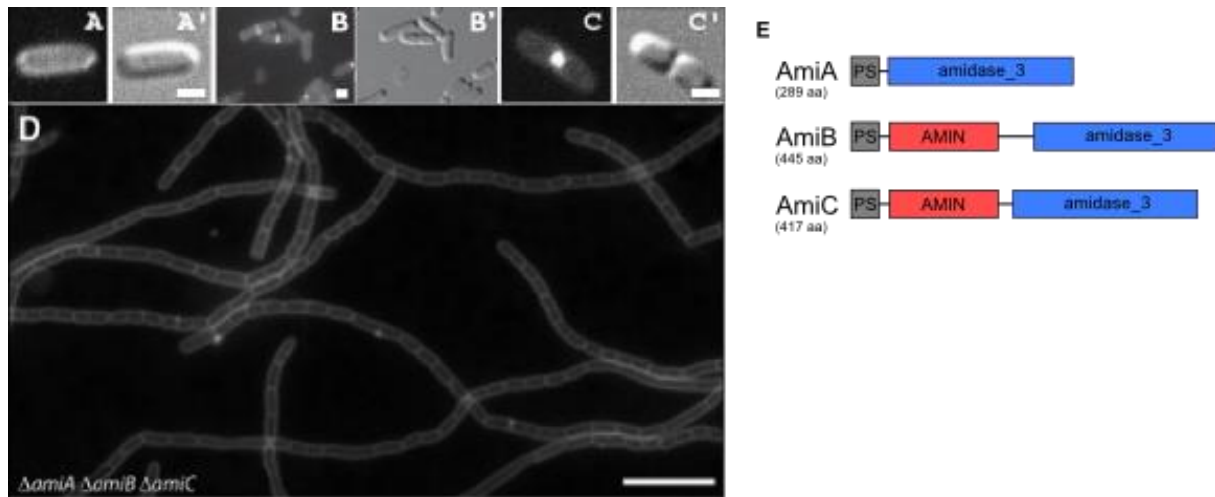


Figure 17. Cell division amidases of *E. coli*. (A-C) Localisation studies with GFP variants of AmiA (A-A'), AmiB (B-B') and AmiC (C-C'). Cells are visualized using GFP (A, B and C) or differential interference contrast (DIC) (A', B' and C'). (D) Triple mutant $\Delta amiA \Delta amiB \Delta amiC$. Cells were stained with the fixable membrane dye FM1-43-FX and visualized by fluorescence. Bars equal 1 μm for (A-B-C) and 8 μm for (D). (E) Topologies of AmiA, AmiB and AmiC.

- Catalytic mechanism of amidase_3 family proteins

Despite different folds, the catalytic site and the catalytic mechanism of the amidase_3 family is similar to that of the amidase_2 domain of the major autolysin AtlE from *Staphylococcus epidermidis* (Figure 18A and B). Upon approach of the substrate, a water molecule bound to the active site Zn^{2+} is shifted toward a conserved glutamic acid which further activates it and favors the nucleophilic attack of the amide bond. This step produces a tetrahedral conformation of the amide carbon and a transient pentameric coordination of the catalytic Zn^{2+} . The tetrahedral intermediate is stabilized by hydrogen interactions involving the carbonyl oxygen of the scissile bond. In the N-acetylmuramoyl-L-alanine amidases, the carbonyl oxygen of the substrate L-Ala and one of the MurNAc oxygen can contribute to the stabilization of the tetrahedral intermediate (Kerff *et al.*, 2010). The proton is transferred to the nitrogen of the scissile bond to form a second transition state characterized by a doubly protonated tetrahedral nitrogen which is potentially stabilized by the MurNAc N-acetyl group (Kerff *et al.*, 2010).

In amidase_2 enzyme, a histidine or a lysine is also found across the active site compare to the glutamate (Figure 18A) and is involved in the stabilization of the tetrahedral conformation of the amide carbon. In the amidase_3 family, no residue equivalent to those has been identified.

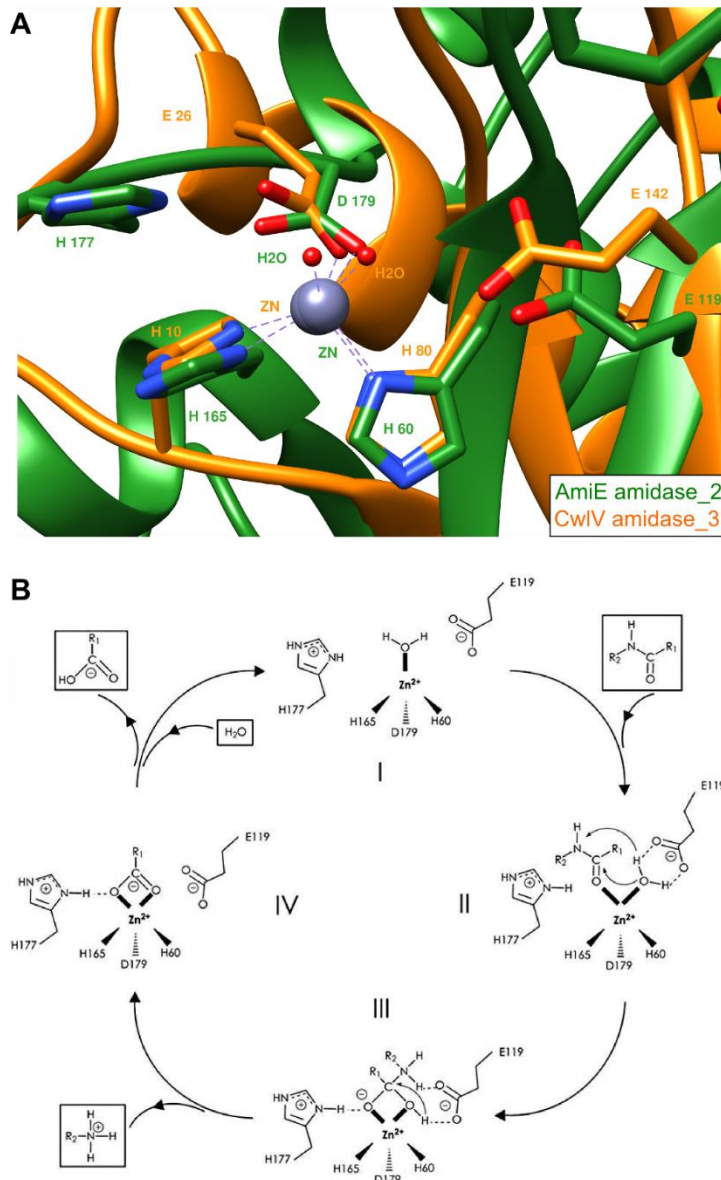


Figure 18. Comparison of amidase_2 and amidase_3 catalytic mechanisms. A. Superposition of the amidase_2 member AmiE (in green) from the major autolysin AtlE (*S. epidermidis*) and the amidase_3 member CwIV (in orange) from *Bacillus polymyxa*. Oxygens and nitrogen are depicted in red and blue respectively. B. Proposed catalytic mechanism of AmiE. See details in text. Adapted from (Zoll *et al.*, 2010)

2.4.6.2. Regulation of septal amidases: the LytM factors

Another set of proteins, containing LytM domains (lysostaphin/peptidase M_23), is involved in peptidoglycan hydrolysis. In *S. aureus*, the LytM protein specifically cleaves the pentaglycine peptide bridge whereas the LytM factor gp13 from the *B. subtilis* phage Φ 29 shows a D,D-endopeptidase activity that cleaves direct cross links in *B. subtilis* peptidoglycan (Browder *et al.*, 1965, Cohen *et al.*, 2009, Firczuk *et al.*, 2005).

In *E. coli*, four proteins (EnvC, NlpD, YebA and YgeR) contain a LytM domain. Deletion of these proteins leads to a severe chaining phenotype with a preponderant effect of the *envC-nlpD* double mutation (Figure 20A). Moreover, EnvC and NlpD were shown to localize at the division site, supporting their role in cell separation (Uehara *et al.*, 2009). Unexpectedly, these two proteins do not exhibit hydrolytic activity against peptidoglycan *in vitro*. Sequence alignment with the active LytM of *S. aureus* highlighted the lack of zinc-chelating residues in the active sites of EnvC and NlpD. Instead, they specifically activate the three aforementioned amidases: AmiA and AmiB for EnvC and Amic for NlpD (Uehara *et al.*, 2010). More insight in the molecular mechanism of septal amidases activation was gained with the crystal structure of the amidase_3 member AmiB from *B. henselae* where an α helix is obstructing the active site (Yang *et al.*, 2012) (Figure 19A-B).

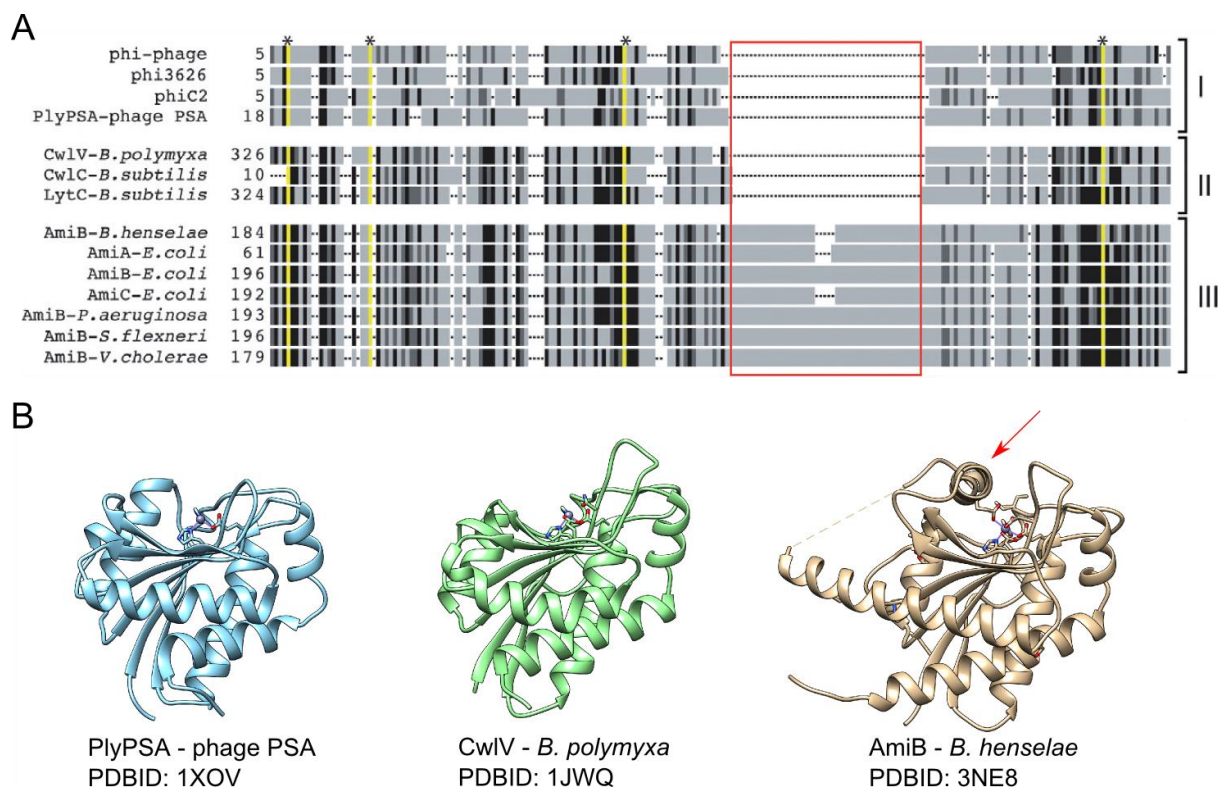


Figure 19. A. Alignment amidase_3 members grouped into the following categories: (I) phage endolysins, (II) bacterial amidases involved in mother cell lysis following sporulation and (III) cell separation amidases. The red box highlights a ~ 50 amino acid insertion region found only in the cell separation amidases. B. Crystal structures of amidase_3 members for each aforementioned category: PlyPSA (phage PSA) (I), CwlV (*B. polymyxa*) (II) and AmiB (*B. henselae*) (III). The amino acid insertion containing the inhibitory helix is shown by the red arrow. Adapted from (Yang *et al.*, 2012)

Mutational screening of the *E. coli* AmiB allowed to isolate variants with uncontrolled lytic activity leading to cell lysis when overproduced. These mutations are mainly located in the obstructing α helix, suggesting a conformational switch induced by the LytM factor EnvC to

allow access to the active site of the amidase (Yang et al., 2012). The crystal structure of EnvC from *E coli* confirmed the lack of critical residues involved in the chelation of the catalytic zinc. Moreover, residues lying in and around the degenerate active site were found to be critical *in vivo* to promote a proper cell separation and *in vitro* to activate the septal amidase AmiB (Peters et al., 2013).

Unlike AmiC and AmiB, EnvC localization is not FtsN-dependent but is mediated via its N-terminal coil-coiled domain (Uehara et al., 2010) (Figure 20B). EnvC was also shown to localize to the division site before its cognate amidase AmiB (Peters et al., 2011). Indeed, EnvC requires the early divisome component FtsE/X for its recruitment to the septal ring (Yang et al., 2011). A direct interaction has been demonstrated between a periplasmic loop of FtsX and EnvC (probably via its coil-coiled domain). Moreover, the ATPase activity of FtsE is a requirement for a proper cell division (Yang et al., 2011). Along with the interaction of FtsE with FtsZ (Corbin et al., 2007), these results strongly suggest a coordination between the cytoplasmic Z ring constriction and the periplasmic hydrolysis of septal peptidoglycan (Yang et al., 2011) (Figure 20C).

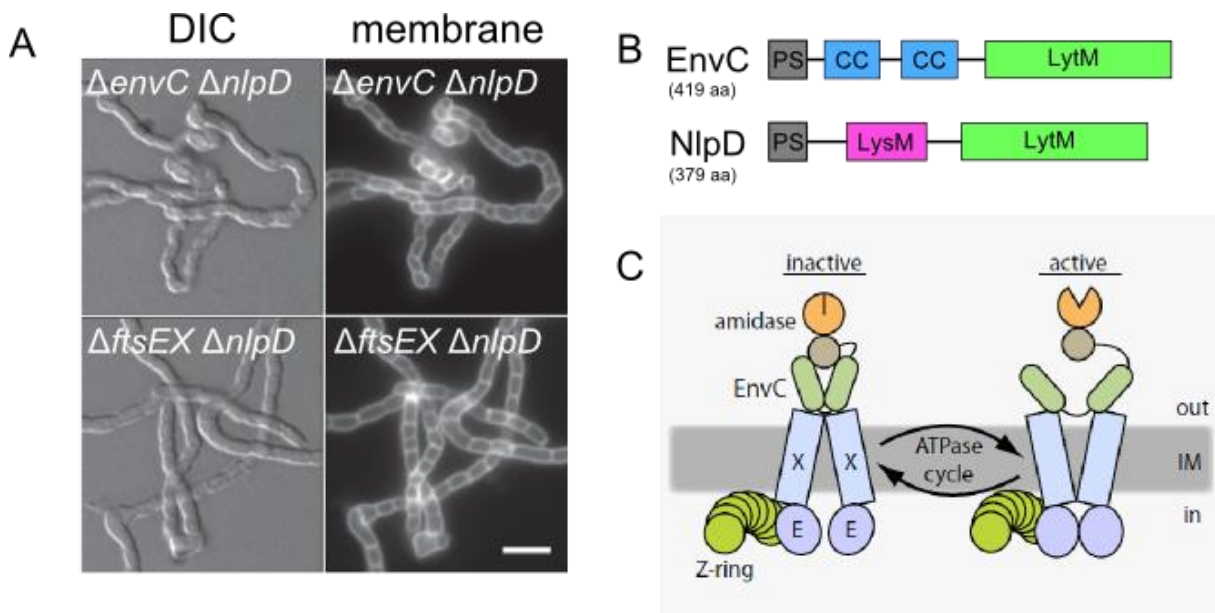


Figure 20. Involvement of LytM factors EnvC and NlpD in bacterial division. A. Mutational study of EnvC, NlpD and FtsEX. Cells are visualized by DIC or by fluorescence thanks to the fixable membrane dye FM1-43-FX. B. Topologies of EnvC and NlpD. (C) Proposed model for the putative FtsEX-EnvC-amidase complex at the division site. The authors suggest that conformational changes in FtsEX induced by the FtsE-mediated ATP hydrolysis are transmitted to EnvC which in turn regulate the amidase activity at the septum (Yang et al., 2011).

The second known amidase activator, NlpD, is a lipoprotein anchored in the outer membrane (Ichikawa *et al.*, 1994, Lange & Hengge-Aronis, 1994). Apart from its LytM domain, NlpD possesses a N-terminal LysM motif known to bind peptidoglycan (Buist *et al.*, 2008) (Figure 20B). The septal localization of NlpD depends on the presence of FtsN and, as for EnvC with AmiB, reach the septum before its cognate amidase AmiC (Peters *et al.*, 2011). The requirement of cell division amidases activation by the LytM factors EnvC and NlpD is supported by the double mutant $\Delta envC\Delta nlpD$ that phenocopies the triple mutant $\Delta amiA\Delta amiB\Delta amiC$ (Figure 17D and Figure 20A)

2.4.6.3. Regulation of murein hydrolysis in the context of septum formation

Apart from the presence of FtsN and FtsE/X, the localization of AmiB and AmiC at the division site also requires a functional synthesis of septal peptidoglycan (Peters *et al.*, 2011). The treatment of cell with the PBP3 inhibitor cephalixin do not disrupt the recruitment of FtsN, EnvC and NlpD but AmiB and AmiC fail to localize at the division site. Consistent with the proposed self-accumulation of FtsN at the division site (Gerding *et al.*, 2009), a model suggests that a small amount of FtsN, localized at the division site, promotes a low level of peptidoglycan synthesis at the septum by PBP3 and/or PBP1B (Müller *et al.*, 2007). This septal peptidoglycan is hydrolyzed by the amidase, leading to glycan strands lacking peptides. These glycan strands are then bound by the SPOR domain of FtsN which accumulates at the division site and further stimulates the synthesis of septal peptidoglycan (Figure 21) (Peters *et al.*, 2011). Thus, the regulated supply of substrate to septal amidases would add another level of control over the peptidoglycan hydrolysis at the division site and ensure a proper cell separation.

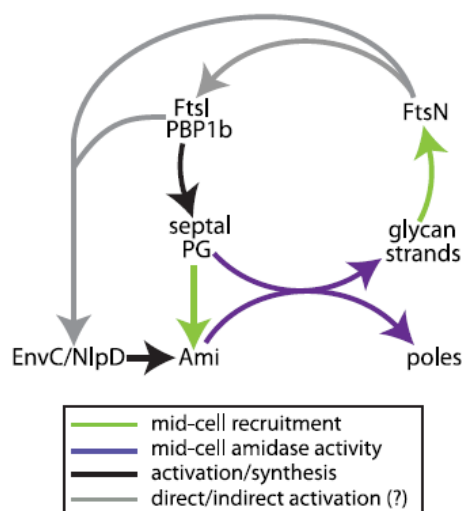


Figure 21. Model for the coordination of septal peptidoglycan synthesis and hydrolysis (Peters *et al.*, 2011).

2.4.6.4. Coupling murein hydrolase activity and Z ring positioning

As mentioned in section 2.2, the FtsZ ring is polymerized at mid-cell thanks to the two spatio-temporal regulating systems (MinCDE system and nucleoid occlusion). Mutational studies showed that low molecular weight PBP (LMW-PBP) also play a role in the positioning of the contractile ring (Potluri *et al.*, 2012). Cells lacking these PBP, and especially the D,D-carboxypeptidase PBP5, exhibit a branching phenotype due to mislocalized FtsZ. PBP5 is known to be involved in the overall shape maintenance of *E. coli* (Ghosh *et al.*, 2008). The authors suggest that the observed changes in the bacterium shape could impair the oscillating mechanism of the MinCDE system and modify the localization of FtsZ-polymerizing antagonists, leading to improper septum formation and division defects (Potluri *et al.*, 2012).

2.5. Divisome network

A tremendous amount of *in vivo* and *in vitro* work has been realized and is still ongoing in order to map the protein-protein interaction network existing within the divisome of *E. coli* (Figure 22). This information along with localization studies constitute a valuable basis in the understanding of the chronology of events leading to the assembly of a functional division machinery. Interestingly, several features of the *E. coli* divisome are shared by other organisms. A two-step assembly is also observed in *B. subtilis* with a comparable delay between the Z ring formation and the assembly of late division proteins (Gamba *et al.*, 2009). Similarities have also been found in the timing of recruitment of divisome proteins in *C. crescentus* (Goley *et al.*, 2011). However, discrepancies are observed, as the late recruitment of FtsA or the non-requirement of FstB (Goley *et al.*, 2011).

A comparative approach between the division proteins of *E. coli* and the Gram positive pathogen *S. pneumoniae* revealed a minimal conserved interactome between the two organisms. Moreover, cross-interactions between *S. pneumoniae* proteins and the corresponding *E. coli* orthologs were detected, supporting the idea of a common core of division proteins (Di Lallo *et al.*, 2003, Maggi *et al.*, 2008). However, both networks are not fully transposable and numerous interactions were shown to be specific to *S. pneumoniae* (Massidda *et al.*, 2013). Thus, the characterization of the *S. pneumoniae* division network is a powerful tool for the identification potential new targets for anti-bacterial therapy (Sham *et al.*, 2012).

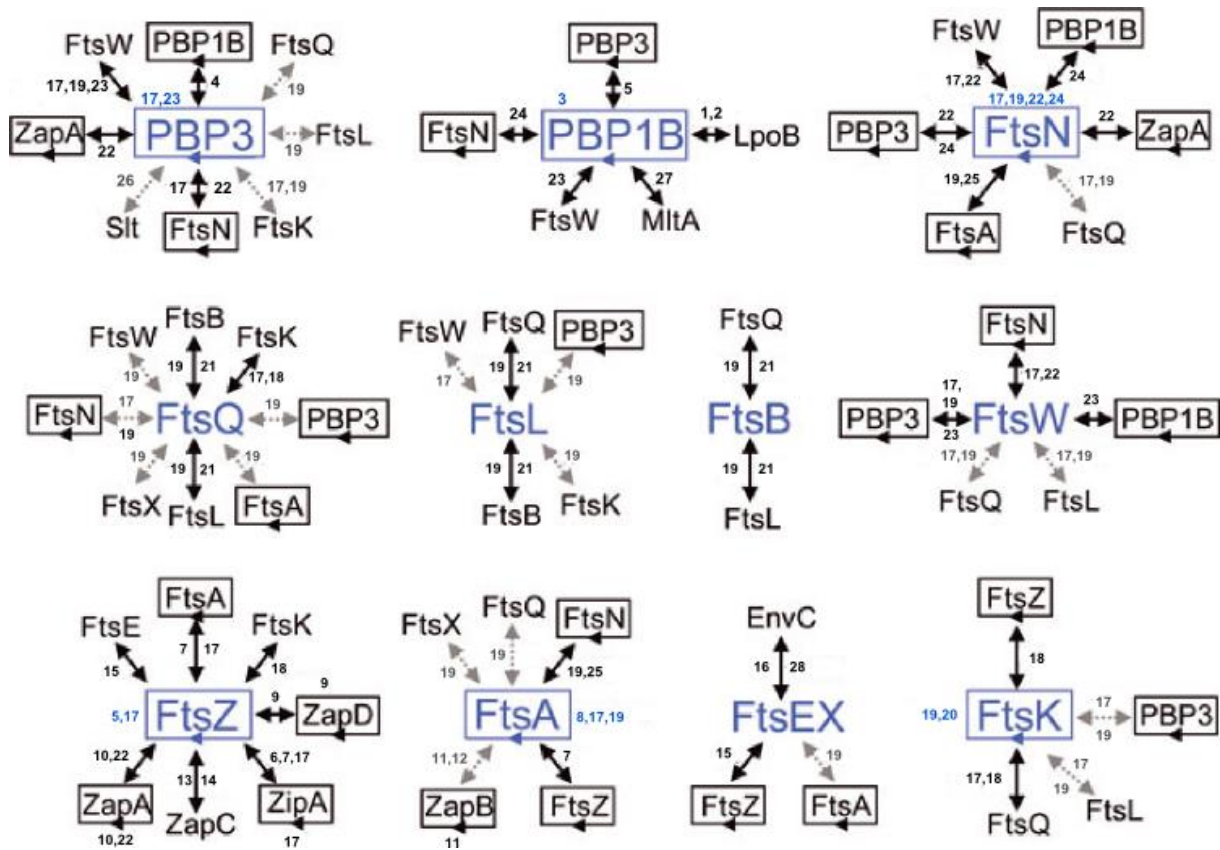


Figure 22. Protein-protein interactions of *E.coli* divisome proteins (Egan & Vollmer, 2013). Solid black lines represent direct interactions identified *in vitro* and in the cell; dashed gray lines represent interactions shown solely by bacterial two-hybrid assays. Rectangular arrows enclosing proteins indicate homodimerization or multimerization. Numbers refer to the following references: 1 (Paradis-Bleau *et al.*, 2010), 2 (Typas *et al.*, 2010), 3 (Bertsche *et al.*, 2005), 4 (Bertsche *et al.*, 2006), 5 (Bi & Lutkenhaus, 1991), 6 (Haney *et al.*, 2001), 7 (Pichoff & Lutkenhaus, 2005), 8 (Szwedziak *et al.*, 2012), 9 (Durand-Heredia *et al.*, 2012), 10 (Low *et al.*, 2004), 11 (Ebersbach *et al.*, 2008), 12 (Galli & Gerdes, 2010), 13 (Durand-Heredia *et al.*, 2011), 14 (Hale *et al.*, 2011), 15 (Corbin *et al.*, 2007), 16 (Uehara *et al.*, 2010), 17 (Di Lallo *et al.*, 2003), 18 (Grenga *et al.*, 2008), 19 (Karimova *et al.*, 2005), 20 (Aussel *et al.*, 2002), 21 (Buddelmeijer & Beckwith, 2004), 22 (Alexeeva *et al.*, 2010), 23 (Fraipont *et al.*, 2011), 24 (Müller *et al.*, 2007), 25 (Busiek *et al.*, 2012), 26 (Romeis & Holtje, 1994), 27 (Vollmer *et al.*, 1999) and 28 (Yang *et al.*, 2011).

Objectives

This thesis work aims to investigate the structural features of three components of the E. coli division machinery: the lipid II flippase FtsW, the N-acetylmuramyl L-alanine amidase AmiC and the LytM factor NlpD. These proteins are recruited at midcell at a late stage of cell division.

FtsW is an integral membrane protein crucial for the translocation of the peptidoglycan precursor from the cytoplasm to the periplasm where it will be processed to produce septal peptidoglycan.

AmiC acts as a septal peptidoglycan hydrolase that allow the separation of the daughter cells. This enzyme has been shown to be activated by the LytM factor NlpD.

The molecular mechanisms involved in the aforementioned activities and activation are poorly understood. After the cloning, production and purification of these proteins, a functional and structural study will allow to gain insight in their respective role in the complex division machinery.

For FtsW, efforts were focused on the cloning of different *ftsW* genes to screen production and purification conditions and obtain a protein suitable for structural studies.

For AmiC and NlpD, activity and interaction tests along with a structural characterization were investigated to better understand the molecular basis of septal peptidoglycan hydrolysis and regulation.

Material and methods

3. Molecular Biology

3.1. Cloning of *amiC*, *nlpD* and variants

Escherichia coli K12 genomic DNA was used for PCR amplification of *amiC*, *nlpD* genes and variants with the following primers: 5'-GCGCATATGGGGCGCGATCGTCCGATTG-3'; 5'-CGCTCGAGTCATCCCCTTCTCGCCAGC-3' for *amiC* and 5'-GCGCATATGTCTGACACTTCAAATCCACCGGCACC-3'; 5'-CGCTCGAGTTATCGCTGCGGCAAATAACGCAG-3' for *nlpD*. For AmiC, the amplified gene codes for a protein without its signal peptide (Gln35-Gly417). NlpD is also produced without its signal peptide (Ser27-Arg380). The gene coding for the AMIN domain (Gln35-Ala145) was amplified with the following primers: 5'-GCGCATATGCAGGTCGTGGCGGTGCGC-3'; 5'-CGCTCGAGTTAGGCCGGATAGAGGTCCATCACC-3'. For the LytM domain of NlpD, the following primers were used: 5'-GCGCATATGGGGGGCAACAAGGGGATTGATATCG-3'; 5'-CGCTCGAGTTATCGCTGCGGCAAATAACGC-3'. PCR products have been cloned into pET28-MHL vector (SGC consortium) between NdeI and XhoI sites allowing the expression of the proteins with a 6xHis Tag followed by a TEV cleavage site at the N-terminal position. The gene coding for AmiC lacking residues Ala287 to Ile329 (called AmiC Δ H5) was synthesized *de novo* (Geneart GmbH, Regensburg, Germany) and cloned into pET28-MHL between NdeI and XhoI. After cleavage of the 6xHis Tag with the TEV protease, all the proteins produced with the pET28-MHL contain three additional N-terminal amino acids (Gly-His-Met).

The sequence coding for AmiC and its signal peptide was PCR amplified with the following primers : 5'-GCACATATGTCAGGATCCAACACTGC-3' and 5'-CGCTCGAGTCATCCCCTTCTCGCCAGC-3'. The PCR product has been cloned into pET-22b between NdeI and XhoI sites. To obtain the construct coding for AmiC Δ H5 with its signal peptide, a BsrGI/XhoI restriction on the pET28MHL-AmiC Δ H5 allowed to isolate the catalytic site devoid of the sequence coding for the inhibitory helix. This DNA fragment was transferred in the pET22b-AmiC to obtain the pET22b-AmiC Δ H5.

3.2. Cloning of *ftsW* from different bacteria

S. aureus and *Aquifex aeolicus ftsW* genes were amplified from the genomic DNA of these microorganisms and the *E. coli ftsw* gene was obtained from pDML2400 (Pastoret *et al.*, 2004) with the following primers:

Bacterial strain	5' primer (including NdeI restriction site)	3' primer (including XhoI restriction site)
<i>E. coli</i>	GCGCATATGCGTTTATCTCTCCCTCG	CGCTCGAGTCATCGTGAACCTCGTACAAACG
<i>S. aureus</i>	GCGCATATGATGAATTATTCATCTCG	CGCTCGAGTTAATTACTTTTTGGATGG
<i>A. aeolicus</i>	GCGCATATGAAATTTGCGGAGAAAATATAC	GCCTCGAGTCATAAGTTTAATACATCGC

These genes were subsequently cloned into the pET28-MHL vector between NdeI and XhoI restriction sites. The gene coding for *ftsW* from *Geobacillus thermodenitrificans* was synthesized *de novo* with the aforementioned restriction sites (Geneart GmbH, Regensburg, Germany) and cloned into the pET28-MHL vector.

Constructions in the pBAD52b vector required 5' NcoI and 3' HindIII cloning sites. pET28-MHL-based constructs were used as template to amplify *ftsW* genes with sequences coding for the N-terminal His-tag followed by the TEV cleavage site. The following primers were used.

Bacterial strain	5' primer (including NcoI restriction site)	3' primer (including HindIII restriction site)
<i>E. coli</i>	GCCCATGGGCCATCATCATC ATCATCACAGCAGCGGC	CCGAAGCTTTCATCGTGAACCTCGTACAAACG
<i>S. aureus</i>		CCGAAGCTTTTAATTACTTTTTGGATGG
<i>G. thermodenitrificans</i>		GGCAAGCTTTTATTAATAAAGGTCAGACCACGTTTC

Cloning sites of the pNZ8148 for production in *L. lactis* are compatible with the pBAD52b (NcoI-HindIII). Transfer of the *E. coli ftsW* gene from the pBAD52b to the pNZ8148 was successful while cloning attempts failed for *ftsW* from *S. aureus* and *G. thermodenitrificans* (see results).

4. Productions and Purifications

4.1. Overexpression and purification of AmiC, NlpD and variants

Transformed *E. coli* C43 (DE3) cells were grown in TB medium supplemented with kanamycin ($50 \mu\text{g}\cdot\text{ml}^{-1}$) until the OD_{600} reached 0.8. The culture was then induced with 0.5 mM IPTG for 3 h at 28°C . The cells were harvested by centrifugation (4000 g , 20 min, 4°C) and the pellet was resuspended in the lysis buffer (30 mM Tris-HCl pH 7.5, 300 mM NaCl, 10% Glycerol, 2 mM MgSO_4 , $1.5 \text{ U}\cdot\text{ml}^{-1}$ benzonase) before disruption using an Emulsiflex C3 homogenizer. The lysate was spun down at $40\,000 \text{ g}$ for 30 min and the supernatant was filtered through a $0.22 \mu\text{m}$ membrane (Millex-GP, Millipore) before purification.

The sample was loaded onto a HisTrap column (GE Healthcare) equilibrated with buffer A (30 mM Tris-HCl pH 7.5, 300 mM NaCl, 10% Glycerol). The column was washed with Buffer A containing 50 mM Imidazole and the proteins were eluted with increasing concentration of imidazole in buffer A: between 50 and 100 mM for NlpD, 300 mM for the LytM domain of NlpD and between 150 and 200 mM for AmiC and the AMIN domain. AmiC Δ H5 was isolated by batch purification with Ni-NTA agarose gel (GE Healthcare) and eluted at 250–300 mM imidazole in buffer A. After SDS-PAGE analysis pure fractions were pooled and dialysed overnight against buffer A, frozen with liquid nitrogen and stored at -80°C at approximately $30 \mu\text{M}$. For interaction and activity tests, His-tags were removed by an overnight incubation at 4°C with the TEV-protease. The cleaved tags, the uncleaved protein and the His-tagged TEV-protease were removed by a second passage on a HisTrap column (GE Healthcare).

4.2. Overexpression and purification of selenomethionyl-AmiC

- Principle

The incorporation of selenomethionine in AmiC was achieved with the methionine biosynthesis pathway inhibition technique (Doublet, 2007). It has been shown that high concentrations of isoleucine, lysine and threonine block methionine biosynthesis in *E. coli* by inhibiting an

aspartokinase, which is the first enzyme involved in this pathway. In addition, leucine and phenylalanine act in synergy with lysine. The main advantage of this technique is that it does not require an auxotrophic strain for methionine and potentially allow methionine incorporation in any *E. coli* production strain.

- Experimental procedure

Glycerol stock of C43 (DE3) for the production of 6H-AmiC was used for an overnight pre-culture of 25 ml in M9 medium (supplemented with 50 µg.ml kanamycin). 1l of fresh M9 medium was then inoculated at 1% and grown to an OD of about 0.8 and amino acids were added as powder at the following concentrations: lysine, phenylalanine and threonine at 100 mg.l⁻¹, isoleucine, leucine and valine at 50 mg.l⁻¹. After 15 minutes of shaking, expression was induced with 0.5 µM IPTG for 4 hours at 28°C.

The subsequent purification step was realized as described for 6H-AmiC except the presence of 1 mM DTT in every buffer to avoid the oxidation of selenomethionines.

4.3. Expression tests of FtsW constructs in *E. coli* C43 (DE3) and membrane preparation

Transformed C43 (DE3) cells were grown in TB medium supplemented with kanamycin (50 µg.ml⁻¹) until the OD₆₀₀ reached 0.8. Cultures were then induced with 1 mM IPTG for 15 h at 18 or 28°C. The cells were harvested by centrifugation (4000 g, 20 min, 4°C) and the pellets were resuspended in the lysis buffer (30 mM Tris-HCl pH 7.5, 300 mM NaCl, 10% Glycerol, 2 mM MgSO₄, 1.5 U.ml⁻¹ benzonase) before disruption using an Emulsiflex C3 homogenizer.

The lysate was first spun down at 10000 g to pellet unlysed cells and the supernatant was centrifuged at 200000 g for 45 min to pellet the membranes. Membranes were kept at -20°C until purification.

4.4. Membrane solubilization and purification of *E. coli* FtsW

Membranes were solubilized at 4°C for 1 hour under moderate stirring in Tris-HCl 30 mM pH7.5, NaCl 100 mM, DDM 1%. Then, the sample was centrifuged at 200000 g to pellet the unsolubilized membranes and the supernatant was filtered through a 0.22 µm membrane (Millex-GP, Millipore) before purification. The sample was loaded onto a HisTrap column (GE Healthcare) equilibrated with buffer A (30 mM Tris-HCl pH 7.5, 100 mM NaCl). The column was washed with Buffer A containing 50 mM Imidazole and the protein was eluted with increasing concentration of imidazole up to 500 mM.

4.5. Expression tests of *E.coli* FtsW in *L. lactis* NZ9000

L. lactis NZ9000 cells were transformed with the pNZ8148-FtsW(*E. coli*) vector by electroporation using a gene pulser (Bio-Rad Laboratories, Richmond, Calif.) with the following parameters: field strength of 2.0 kV/2 mm, 25 µF capacitance, and 200 Ω resistance. Cells were grown in M17 medium (5g Neopeptone, 5g Bactosoytone, 5g Beef extract, 2.5g Yeast extract, 0.5g Ascorbic acid, 1g 2-Glycerolphosphate for one liter) supplemented with 0.5% (w/v) glucose and 5 µg/mL chloramphenicol. Cell were induced at an optical density of 0.4 with 1, 5 and 10 ng.ml⁻¹ of nisin for 4 hours. Cell extracts were analysed for each induction condition by SDS-PAGE 12%.

5. Structural study of AmiC

5.1. Crystallization and data collection

His-tagged AmiC was concentrated to 13 mg.ml⁻¹ and crystallized using the hanging-drop vapour diffusion method. 1 µl of protein was mixed with 1 µl of precipitant buffer (20% PEG 8000, 0.1 M CABS pH 12, 20 mM CoCl₂) and crystals grew at room temperature. The crystals

were transferred into a cryoprotectant solution containing 50% glycerol before flash-freezing in a liquid nitrogen bath. Diffraction data were collected at the European Synchrotron Radiation Source Facility FIP-BM30a beamline (Grenoble).

5.2. Data processing

Data were integrated with Mosflm (Leslie & Powell, 2007) and scaled with Scala from the CCP4 software package (1994). A first model of the catalytic domain of AmiC was determined by molecular replacement using the structure of AmiB from *B. henselae* as a search model (PDB ID: 3ne8). Five poly-alanine β -strands of the N-terminal AMIN domain were built in the electron density and subjected to a DALI search. The most structurally related structure, the chaperone Hsp26, was used as a template to build seven poly-alanine β -strands of the AMIN domain. This partial model was provided to the software ARP/wARP (Morris *et al.*, 2003) to build and assign the whole domain. Helix α 2 was solved by fitting the Leu140-Leu144 (LLALL) segment in the electron density and, although the density was less clear for the residues, the helix could be completed from Pro139 to Asn148.

5.3. Structure analysis

The ConSurf server was used to analyze the amino acid conservation on the surface of AmiC (<http://consurf.tau.ac.il/>) (Ashkenazy *et al.*, 2010) The homologous sequences were selected using three iterations of CSI-Blast within the UNIREF-90 database and the 150 most representative sequences were used to generate conservation scores (Table S1 of the Annexe 2). The PISA server provided an analysis of the interface between N and C-terminal domains (http://www.ebi.ac.uk/msd-srv/prot_int/pistart.html) (Krissinel & Henrick, 2007). The different figures were generated with Chimera (Pettersen *et al.*, 2004).

PISA (Protein Interfaces, Surfaces and Assemblies) is a software for the analysis of macromolecular interactions based on crystallographic data. The program was used for the analysis of the interaction surface between the AMIN domain and the catalytic domain of AmiC. The significance of the assembly formation is indicated by the CSS factor

(Complexation Significance Score). This score ranges from 0 to 1 with increasing values reflecting a corresponding increase in complexation relevance and is defined as a maximal fraction of the total free energy of binding that belongs to the interface in stable assemblies.

6. Activity tests

6.1. Preparation of peptidoglycan sacculi

Peptidoglycan sacculi were prepared from MC1061 cells as described earlier (Glauner *et al.*, 1988) with few modifications. Cells grown in 6 liters of LB were harvested at an optical density of 0.7 by centrifugation at 4000 g for 20 minutes at 4°C. Pellet was resuspended in 60 ml of cold PBS and added to a flask containing 60 ml of boiling 8% ultra-pure SDS (MPbiomed, CA) with vigorous stirring. The lysate was boiled for 30 min and incubated overnight at room temperature. The next morning, the sample was centrifuged at 160000g (Beckman L2-65B ultracentrifuge, rotor 60Ti) for 30 minutes and the pellet was washed several times with MilliQ water until the Hayashi test remained negative (see below). Then the pellet was resuspended in 900µl of Tris/HCl 10mM pH7.0, NaCl 10mM, 100µl 3.2M Imidazole supplemented with 1µl of 200mg.ml⁻¹ α-amylase and incubated for 2H at 37°C. 20µl of 10mg.ml⁻¹ pronase were added and the sample was incubated 1H at 60°C. 1ml of 4% pure SDS was added and the sample was boiled for 15 min. The sacculi were washed free of SDS as described above and resuspended in water 0.02% sodium azide.

6.2. SDS detection method (Hayashi)

The presence of SDS was assayed by the method developed by Hayashi (Hayashi, 1975). This test detects the formation of complex of SDS with methylene blue, insoluble in water. A sample of 335 µl was mixed with 170 µl of 0.7 M sodium phosphate, 7 µl of 0.5% methylene blue and 1 ml chloroform. After vigorous mixing, two phases are observed. The sample is considered

SDS-free when the bottom phase of chloroform shows a pink color. In the presence of SDS, the organic phase shows a blue color.

6.3. Labelling of peptidoglycan with Remazol Brilliant Blue

The RBB-labelled peptidoglycan was prepared as described (Uehara et al., 2009). The sacculi were incubated overnight with 20 mM RBB (Sigma) in 0.25 M NaOH at 37°C. The next morning, the sample was neutralized by addition of HCl before centrifugation (16 000 *g*, 20 min, room temperature). The pelleted sacculi were then washed with MilliQ water until no more soluble RBB was detected after centrifugation. The labelled sacculi were finally resuspended in water with 0.02% sodium azide and stored at 4°C.

6.4. Activity tests with RBB-labelled peptidoglycan

For activity tests, 10 µl of the RBB-PG were incubated with 4 µM of AmiC and/or NlpD (without His tag) in 30 mM Tris-HCl buffer pH 7.5, 300 mM NaCl and 10% glycerol (100 µl total) for 30 min to 15 h (overnight) in a total volume of 100 µl. The samples were centrifuged for 10 min at 14 000 *g* and the absorbance of the supernatant was measured at 595 nm (Tecan Infinite 200 PRO microplate reader, Tecan Austria GmbH, Austria). Reported results were standardized with a negative control consisting of 10 µl of RBB-PG and 90 µl of the aforementioned buffer. Lysozyme was used as a positive control at a 4 µM concentration. The peptide corresponding to the $\alpha 5$ helix (Thr288-Gly306) was synthesized by Genscript (NJ, USA).

6.5. Peptidoglycan-binding assay

The pull down experiments were carried out with the untagged AMIN domain. 10 µg of protein was incubated 2 h either with or without peptidoglycan in the binding buffer (30 mM Tris-HCl pH 6.8, 50 mM NaCl, 10 mM MgCl₂) in a total volume of 100 µl. The samples were centrifuged

for 20 min at 14 000 *g*. The pellets were washed twice in 150 μ l of binding buffer and then resuspended in 40 μ l of SDS 2% and incubated for 1 h. The supernatants of the binding step, the washing steps and the resuspended pellet were analysed by SDS-PAGE 15%.

7. Interaction study

- Microscale thermophoresis

Interactions between freshly prepared AmiC and NlpD (without 6x His Tags) were measured using microscale thermophoresis (Jerabek-Willemsen *et al.*, 2011) with a Monolith NT.115 (NanoTemper Technologies GmbH, Munich, Germany). Each protein was in turn labelled with DyLight 650 (Thermo Scientific) and mixed with sixteen twofold serial dilutions of the other unlabelled protein starting from 272 μ M for AmiC and 426 μ M for NlpD. The final buffer contained 50 mM Tris-HCl pH 7.5, 150 mM NaCl, 10 mM MgCl₂, 0.05 % Tween-20 and measurement were performed in hydrophilic capillaries with 100% Led power and 80% IR-laser power. NanoTemper Analysis 1.2.101 software was used for the fitting of the data and the determination of the apparent K_d values. The experiments were performed three times for each combination.

Results

8. Cloning, Production and Purification

8.1. Cloning, production and purification of FtsW

The integral membrane protein FtsW is responsible for the translocation of the lipid II precursor of peptidoglycan from the cytoplasm to the periplasm. This protein contains ten trans-membrane segments connected by loops. Therefore, production in hosts suitable for over-production of membrane proteins is required as well as the use of detergents to extract the recombinant protein from the cytoplasmic membrane and obtain sufficient amounts for structural studies.

8.1.1. *ftsW* cloning in production vectors

The different genetic constructs including *ftsW* genes of the Gram negative *E. coli*, the Gram positive *S. aureus* and two thermophilic species: *G. thermodenitrificans* (Gram positive) and *A. aeolicus* (Gram negative) are listed in Table 1.

<i>ftsW</i> source	Production Vector	Production host	Fusion protein
<i>E. coli</i> K12	pET28-MHL	<i>E. coli</i>	N-terminal His-tag followed by a TEV cleavage site
	pBAD-52b		
	pNZ8148	<i>Lactococcus lactis</i>	
<i>G. thermodenitrificans</i>	pET28-MHL	<i>E. coli</i>	
	pBAD-52b		
<i>S. aureus</i>	pET28-MHL	<i>E. coli</i>	
	pBAD-52b		
<i>A. aeolicus</i>	pET28-MHL	<i>E. coli</i>	

Table 1. Genetic constructs for the overproduction of FtsWs from *E. coli* K12, *G. thermodenitrificans*, *S. aureus* and *A. aeolicus*

Cloning of the genes coding for FtsW from *G. thermodenitrificans* and *S. aureus* in pNZ8148 could not be realized due to the absence of growth in liquid medium for the transformants in cloning (MACH1) cells. One possibility could be an expression leakage of the FtsW protein that would be toxic for the cell. This is supported by the observation under the microscope of a filamentous phenotype and lysed cells of the transformants grown on agar plates (data not shown).

8.1.2. Production and purification tests

8.1.2.1. Production and purification of *E. coli* FtsW

- Production test in *E. coli* C43 (DE3) cells

Expression of FtsW was assessed in C43 (DE3) after 15 hours of induction with IPTG (1mM) at 18°C and 28°C with the pET28-MHL production vector (Figure 23). The band corresponding to the full length protein migrates at a molecular weight of 37 kDa whereas the expected mass is 48.3 kDa. Altered migration is common for membrane proteins and can be explained by an excess of detergent binding (Rath *et al.*, 2009).

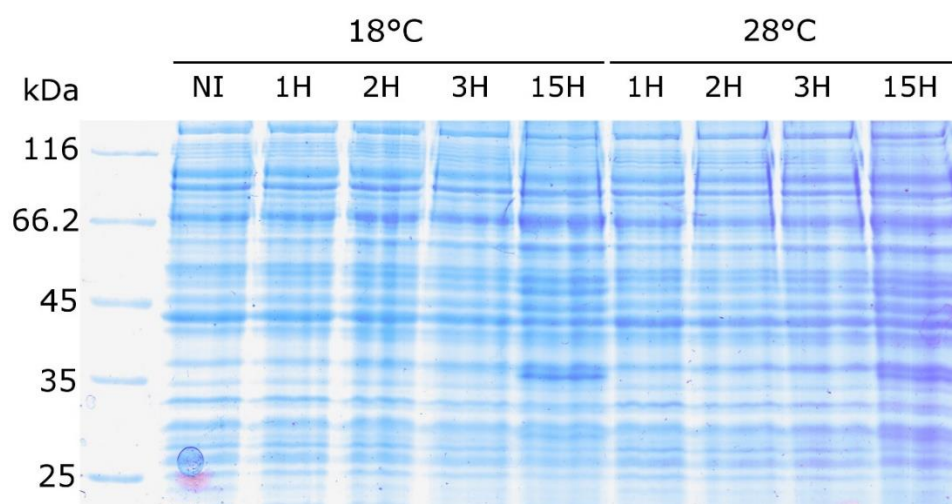


Figure 23. Production test of FtsW from *E. coli*. SDS PAGE analysis of crude extracts from induced and non-induced *E. coli* cultures at different time periods. (NI) Non induced culture; (1-15H) Hours after induction with 1mM IPTG

- Production and purification of *E. coli* FtsW

Based on the previous production tests, the pET28-MHL vector coding for the *E. coli* FtsW was selected for expression in C43 (DE3) cells in 3L TB medium at 28°C. After 15 hours of induction (1 mM IPTG), cells were harvested and the membrane fraction prepared (see material and methods). The membranes were solubilized in a buffer containing 1% DDM and the soluble fraction, after ultra-centrifugation, was loaded on a Ni²⁺-NTA column. The majority of the recombinant protein is eluted at 300 mM imidazole (Figure 24A). The fractions were pooled and the purity of FtsW was estimated at around 50%. A slight band migrating at a molecular weight of 27 kDa was shown to be a degradation product of FtsW by mass spectrometry (data not shown).

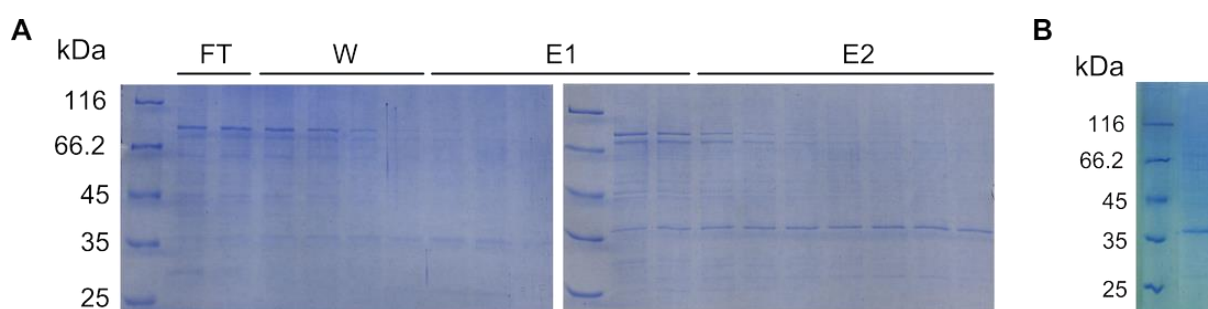


Figure 24. SDS-PAGE analysis of the elution profile of FtsW (*E. coli*) for the Ni²⁺ affinity chromatography step. A. Flow-through (FT), wash step (W) and elutions at 100 (E1) and 300 mM (E2) imidazole. B. Pool of the best fractions concentrated 4 times on a 50 kDa cut-off filter unit.

A final yield of 150 μ g.L⁻¹ of His-tagged FtsW from *E. coli* was obtained with the pET28-MHL. Consequently, a cell culture in a 15-liter fermenter was undertaken in the same conditions but the analysis of the crude extracts showed a majority of 27 kDa degradation product mentioned above. Due to lack of time, the production in flask of a sufficient amount of recombinant FtsW protein for structural studies could not be achieved.

- Production of *E. coli* FtsW in *L. lactis* NZ9000

The production of the *E. coli* FtsW in *L. lactis* NZ9000 with the pNZ8148 production vector was tested at 30°C in M17 medium with different nisin inducer concentrations (1, 5 and 10 ng.ml⁻¹) added at an optical density (600nm) of 0.9. Growth curves show an alteration of the biomass production upon induction by nisin but no production of FtsW was detected in crude extracts by SDS-PAGE analysis. This could be due to a low production amount of recombinant protein and/or toxicity of FtsW from *E.coli* against *L.lactis* cells. Consequently, the *L. lactis* production host was found unsuitable for the overproduction of FtsW of *E. coli*.

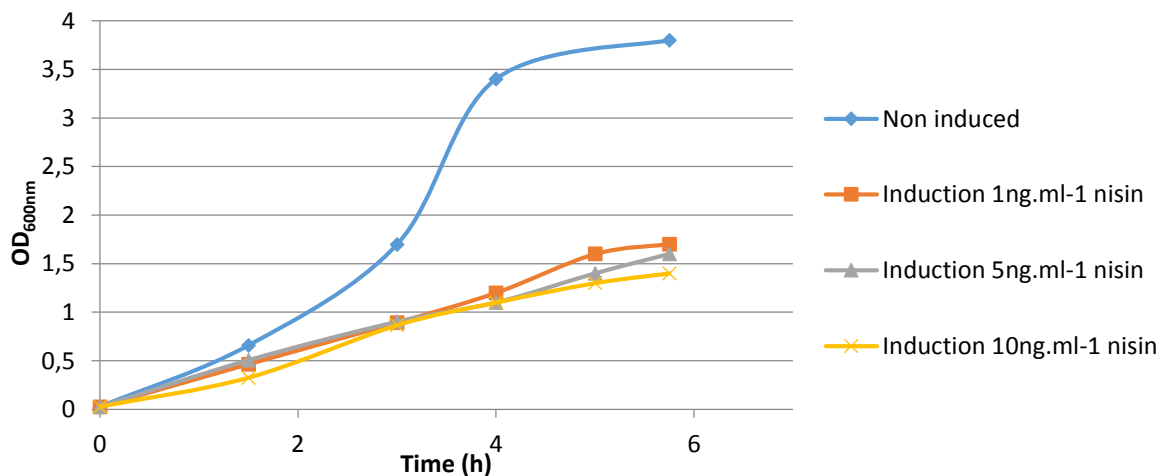


Figure 25. Growth curves of the *L. lactis* producing *E. coli* FtsW.

8.1.2.2. *G. thermodenitrificans*, *A. aeolicus* and *S. aureus* FtsWs

Overproduction was tested for *G. thermodenitrificans*, *A. aeolicus* and *S. aureus* FtsWs in *E.coli* C43 (DE3) cells with pET-28-MHL vectors, based on the successful conditions obtained for FtsW from *E. coli*. SDS-PAGE analysis did not reveal overproduction in crude extracts for cultures at 18 and 28°C induced with 1 mM IPTG at an optical density (600 nm) of 0.8. Nevertheless, Ni²⁺ affinity purification tests of the solubilized membranes were realized for *G. thermodenitrificans* and *S. aureus* FtsWs production and recombinant proteins were detected but in low amounts and with a high proportion of degradation products (data not shown).

Consequently, productions based on pET28-MHL were not further investigated for FtsWs of *G. thermodenitrificans* and *S. aureus*.

Genes coding for His-tagged FtsW of *G. thermodenitrificans* and *S. aureus* from the pET28-MHL constructs were transferred into a pBAD vector (pBAD52b) known to limit expression leakage before induction. Cultures were grown in rich medium (TB) and induced with 0.2% arabinose. Unfortunately, no production was detected in crude extracts for both constructs. One explanation for this lack of detectable heterologous expression could be an improper insertion of recombinant proteins in the membrane leading to their proteolysis.

Due to cloning problems, FtsWs from *G. thermodenitrificans*, and *S. aureus* could not be tested for overproduction in *L. lactis*.

8.2. *E.coli* AmiC & NlpD

The AmiC-NlpD couple is involved in the septal hydrolysis of the peptidoglycan leading to the separation of the daughter cells. AmiC exhibits a N-acetylmuramyl-L-alanine amidase activity and is responsible for the cleavage of peptidoglycan. The LytM factor NlpD was shown to specifically activate AmiC. The following section covers the results obtained for both proteins.

8.2.1. Cloning of *amiC* and *nlpD*

The AmiC protein is composed of two domains: the AMIN domain (30-145) responsible for the septal localization of AmiC and the catalytic domain (175-417) involved in the N-acetylmuramyl-L-alanine amidase activity (Bernhardt & de Boer, 2003, Heidrich et al., 2001). AmiC is exported to the periplasm via the Twin arginine pathway (Bernhardt & de Boer, 2003). Two genetic constructs were designed in the pET22b to produce the full length protein with the exporting signal peptide with or without the inhibiting helix $\alpha 5$. Four other constructs using the pET28-MHL allow the cytoplasmic production of His-tagged AmiC variants without signal peptide: AmiC with or without the inhibiting helix $\alpha 5$, the catalytic domain alone and the AMIN domain alone (Table 2). The His-tag is followed by a TEV cleavage site to facilitate the purification of the protein and allow the subsequent cleavage of the His-tag, leaving three N-terminal non-native amino acids (Gly-His-Met).

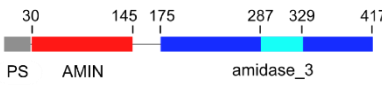
AmiC variant	Name	Molecular Mass (kDa)	Production vector
	AmiC-FL	45.6	pET22b
	AmiC-FL- Δ H5	41	pET22b
	6H-AmiC	44.6	pET28-MHL
	6H-AmiC Δ H5	40	pET28-MHL
	6H-AmiCcat	28.1	pET28-MHL
	6H-AMIN	15	pET28-MHL

Table 2. AmiC variants. Four amino-acid domains are highlighted: signal peptide (grey), AMIN domain (red), amidase₃ domain (blue) and the inhibitory helix (light blue). FL: full length, Δ H5: deletion of the Ala287-Ile329 fragment, cat: catalytic domain, SP: signal peptide, 6xHis-TEV and 6H: 6xHis-tag followed by a TEV cleavage site.

NlpD is a lipoprotein anchored to the outer membrane of *E. coli* (Ichikawa et al., 1994). This protein contains a N-terminal peptidoglycan-binding LysM domain (Pfam ID: PF01476), a C-terminal LytM domain belonging to the peptidase_M23 family (PF01551) and a linker of about 100 amino acids before each domain. Two constructs were designed in the pET28-MHL to over-produce a soluble form of NlpD without its signal peptide (1-27) and the LytM domain alone in the cytoplasm (Table 3).

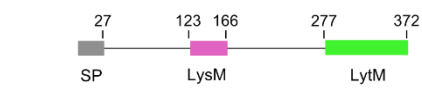
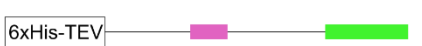
NlpD variant	Name	Molecular Mass (kDa)	Production vector
	NlpD-FL	40.1	-
	6H-NlpD	39.9	pET28-MHL
	6H-LytM	13.6	pET28-MHL

Table 3. NlpD variants. Three amino-acid sequences are highlighted: signal peptide (grey), LysM domain (violet), LytM domain (green). SP: signal peptide, FL: full length, 6xHis-TEV and 6H: 6xHis-tag followed by a TEV cleavage site.

8.2.2. Production & Purification of AmiC and NlpD

- Production and purification of AmiC

Overproductions in C43 (DE3) cells of 6H-AmiC, 6H-AmiCΔH5, 6H-AmiC-cat and 6H-AMIN were achieved using the pET28-MHL-based constructs and a 0.5 mM IPTG induction at 28°C (at a $OD_{600nm} = 0.8$). Each protein was purified on Ni^{2+} -NTA affinity column and eluted in the same conditions as AmiC (Figure 26).

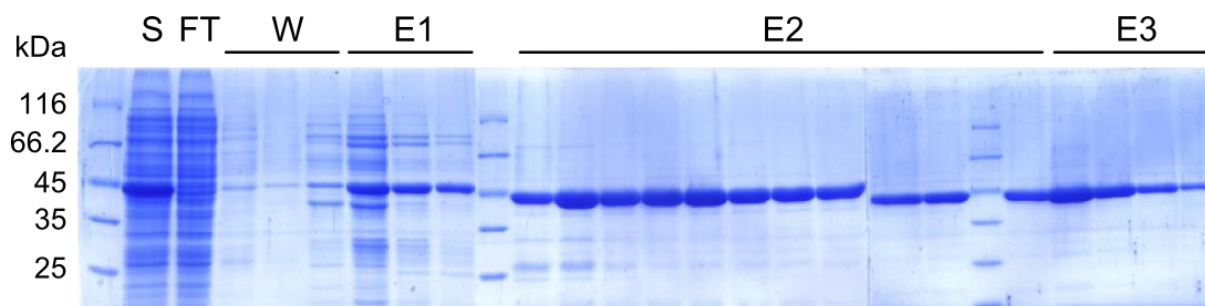


Figure 26. Coomassie blue stained SDS-PAGE of 6H-AmiC fractions after the Ni^{2+} affinity chromatography step. Sample before purification (S), flow through (FT) wash step at 50 mM imidazole (W), elution at 150 (E1), 250 (E2) and 350 mM (E3) mM imidazole.

For 6H-AmiC Δ H5, on-column purification showed poor binding of the target protein. Better results were obtained by batch purification with a Ni²⁺-NTA agarose gel. The best eluted fractions were pulled and purity was estimated at 75%.

In order to improve the protein purity and obtain a protein close to the natural form, a TEV protease treatment was realized for each AmiC variant in order to remove the His-tag. A 10:1 (protein:TEV protease) ratio was used overnight at 4°C to reach a complete digestion. The migration shift of the untagged protein observed on SDS-PAGE corresponds to the loss of the His-tag and the six first residues of the TEV cleavage site (2.15 kDa total) (Figure 27).

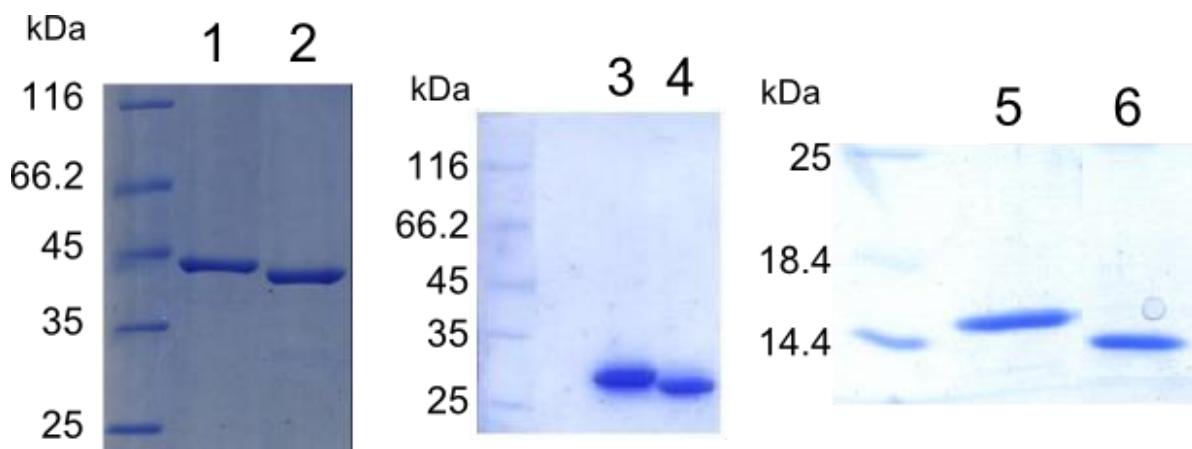


Figure 27. Coomassie blue stained SDS-PAGE analysis of the TEV protease treatment on 6H-AmiC (1-2), 6H-AmiC-cat (3-4) and 6H-AMIN (5-6) before (1, 3 and 5) and after (2, 4 and 6) an overnight digestion at 4°C at a protein:TEV protease molar ratio of 10:1.

A second step on Ni²⁺ affinity column allowed the capture of remaining contaminants from the first purification step and the His-tagged TEV protease. The untagged target protein is eluted in the flow-through fractions. Figure 28 shows an example with the AMIN domain purification. The band of 27 kDa is the His-tagged TEV protease.

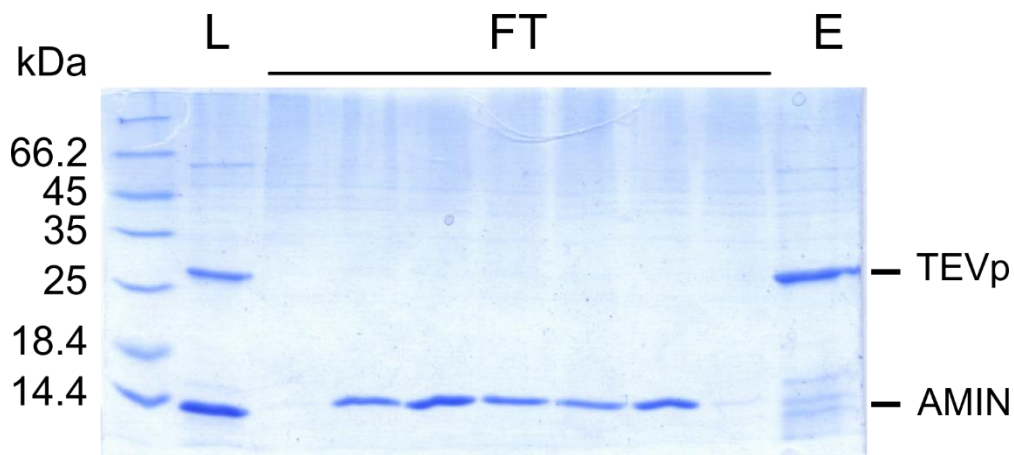


Figure 28. Coomassie blue stained SDS-PAGE analysis of the purification of the untagged AMIN domain. Load (L), Flow through (FT) and elution at 250 mM imidazole (E).

A selenomethionyl AmiC protein was produced to facilitate the structure determination by x-ray crystallography using the anomalous signal of the selenium to obtain initial phases. The protein was produced in minimal medium with selenomethionine instead of methionine (see material and methods) in the same conditions of temperature, time and induction as for the native AmiC. A single purification step on Ni²⁺ affinity column was efficient enough to reach a purity suitable for crystallization trials (95% purity) (Figure 29).

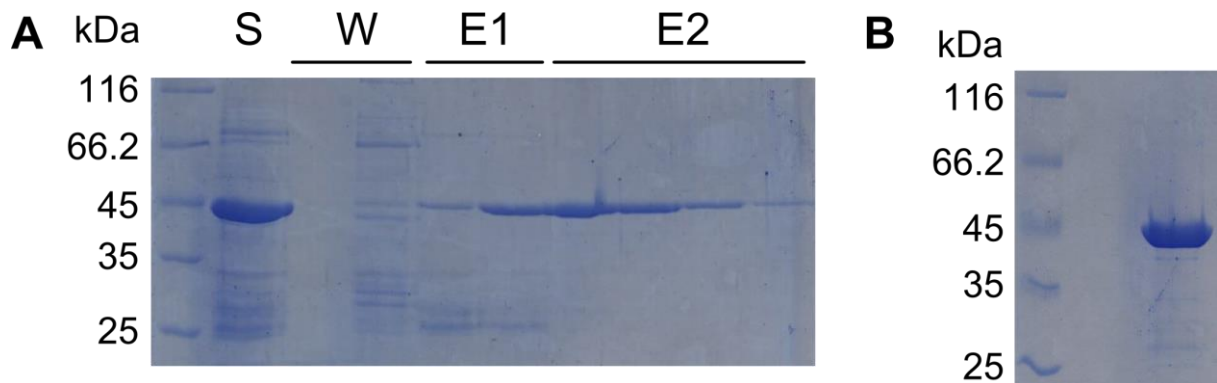


Figure 29. Coomassie blue stained SDS-PAGE analysis of the Ni²⁺ affinity chromatography of the selenomethionyl AmiC. A. Soluble extract (S), wash fractions (W), Elutions at 50mM (E1) and 250 mM (E2) imidazole. B. Pool of the purest fractions.

- NlpD

The same strategy as for 6H-AmiC was undertaken with 6H-NlpD and the 6H-LytM. Both proteins were produced in C43 (DE3) at 37°C with a 0.5 mM IPTG induction at an optical density (600nm) of 0.8. The subsequent Ni²⁺-NTA purification showed an elution of NlpD starting at an unusually low (50mM) imidazole concentration (Figure 30A). The pooled elution fractions were then treated with TEV protease (protease:protein molar ratio of 1:10) for 5 hours at room temperature to remove the N-terminal His-tag (Figure 30B). The second Ni²⁺-NTA purification step allowed to reach a high purity (>95%) for this protein.

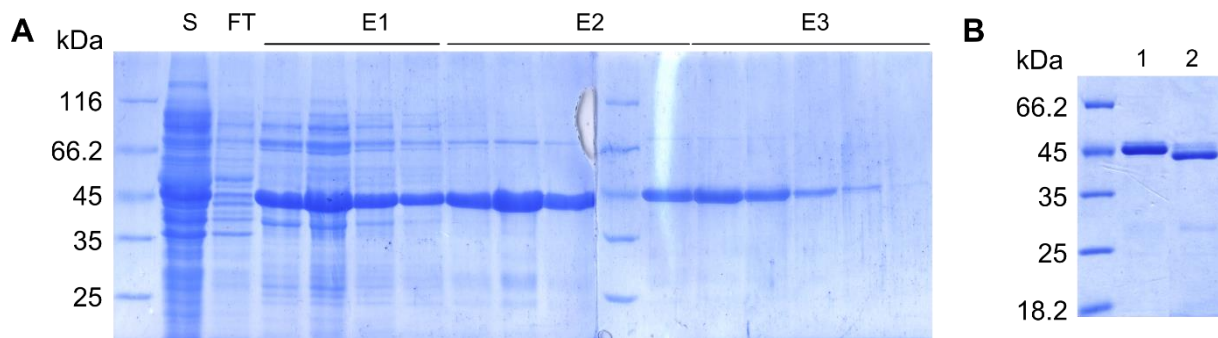


Figure 30. Coomassie blue stained SDS-PAGE analysis of the first Ni²⁺ purification of 6H-NlpD and the TEV protease treatment. A. Sample (S), flow through (FT), elutions at 50 (E1), 100 (E2) and 250 mM (E3) imidazole.

For the LytM domain of NlpD, the first Ni²⁺-NTA purification step was carried out using a gradient of imidazole between 0 to 500 mM and the elution peak was detected at around 320 mM (

Figure 31A). The TEV protease treatment and a second Ni²⁺-NTA purification step led to a pure, untagged LytM domain (Figure 31B).

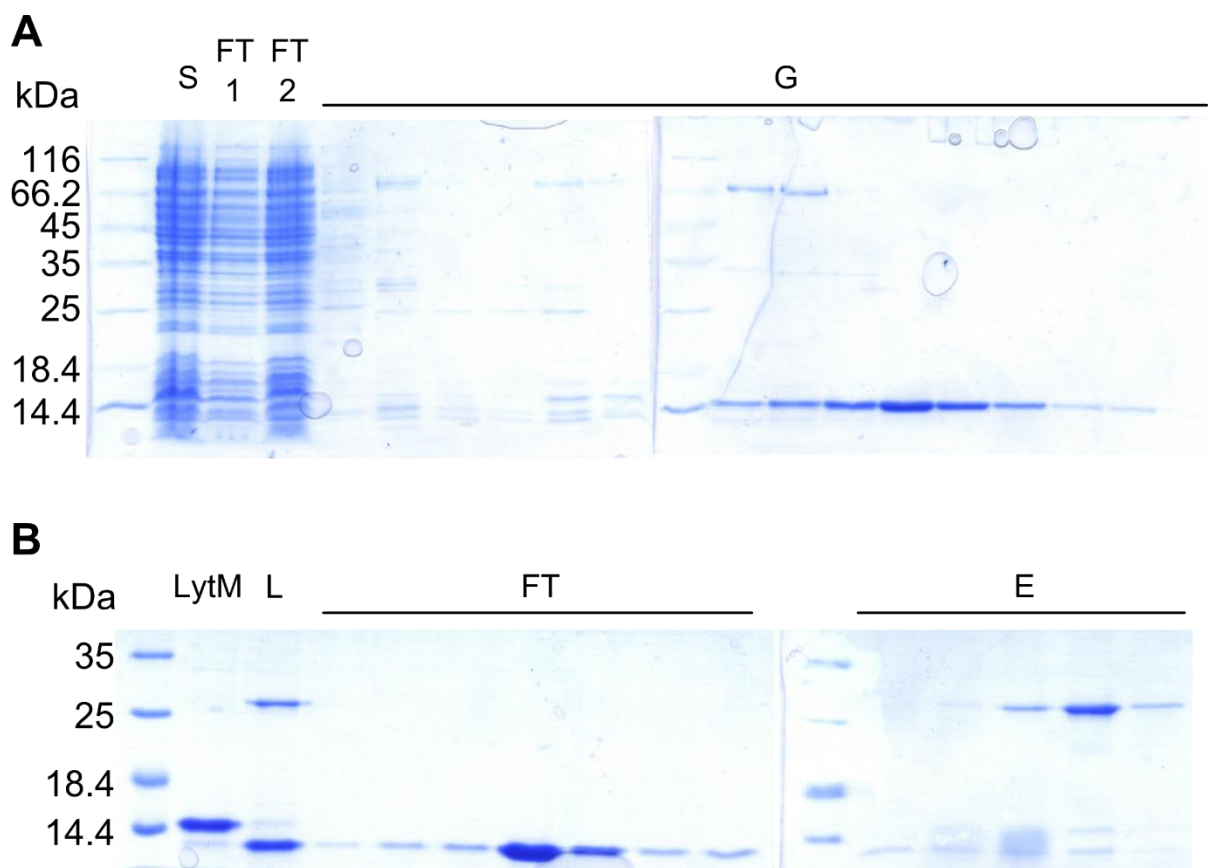


Figure 31. LytM domain purification. A. Coomassie blue stained SDS-PAGE analysis of the first Ni²⁺-NTA purification step. Soluble extract (S), flow through (FT1 & 2) and elution gradient from 0 to 500mM imidazole (G). Coomassie blue stained SDS-PAGE analysis of the second Ni²⁺-NTA purification step. His-tagged LytM (LytM), Load (L), flow through (FT), elution at 250 mM imidazole (E).

9. Crystallogenesi and data collection

9.1. Crystallogenesi

- AmiC

Both 6H-AmiC and untagged AmiC were concentrated up to 13 mg.ml⁻¹ (in 30 mM Tris-HCl pH 7.5, 300 mM NaCl and 10 % glycerol) with a 30 kDa cut-off Amicon Ultra-15. Then they were directly used for crystallization tests in 24-well plates at room temperature with commercially available kits of precipitants (see material and methods) for a total of 528 unique conditions for each protein. The hanging-drop vapor diffusion method used for these screenings gave five positive hits at room temperature for the two proteins as listed in Table 4.

Most of the crystals grew in a short period of time (24-72 hours) in the form of needles. 6H-AmiC crystallized at highly basic pHs (11-12) whereas untagged AmiC crystals grew in more acidic conditions with pH values ranging from 5 to 6.5. The presence of cobalt chloride in the precipitants for 6H-AmiC was a major drawback for reproducibility. This salt precipitated at the basic pHs used in the crystallization screen in a time-dependent manner. Screening of cobalt chloride concentrations were made to mimic the composition of the crystallizing conditions but remained unsuccessful. Glycerol was also added to the precipitant solution in order to obtain less but bigger crystals. Glycerol is known to slow down the crystal growth by modifying the hydration shell of the proteins and thus limiting the proportion of crystal contacts (Vera *et al.*, 2011). Unfortunately, no crystals were obtained for these attempts. Crystallization trials at low temperature (4°C) remained also unfruitful.

Crystals of untagged AmiC were not reproduced due to a lack of diffraction pattern when exposed to X-rays (see below).

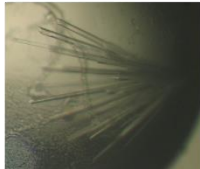
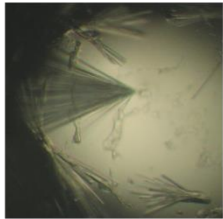
AmiC variant	Crystallization kit condition	Composition	Crystal
AmiC	Base II C4	20% PEG8K 0.1 M CAPS pH 11 20 mM CoCl ₂	
6H-AmiC	Base II D4	20% PEG8K 0.1 M CABS pH 12 20 mM CoCl ₂	
untagged AmiC	Crystal Screen I (Hampton Research) Cond. 15	30% PEG8K 0.1 M Cacodylate pH 6.5 0.2 M NaAc, 3H ₂ O	
untagged AmiC	Crystal Screen II (Hampton Research) Cond. 26	30% PEG MME 5K 0.1 M MES pH 6.5 0.2 M Ammonium sulfate	
untagged AmiC	SPE I C4	50% PEG MME 5K 0.2 M Citrate pH 5	

Table 4. Protein crystals obtained for AmiC and untagged AmiC obtained with the hanging drop vapor diffusion method in 24-well plates.

In order to circumvent a potential phase problem during the data processing, a selenomethionyl 6H-AmiC variant was produced and purified. Indeed, the catalytic domain of AmiC is a member of the structurally known amidase₃ family but the AMIN domain structure has never been described, discarding the molecular replacement technic for the latter. A single crystal was obtained with SeMet-6H-AmiC in conditions allowing the formation of 6H-AmiC crystals (20% PEG 8K, 0.1 M CABS pH12, 20 mM CoCl₂).

- Catalytic domain of AmiC

Both AmiC-cat and the untagged variant were concentrated up to 10 mg.ml⁻¹ in 30 mM Tris-HCl pH 7.5, 300 mM NaCl and 10% Glycerol and an initial screening was realized in micro-plates with a crystallization robot (Mosquito) at room temperature. One condition (45% MPD, 0.1 M BisTris-HCl pH 6.5, 0.2 M NH₄Ac) gave one crystal for the His-tagged version of the catalytic domain of AmiC. Crystallogenesis experiments were no further investigated for this variant because crystals of the full length protein allowed us to collect interpretable data (see below).

- NlpD

Two initial screenings were realized in micro-plates at room temperature with different protein concentrations and protein buffer composition. For the first one, NlpD was concentrated at 15 mg.ml⁻¹ in 30 mM Tris-HCl pH 7.5, 300 mM NaCl and 10 % glycerol. For the second screening, NlpD was used at 27 mg.ml⁻¹ in 30 mM Tris-HCl pH 7.5, 150 mM NaCl, 10 mM MgCl₂ and 0.05% Tween. The later came from the protein solution stock used for thermophoresis experiments (see 13), which explains the presence of the Tween detergent. Neither of these two initial screening gave crystallization hits. This could be explained by the presence of two large linkers exceeding a hundred residues located at the N-terminal extremity and between the LysM and LytM domains (Table 3). These long and unstructured amino acids stretches increase the overall flexibility of the protein, potentially preventing crystallogenesis events. We therefore also realized crystallization tests on the LytM domain alone.

- LytM domain of NlpD

The LytM domain was concentrated at 7.2 mg.ml⁻¹ in 30 mM Tris-HCl pH 7.5 and 100 mM NaCl. An initial screening allowed obtaining one crystal with a precipitant condition containing 0.2 M NaCl, 0.1 M Tris-HCl pH 8.5 and 25 % PEG 3350. This promising condition has not been optimized yet but the grown crystal showed a diffraction pattern characteristic of a protein crystal upon X-ray exposure (see below), excluding the possibility of salt crystals. This test was done at the Proxima 1 beamline of the Soleil synchrotron (Orsay, France).

- AmiC-NlpD complex

Both 6H-AmiC and 6H-NlpD were concentrated to 17 mg.ml^{-1} in 30 mM Tris-HCl pH 7.5, 150 mM NaCl and 10% Glycerol. The initial screening did not give crystallization hits. The aforementioned flexibility of NlpD and a potential low stability of the complex could be detrimental for crystal formation.

9.2. Diffraction and data collection

- AmiC

Crystals were tested on the FIP-BM30a beamline at the European Synchrotron Radiation Source Facility (ESRF Grenoble, France). Diffraction patterns were observed only for 6H-AmiC and not for untagged AmiC and selenomethionyl 6H-AmiC crystals.

Different cryo-protectant conditions were tested in order to limit radiation damage during X-ray exposure. The transfer of 6H-AmiC crystals in a drop containing 50% glycerol followed by flash-freezing in a liquid nitrogen bath did not alter their physical aspect or X-ray diffraction and no ice rings were observed in the collected images. The best crystal diffracted up to a 2.5 Å resolution and a dataset was collected over a 360° oscillation. The crystal belongs to the P212121 space group with unit cell axes $a = 59.03$, $b = 68.44$, $c = 90.58$ Å

- LytM domain of NlpD

Preliminary tests were positive for the LytM domain of NlpD. The crystal obtained allowed to obtain 7 Å resolution data upon X-ray exposure. This is clearly not sufficient for atomic resolution of the LytM domain but promising whether crystals are reproducible and optimized through a fine screening around the hit condition.

10. AmiC crystal structure

- *Data processing and structure determination*

The 2.5 Å resolution structure of 6H-AmiC was solved by molecular replacement for the catalytic domain and model building for the AMIN domain (Figure 32). Data were integrated with Mosflm (Leslie & Powell, 2007) and scaled with Scala from the CCP4 software package (1994). A first model of the catalytic domain of AmiC was determined by molecular replacement using the structure of AmiB from *B. henselae* as a search model (PDB ID: 3ne8). Five poly-alanine β-strands of the N-terminal AMIN domain were built in the electron density and subjected to a DALI search. The most structurally related structure, the chaperone Hsp26, was used as a template to build seven poly-alanine β-strands of the AMIN domain. This partial model was provided to the software ARP/wARP (Morris et al., 2003) to build and assign the whole domain. Helix α2 was solved by fitting the Leu140-Leu144 (LLALL) segment in the electron density and, although the density was less clear for these residues, the helix could be completed from Pro153 to Asn162.

The R_{cryst} and R_{free} values after refinement are 17.6% and 23.1% respectively. Table 5 summarizes the main statistics about data collection, refinement and model validation of the 6H-AmiC crystal structure. The final electron density map shows a clear density for the whole protein except for five disordered segments consisting of the first fifteen residues of the N-terminal purification tag, Asn146-Asp152, Lys163-Gln174, Lys310-Phe321 and the last nine residues at the C-terminus. AmiC is made of two structurally distinct domains linked by a flexible segment (Asn146-Gln160) containing the poorly defined α2 helix.

<i>Diffraction data statistics</i>	
Space group	P2 ₁ 2 ₁ 2 ₁
a, b, c (Å)	59.03, 68.44, 90.58
Resolution range (Å)	49.6 - 2.5 (2.56 - 2.5)
Unique reflections	13337 (1907)
Completeness (%)	99.9 (99.8)
Redundancy	12.7 (7.3)
R _{merge} (%) ^a	20.1 (100.5)
R _{pim} (%) ^b	5.7 (39.7)
Average I/σ	12.8 (2.2)
<i>Refinement statistics</i>	
Resolution range (Å)	90.58 - 2.5 (2.56 - 2.5)
R _{cryst} (%) ^c	17.6 (24.2)
R _{free} (%) ^d	23.1 (31.4)
RMS deviations	
Bond lengths (Å)	0.016
Bond angles (°)	1.625
Ramachandran analysis	
Favoured region (%)	95.9
Allowed region (%)	4.1
Outlier region (%)	0

Table 5. Crystallographic data and model refinement statistics.

a. $R_{\text{merge}} = \sum |I_i - I_m| / \sum I_i$, where I_i is the intensity of the measured reflection and I_m is the mean intensity of all symmetry related reflections.

b. R_{pim} denotes the precision-indicating merging R factor (Weiss and Hilgenfeld, 1997)

c. $R_{\text{work}} = \sum |F_o - F_c| / \sum |F_c|$, where F_o denotes the observed structure factor amplitude, and F_c denotes the structure factor amplitude calculated from the model.

d. R_{free} is similar to R_{work} but calculated with randomly chosen reflections that are omitted from the refinement.

The N-terminal AMIN domain (Phe30-Ala145) adopts an α -crystallin-like fold with two four-stranded anti-parallel β -sheets. The C-terminal zinc-dependent catalytic domain (Ser175-Ala408) has an α/β fold with a six-stranded β -sheet flanked by α helices, and belongs to the amidase_3 family (Figure 32A) (Korndörfer *et al.*, 2006)

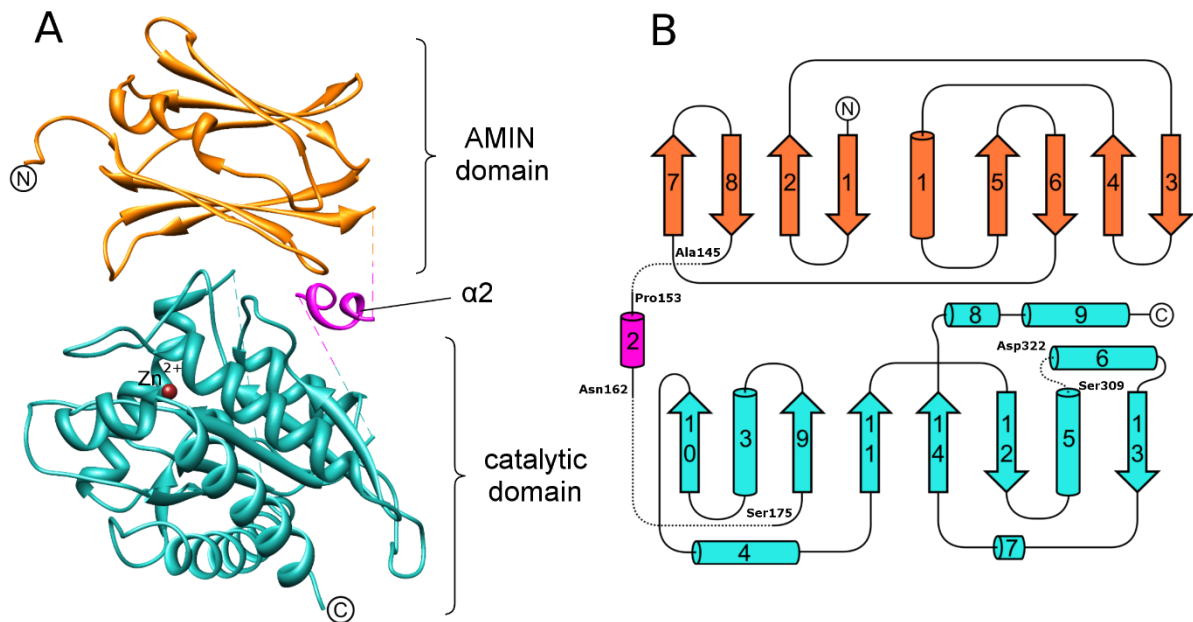


Figure 32. Crystal structure of AmiC. A. The AMIN domain, the linker and the catalytic domain are respectively shown in orange, violet and cyan B. Topology of AmiC. α -helices are colored in blue and β -strands in red. Stretches of missing residues are represented as dashed lines. Residues preceding and following the missing segments are labeled.

- *AMIN domain (Phe30-Ala145)*

One of the two β -sheets (β -sheet1) of the AMIN domain of AmiC is composed of strands β 1-2-8-7 and the second one (β -sheet2) of strands β 5-6-4-3. An additional short α -helix (α 1) located near the β 1 and β 5 strands closes one side of the β -sandwich (Figure 32).

A striking feature of the AMIN domain is the presence of four RxxxD/E motifs on strands β 2 (Arg49xxxGlu53), β 4 (Arg70xxxAsp74), β 6 (Arg112xxxGlu116) and β 8 (Arg137xxx-Asp141). These residues lie on the external face of the two central strands of each β -sheet (Figure 33). Arg49 and Arg112 are involved in salt bridges with the aspartates of the motifs located on the adjacent antiparallel strands (Asp141 and Asp 74 respectively) whereas Glu53, Arg70, Glu116 and Arg137 do not share any hydrogen bond. Instead, Glu53 is hydrogen bonded to Arg26, which is located on the strand β 1 and Arg137 interacts with Glu199, an electrostatic anchor of the catalytic domain (see below). This organization suggests that the repetition of the RxxxD/E motifs originates from the double duplication of a two-stranded ancestor encompassing one RxxxD/E motif on the second strand to form the AMIN domain (de

Souza *et al.*, 2008). Both interactions Arg49/Asp141 and Arg112/Asp74 could be important to stabilize a folding intermediate or the final scaffold of the AMIN domain.

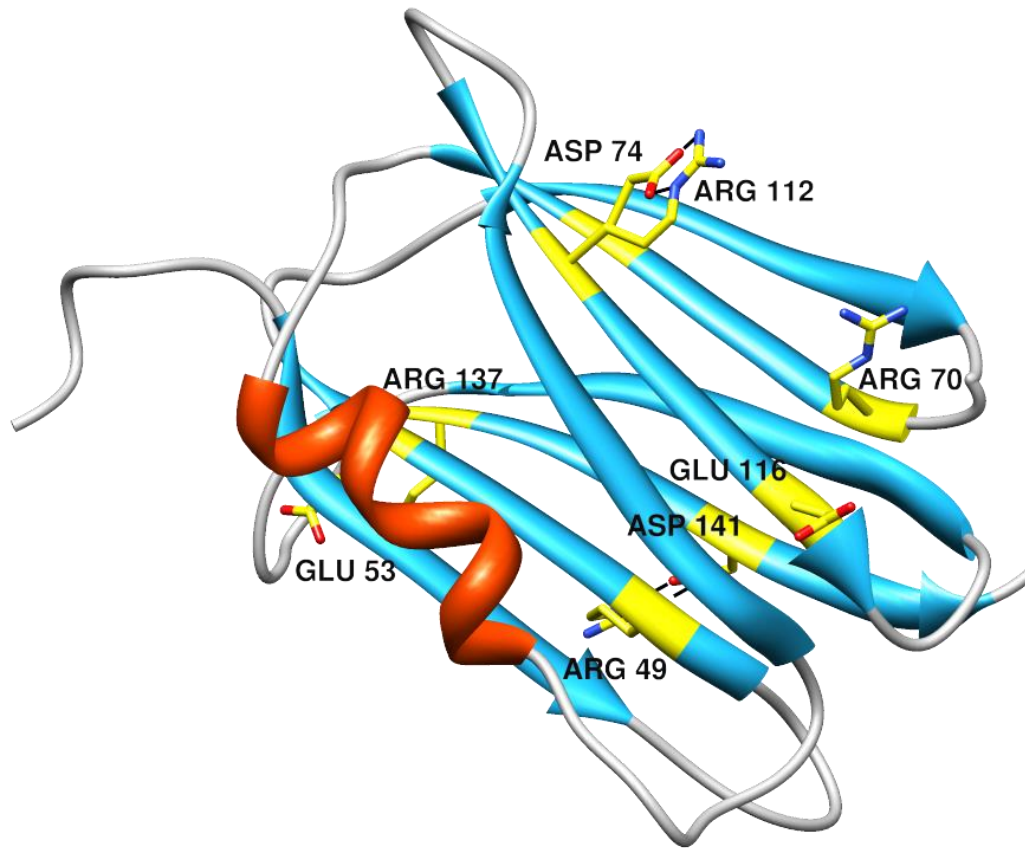


Figure 33. RxxxD/E motifs of the AMIN domain. The residues involved in the RxxxD/E motifs are depicted in yellow. α -helix and β -strands are shown in orange and cyan respectively. Salt bridges are represented as dashed lines.

A ConSurf analysis with AmiC related proteins (Ashkenazy *et al.*, 2010) reveals a patch of conserved residues on the outer face of both β -sheets. Moreover, the superposition of β -sheet1 and β -sheet2 reveals a striking similarity between them (RMSD of 0.64Å on 25 residues). Indeed, on each face, two small residues (Thr51 and Val139 on β -sheet1, Val72 and Val114 on β -sheet2) are surrounded by five charged ones (Arg40, Arg49, Glu53, Arg137 and Asp141 on β -sheet1; Arg102, Arg112, Glu116, Arg70 and Asp74 on β -sheet2) and two hydrophobic residues (Phe126 and Leu128 on β -sheet1; Phe63 and Leu65 on β -sheet2) (Figure 34C). ConSurf scores range from 9.8 to 9.9 for each of these residues except for Phe63 and Leu65 with scores of 7.6 and 8.7 respectively. These residues are therefore strictly conserved between β -sheet1 and β -sheet2 except for the Thr51 that is replaced by the shape-equivalent Val114 in

β -sheet2. The superposed Arg40 and Arg102 side chains do not show the same orientation but this can be explained by the interaction of Arg40 with the catalytic domain (see below). Two lysines (Lys59 and Lys122) lie in the same positions in their respective β -sheets but are not conserved in AMIN domains.

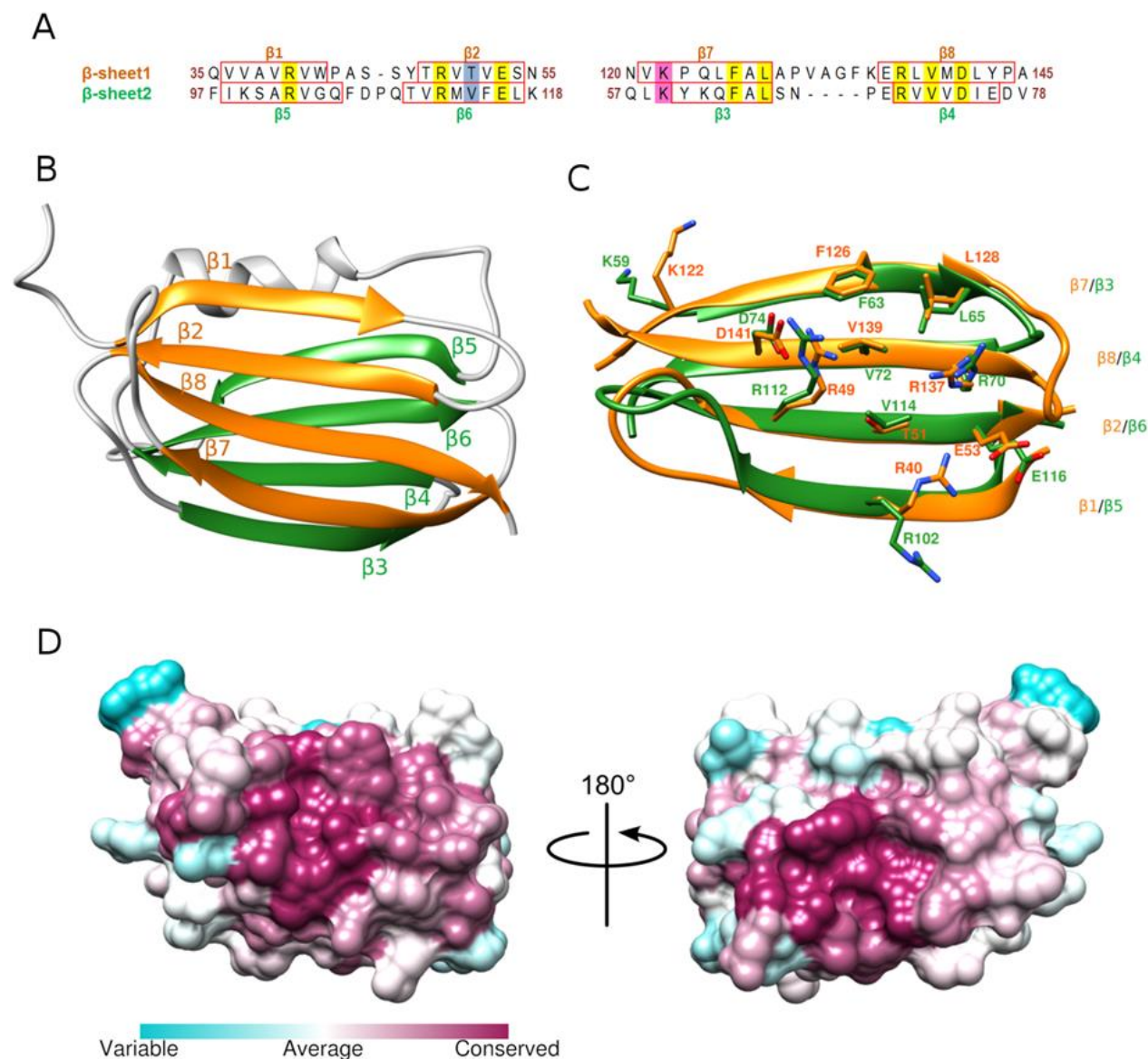


Figure 34 AMIN domain of AmiC. A. Sequence alignment of the two β -sheets composing the AMIN domain. β -strands are represented by red boxes. Surface residues conserved in the AMIN domains of amidases are highlighted : in yellow, for residues identical in β -sheet1 and β -sheet2 and in blue for residues of similar shape. Residues not conserved in AMIN domains but identical in the two β -sheets are represented in pink. B. Cartoon representation of the AMIN domain. The β -sheet1 (strands β 1-2-8-7) and the β -sheet2 (strands β 3-4-6-5) are depicted in orange and green respectively. Coils and helix α 1 are shown in grey. C. Superposition of the two β -sheets of the AMIN domain. The color code is the same as in Figure 2B. Amino-acids highlighted in Figure 2A are represented as sticks (nitrogens and oxygens are shown in blue and red respectively). D. Surface representation of the AMIN domain. Conservation of amino-acids of AmiC related proteins is mapped onto the surface from poorly conserved in blue to highly conserved in purple.

β -Sheet1 shares numerous interactions with the catalytic domain. In particular, Glu199 of the catalytic domain seems to play the role of electrostatic anchor by sharing multiple hydrogen bonds with the AMIN domain via amino acids that form a hydrophilic pocket (Arg40, Trp42, Thr51 and Arg137). Moreover, Arg49 which belongs to the RxxxE motif of strand β 2 interacts with the main chain carbonyl of Gly307 in the catalytic domain (Figure 35). The AMIN domain also interacts with the C-terminus of helix α 5 of the catalytic domain via hydrophobic interactions between Val131/Ala132/Phe134 and Leu304/Ile305 respectively. However, a PISA analysis (Krissinel and Henrick, 2007) of the interaction surface between the AMIN and catalytic domains provides a Complex Significance Score of 0 (see material and methods) and thus may indicate a crystal packing artifact rather than a specific binding. This suggests a relative flexibility of the AMIN domain that could expose both its conserved surfaces for a simultaneous interaction with two similar partners.

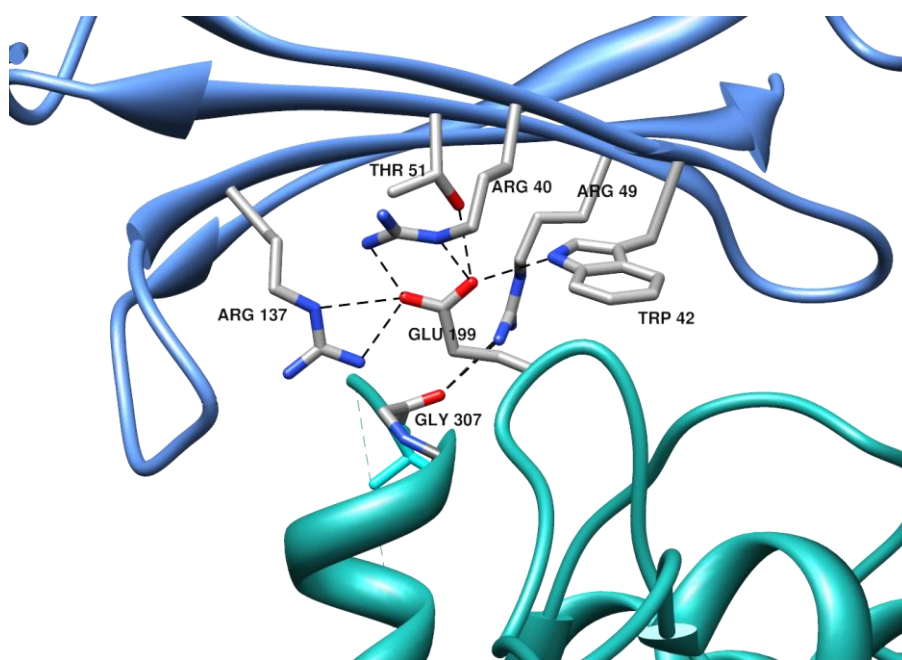


Figure 35. AMIN domain/catalytic domain interface. The AMIN domain and the catalytic domain are colored in blue and cyan respectively. Amino acids involved in interactions are shown in sticks (nitrogens and oxygens are shown in blue and red respectively)

The AMIN domain shows a high fold similarity with the heat shock protein Hsp26 (DALI score of 7.1 on 93 residues) where seven of the eight β -strands of the AMIN domain are conserved. Consequently, the conserved area located on the outer faces of the two β -sheets of the AMIN

domain along with the fold homology with the chaperone protein Hsp26 suggest that this domain interacts with components of the septal ring.

- *Catalytic domain (Ser175-Ala408)*

The catalytic domain of AmiC consists in a strongly twisted six-stranded β sheet flanked by six α -helices (Figure 32). The overall fold is conserved when compared to the five solved structures of the amidase_3 family (Korndörfer *et al.*, 2006; Mayer *et al.*, 2011; Yang *et al.*, 2012). RMSDs between alpha carbons range from 0.8 Å (138 alpha carbons) with the N-acetylmuramoyl-L-alanine amidase from *Bacillus polymyxa* (PDBID: 1JWQ) to 1.13Å (85 alpha carbons) with the putative N-acetylmuramoyl-L-alanine amidase from *Neisseria meningitidis* (PDBID: 3CZX).

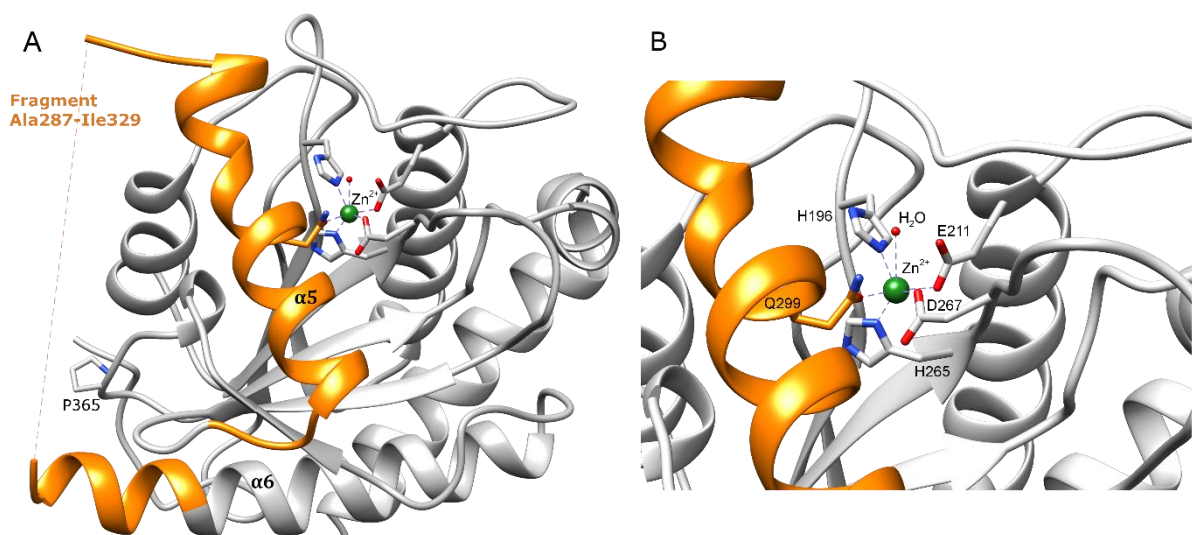


Figure 36. Catalytic domain of AmiC. A. Cartoon representation of the catalytic domain. The fragment removed to produce the mutant AmiC Δ H5 (see in text) is depicted in orange. The catalytic zinc is shown in green. B. Close-up on the catalytic site of AmiC. The catalytic zinc and the obstructing helix α 5 are shown in green and orange respectively. The chelating residues are represented as sticks (nitrogens and oxygens are shown in blue and red respectively).

In the amidase_3 family, four residues involved in the catalytic activity are strictly conserved. Two histidines (His196 and His265) and one glutamate (Glu211) chelate the catalytic zinc ion. The fourth conserved residue (Glu373) is thought to be involved in the proton transfer during the catalysis in metallo-proteases (Christianson *et al.*, 1989) (Figure 36). A striking feature, also observed in the amidase ortholog AmiB from *Barthionella hensealae* (PDBID: 3NE8, (Yang *et al.*, 2012)), is the presence of an additional 43 amino-acid segment from Ala287 to Ile329 that

contains an extension to the $\alpha 6$ helix and the $\alpha 5$ helix (Thr290-Gly306) that obstructs the active site. This insertion induces slight conformational rearrangements in the loop connecting the strands $\beta 11$ and $\beta 12$ when compared with the amidase_3 members with accessible active sites. The most striking one is the position of Asp267 which is flipped in the direction of the catalytic site and coordinates the zinc ion. In the other amidase_3 members lacking the obstructing helix (PDB IDs: 1XOV, 3CZX and 1JWQ), this aspartate is replaced by an asparagine oriented to the solvent. This conformation would be unfavorable in AmiC because of a steric hindrance with Leu295 present on helix $\alpha 5$. Therefore, the zinc chelation of Asp267 could simply result from the blocking of the active site by helix $\alpha 5$ and this residue would not be involved in the catalysis. Helix $\alpha 5$ also contains a glutamine residue (Gln299) which chelates the zinc ion. Two neighboring residues (Asn300 and Asp303) are highly conserved in the amidase_3 members exhibiting the additional loop that contains the inhibitory helix. Asn300 is in close contact with the loop connecting strands $\beta 13$ and $\beta 14$, while Asp303 interacts with the main chain nitrogen of Leu246 located at the beginning of helix $\alpha 4$ (Figure 37).

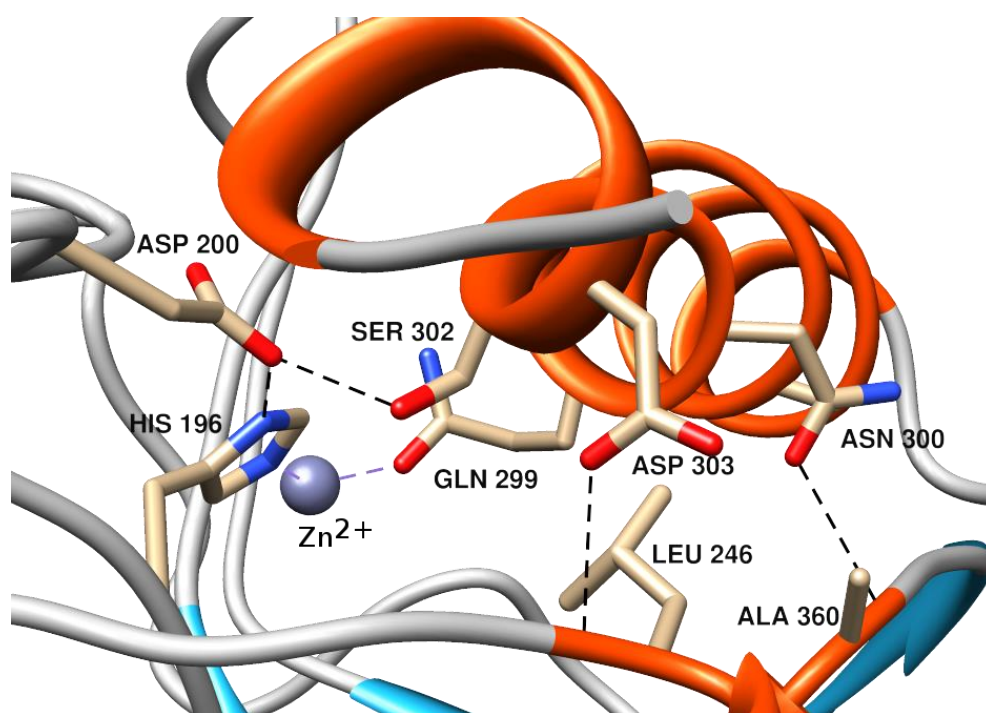


Figure 37. Interactions stabilizing the helix $\alpha 5$ in the active site of AmiC. Nitrogens and oxygens atoms of the amino acids represented as sticks are depicted in blue and red respectively. Hydrogen bonding and electrostatic interactions are shown as dotted lines. The catalytic zinc ion is shown in grey.

Asn300, Asp303 as well as Ser302, which is not a conserved residue, appear to be important for the stabilization of the helix in the active site and the interactions that they share with the rest of the catalytic domain have to be disrupted during the activation process.

Moreover, the displacement of the obstructing helix requires a relative flexibility of the whole additional segment. This is supported by the absence of interpretable density for the Lys310-Phe321 segment connecting the helices $\alpha 5$ and $\alpha 6$. The corresponding segment (Glu303-Thr308) in the crystal structure of AmiB catalytic domain from *B. henselae* is also missing.

Sequence conservation analysis highlights a proline in position 365 surrounded by polar residues (Gln254, Asp322, Lys363 and Asp366). This highly conserved patch (ConSurf scores ranging from 9,8 to 9,9) is located at the beginning of helix $\alpha 6$, close to the flexible loop connected to the obstructing helix $\alpha 5$ and thus constitutes a potential interaction surface with the activator NlpD. Such an interaction could induce slight conformational changes, like the disruption of the hydrogen bonds shared by Asn300 (see above), and release the obstructing helix from the active site.

11. Role for the auto-inhibiting α -helix

In order to characterize the activation mechanism of AmiC by the LytM factor NlpD, activity tests based on dye-release assay with Remazol Brilliant Blue (RBB)-labeled peptidoglycan were conducted (Figure 38). This technique allows a rapid assessment of peptidoglycan digestion by the release of labelled peptidoglycan fragments. Both purified proteins were used at a $4\mu\text{M}$ concentration in the activity assay for 30 minutes or 15 hours.

The activation of AmiC by NlpD (Uehara et al., 2010) was confirmed, as was the weak activity of AmiC for the shortest incubation time. NlpD did not show any significant activity even for longer incubation times (overnight). Moreover, upon the addition of the chelating agent EDTA at 1 mM concentration; the apparent activity of the AmiC/NlpD couple is reduced by a factor 11 after 30 minutes. This observation confirms the central role of the zinc in the catalytic mechanism of AmiC.

Based on the structural data, we also produced and purified an AmiC mutant lacking the Ala287-Ile329 segment that includes helix $\alpha 5$ (AmiC Δ H5) (Table 2). This construct was designed on the basis of the available structures of amidase_3 members lacking the obstructing loop in order to maintain the overall fold of AmiC. The level of activity of AmiC Δ H5 against the RBB-labeled peptidoglycan is equivalent to that of AmiC activated by NlpD. Moreover, by

adding a peptide mimicking helix $\alpha 5$ (Thr288-Gly306) at 50 μ M, the measured activity of AmiC Δ H5 was decreased approximately by a factor 2. These results demonstrate that in the absence of helix $\alpha 5$, the AmiC Δ H5 variant becomes unregulated and exhibits maximal activity without activation by NlpD. *In vivo*, such uncontrolled hydrolase activity would have severe consequences for the integrity of the bacterium leading to cell lysis.

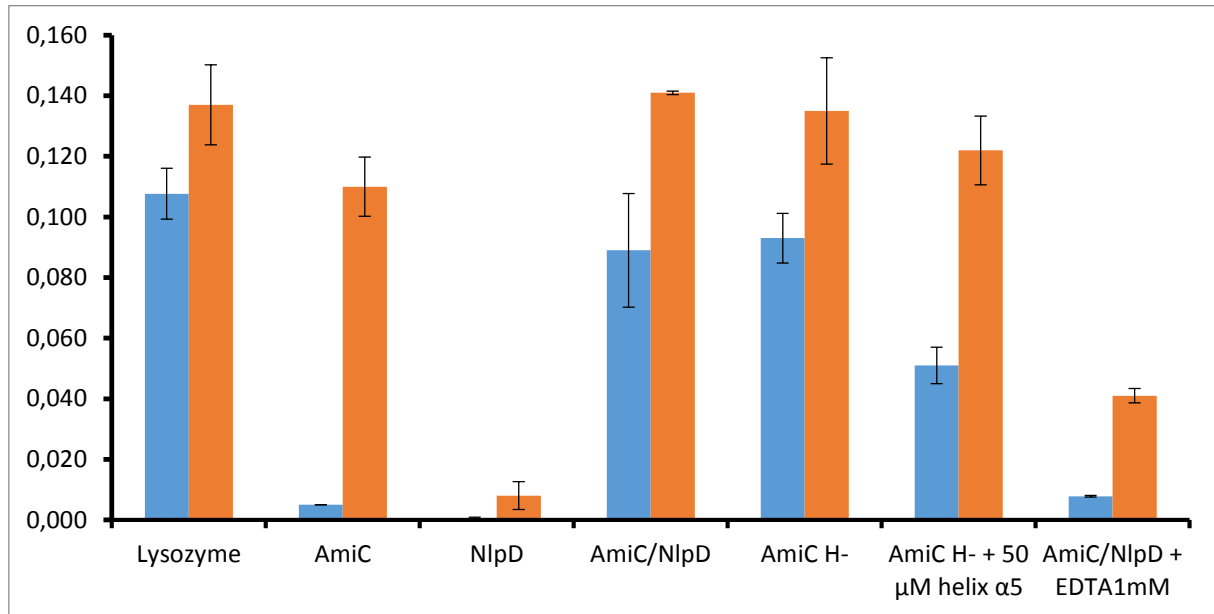


Figure 38. Helix $\alpha 5$ of AmiC is involved in the activation mechanism by NlpD. The dye-release assay allows the following of the hydrolysis of RBB-labeled peptidoglycan. Each protein was used at 4 μ M during 30min (blue bars) or overnight (orange bars). Lysozyme was used as positive control. AmiC Δ H5 is the AmiC mutant lacking the Ala287-Ile329 segment. The α -helix is the peptide mimicking the Thr288-Gly306 segment of AmiC. Error bars represent standard deviations from three independent measurements.

- Effect of AmiC Δ H5 expression in *E. coli*

Activity tests with RBB-labeled peptidoglycan demonstrated the importance of the inhibitory helix in the regulation mechanism of AmiC by the LytM factor NlpD.

In order to confirm the loss of regulation for the AmiC Δ H5 variant *in vivo*, the gene coding for this protein or the wild-type AmiC were cloned in a pET-22b production vector and expressed in *E. coli* BL21 (DE3) cells. Monitoring of the growth of the transformants did not show any alteration of the growth curves in both cases. To explain this unexpected result, the cellular fractions (periplasm and cytoplasm) were prepared and analysis by SDS-PAGE. The gel shows

that both AmiC and AmiC Δ H5 were over-produced but not exported to the periplasm and remained in the cytoplasm in an insoluble form (at 45 kDa for AmiC and 42 kDa for AmiC Δ H5). Future tests will involve an arabinose inducible gene expression to lower the amount of recombinant proteins in order to avoid inclusion body formation and assure the proper export of the recombinant proteins.

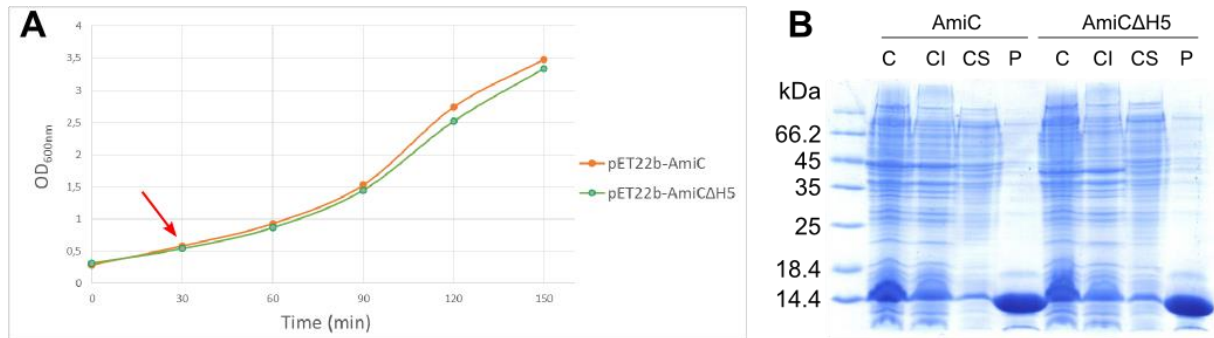


Figure 39. A. Growth curves of BL21 (DE3) cells after the 150 mM IPTG induction (red arrow). B. Fractionation of the cell culture three hours after the IPTG induction. Cytoplasm (C), soluble (CS) and insoluble (CI) fractions and periplasm (P) fractions.

12. AMIN domain interaction with peptidoglycan sacculi

The AMIN domain of AmiC is known to be necessary and sufficient for the proper localization to the division site (Bernhardt & de Boer, 2003). However, no binding partners have been identified so far. The interaction between the untagged AMIN domain of AmiC and peptidoglycan sacculi was tested by pull-down experiments (Figure 40). After two washing steps, a significant amount of the AMIN domain is released from the pelleted peptidoglycan in comparison with the control experiment without peptidoglycan. This assay clearly shows an interaction between the AMIN domain of AmiC and the peptidoglycan.

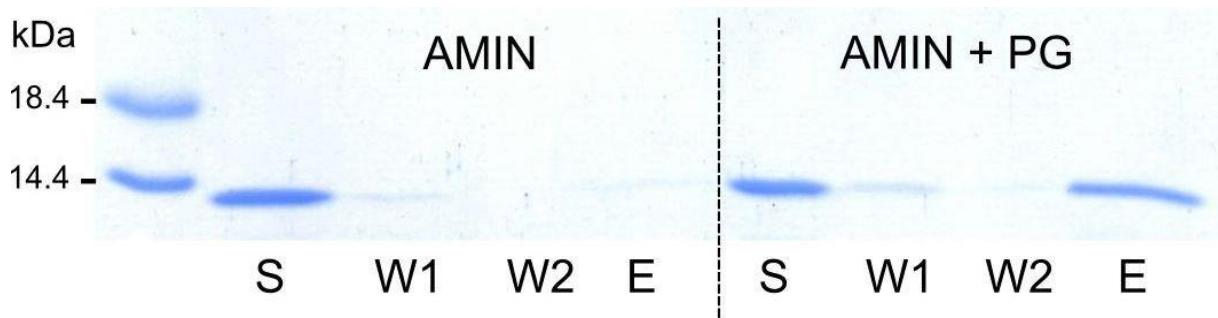


Figure 40. The AMIN domain of AmiC interacts with the peptidoglycan (PG). 10 μ g of the purified AMIN domain were incubated with peptidoglycan sacculi for two hours at 4°C in the binding buffer. The supernatant (S) was collected after centrifugation at 14000g during 20 minutes. The supernatants of two washes followed by centrifugation (W1 and W2) and the remaining pellet resuspended with 2% SDS (E) were analyzed by SDS-PAGE.

Another requirement for the localization of AmiC to the division site is the presence of the bitopic protein FtsN (Bernhardt & de Boer, 2003). The interaction between these two septal components has also been tested by a pull-down assay (Figure 41). The membrane protein FtsN with a N-terminal His-tag was incubated with the untagged AMIN domain in the presence of agarose beads charged with Ni^{2+} (see material and methods). Two washing steps (with 50mM NaCl) discarded the majority of the AMIN domain and only FtsN was eluted upon the addition of 500 mM of imidazole. Based on this pull-down assay, FtsN is unlikely to be an interaction partner of the AMIN domain and suggests that the FtsN-dependent localization of AmiC is likely indirect. This observation is in good agreement with the model proposed by Peters *et al*, where FtsN could stimulate peptidoglycan hydrolysis by promoting the recruitment of NlpD to the septum and stimulating the production of peptidoglycan at the division site *via* the activation of PBP3 and PBP1B and thus providing substrate for the septal amidases (Peters *et al.*, 2011).

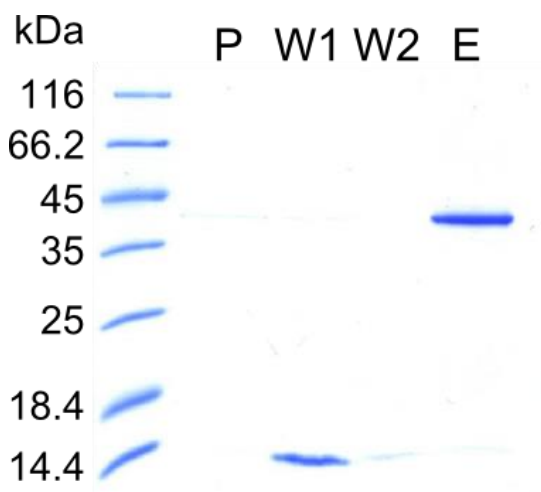


Figure 41. Pull down assay with FtsN and the AMIN domain. Pellet after 1h incubation of FtsN and the AMIN domain and before the addition of Ni^{2+} -charged beads (P), Wash steps (W1 and W2) with 50 mM NaCl and elution (E) with 500 mM imidazole.

13. The AmiC-NlpD interaction

In vitro activation of AmiC by NlpD suggests a direct interaction between these two cell division components. We tested the interaction by microscale thermophoresis, an immobilization-free technique that allows the monitoring of the displacement of molecules in a temperature gradient generated by an infra-red laser. The behavior of a particle in this gradient rests upon its mass, charge and solvation shell (Jerabek-Willemsen et al., 2011). These properties are then altered when a binding partner is added to the system and titration series allow the determination of the binding affinity.

Each protein was labeled with Dylight 650 and titrated against its potential unlabeled partner or lysozyme, used as a negative control. Binding was detected for each titration involving the couple AmiC/NlpD and no binding is observed between AmiC and lysozyme (Figure 42). Experiments were realized in triplicate and the apparent K_d values are $11.3 \pm 1.5 \mu\text{M}$ with labeled NlpD and $15.5 \pm 7.2 \mu\text{M}$ with labeled AmiC.

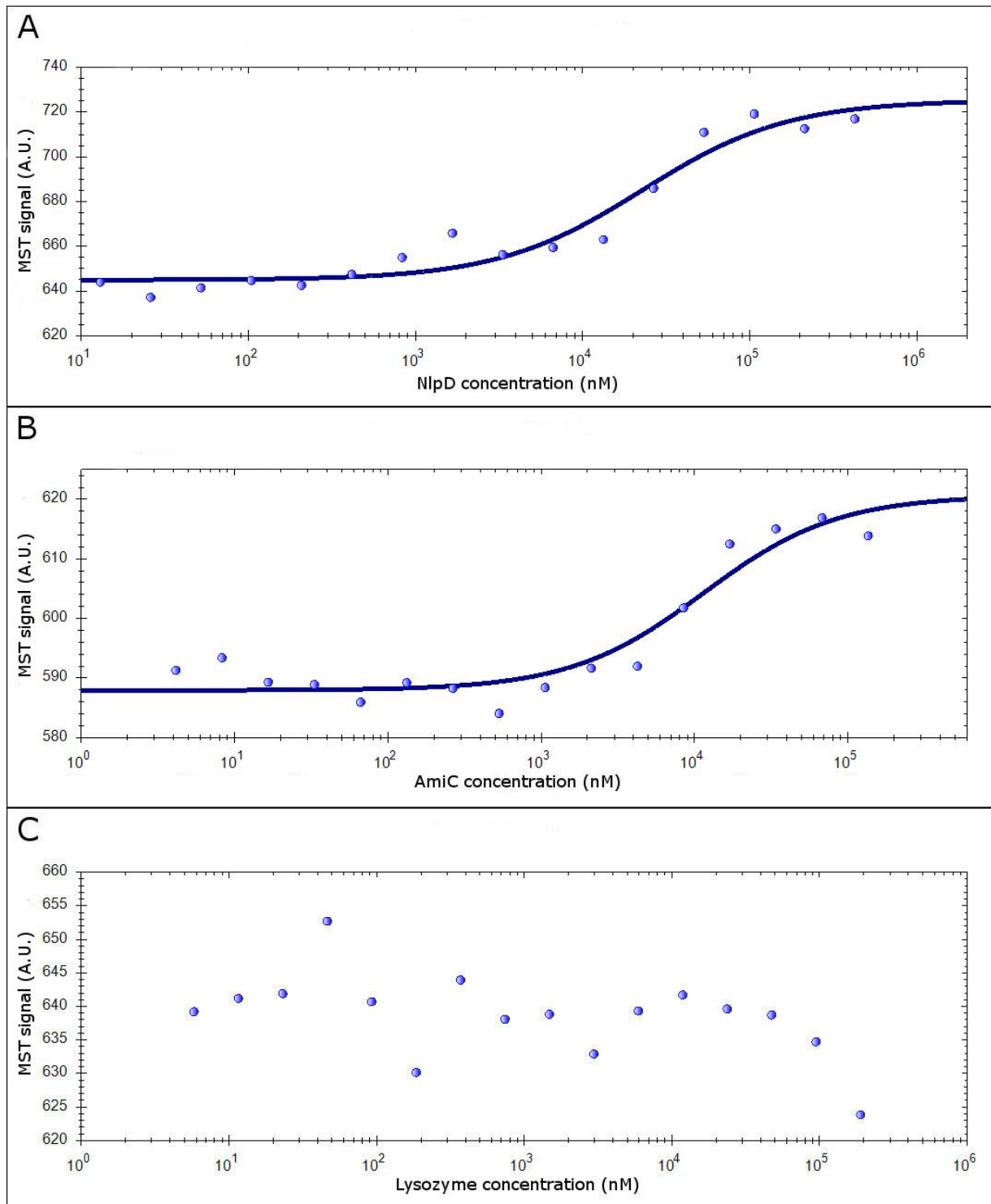


Figure 42. AmiC directly interacts with NlpD. Thermophoresis assays were realized with either AmiC labeled (A and C) or NlpD labeled (B) with Dylight 650 (see experimental procedures for details). The negative control with lysozyme as binding partner did not exhibit the typical binding curve (C). Measures are represented by blue dots and fitted curves by blue lines. NanoTemper Analysis 1.2.101 software was used for the fitting of the data and determination of the apparent K_d values.

Discussion

The lipid II flippase FtsW

FtsW is an essential protein of the *E. coli* division machinery. This integral membrane protein of ten transmembrane segments, member of the SEDS (shape, elongation, division and sporulation) family, was shown to be responsible for the translocation of the lipid II (peptidoglycan precursor) across the cytoplasmic membrane (Mohammadi et al., 2011). Its essential but yet non understood flippase activity at the division site along with the multiple interactions shared with the other septal components (Figure 22) made FtsW an attractive candidate for structural investigations.

Experimental results and perspectives

The first bottleneck of structural investigation of membrane proteins is the production of sufficient amounts of recombinant protein. We tried to address this problem by cloning four different *ftsW* genes from the model organism *E.coli*, the Gram positive pathogen *S. aureus*, and the two thermoresistant strains (*A. aeolicus* and *G. thermodenitrificans*) into pET-based production vectors for the production in *E. coli* and nisin- inducible vectors for *L. lactis* productions.

Overproduction was only detected for FtsW from *E. coli* cloned into a pET-based vector and in *E. coli* C43 (DE3) cells. The lack or very low rate of production for the others FtsW may be due to improper insertion of the recombinant proteins into the cytoplasmic membrane, leading to proteolysis or toxic effect. An alternative consisted in a more tunable induction of protein production with the arabinose-inducible pBAD vector (Guzman *et al.*, 1995). Unfortunately, this system did not result in better productions.

Expression of FtsW from *E. coli* also showed the presence of a degradation product during the production. Identification by mass-spectrometry of the cleavage site and mutagenesis of the involved residues could limit proteolysis. Another strategy involves the production of FtsW with its cognate PBP. Indeed, FtsW is known to form a discrete pre-complex with the D,D-transpeptidase PBP3 before its recruitment at the septum (Fraipont et al., 2011). Interesting results were obtained with the *B. subtilis* couple SpoVD-SpoVE (involved in sporulation events) where both proteins were co-expressed in *E. coli* (Fay *et al.*, 2010). SpoVD, a non-essential PBP, was shown to increase the stability of the SEDS member SpoVE and limit the

proteolysis observed when SpoVE was expressed alone. Moreover, a fusion of the two proteins was found to complement the double $\Delta spoVD \Delta spoVE$ mutant indicating a functional fusion with both protein activities (Fay et al., 2010). Accordingly, co-expression of FtsW with PBP3 and expression of a fusion FtsW-PBP3 are currently tested in the lab.

The genetic constructs realized so far code for recombinant proteins with a N-terminal His-tag followed by a TEV cleavage site. During the purification steps of FtsW from *E. coli*, both full length protein and degradation product are captured on a Ni²⁺ affinity column, arguing for a C-terminal degradation. Therefore, an additional purification tag (e.g. Strep-tag) located at the C-terminus of FtsW could help to isolate the full length version of FtsW and improve its purity.

Finally, efforts should be pursued to screen other FtsWs from other strains in order to increase the chances to obtain a sufficient purified amount of this highly challenging protein.

AmiC & NlpD, actors of the daughter cells separation

Enzymes exhibiting a hydrolase activity against the peptidoglycan were commonly associated with potentially lethal agents as lysozyme. Peptidoglycan hydrolases actually play major roles in critical physiological contexts such as bacterial growth, peptidoglycan turnover or cell wall shape (Vollmer et al., 2008) and have been found recently to be essential for growth (Singh *et al.*, 2012). In *E. coli*, separation of daughter cells at the late stage of bacterial division was found to be mainly accomplished by one murein hydrolase family, the N-acetylmuramyl amidases. At the septum of *E. coli*, AmiA, AmiB and AmiC cleave the amide bond between the lactyl group of the muramic acid and the L-Alanine of the peptide moiety. These enzymes have been recently shown to be regulated by LytM factors: EnvC activates AmiA/AmiB and NlpD activates AmiC (Uehara et al., 2010).

AmiC and the regulation of its amidase activity

The crystal structure of AmiC described in this work highlights two structurally independent domains: the N-terminal AMIN domain and the C-terminal catalytic domain. The structure of the C-terminal amidase_3 domain clearly shows the obstruction of the active site by an α -helix confirming the observation made with the septal amidase AmiB from *B. henselae* (Yang et al., 2012). This α -helix shares several contacts with the rest of the protein including a glutamine that chelates the catalytic zinc ion. The helix has to be displaced in order to accommodate the peptidoglycan. For AmiC, this activation, likely involving conformational change, has been shown to be induced by the LytM factor NlpD (Uehara et al., 2010).

In vitro, AmiC exhibits a basal activity suggesting a competition between the auto-inhibitory helix and peptidoglycan, with a clear preference for the closed state. In the presence of NlpD, the equilibrium is displaced towards the open state and the active site becomes freely accessible to peptidoglycan. With the mutant of AmiC which is devoid of the inhibitory helix and therefore constitutively active, we have shown that the addition of a synthetic form of the $\alpha 5$ helix partially restores the inhibited form of the enzyme further suggesting a competition between this helix and peptidoglycan.

In the context of daughter cell formation, one hypothesis is that amidase activity targets preferentially cross linked peptides, leading to the separation of adjacent glycan chains and eventually, contributes to the formation of the future cell poles. Preliminary results of HPLC analysis of peptidoglycan digested over an extended period of time (overnight) by the couple AmiC/NlpD did not show a strict substrate specificity of AmiC or of the AmiC/NlpD complex for cross-linked peptides. However, further investigation is needed to demonstrate or rule out our hypothesis.

AMIN domain and PG recognition

In the N-terminal AMIN domain, conserved residues on both outer faces suggest two symmetric interaction regions. The two RxxxD/E motifs present on each face of the AMIN domain represent almost half of the conserved residues. Their conservation and the striking symmetry of this domain suggest the recognition of a repeated pattern like the building blocks of peptidoglycan or the simultaneous binding to two identical divisible components. We have tested two potential binding partners of the AMIN domain: FtsN because of its importance for the recruitment of AmiC at the division site, and the peptidoglycan. Our attempts to find an interaction between purified FtsN and the AMIN domain by different pull-down assays were unsuccessful (data not shown), but we were able to show that the AMIN domain directly interacts with the peptidoglycan. Furthermore, although the AMIN domain is packed onto the C-terminal domain in the crystal structure, the presence of a 30 amino acids linker suggests a high flexibility between these two domains. The PISA analysis and the high homology between the AMIN exposed surface and the AMIN surface in contact with the catalytic domain also argue in favor of a crystallographic artifact for the interaction between these two domains. Moreover, because the AMIN domain is known to be sufficient for the localization of AmiC at the division site, it potentially recognizes a specific characteristic of the septal peptidoglycan which remains however to be identified.

A modeling of two cross-linked glycan chains provided by Dr Sauvage suggests at least two possible interaction modes for the AMIN domain. The opposite conserved faces of the domain could interact either with the sugar moieties of two parallel glycan strands or with two consecutive peptide cross links (Figure 43). Both models raise questions concerning the

processivity of AmiC in the context of coordinated septal peptidoglycan synthesis and hydrolysis. Indeed, such model implies a high frequency of targeting-release events of the AMIN domain to follow the septal peptidoglycan synthesis machinery. Alternatively, the cleavage of the peptide cross-links could be part of the processive mechanism of hydrolysis via an alternate anchorage of the catalytic and the AMIN domains on the peptidoglycan.

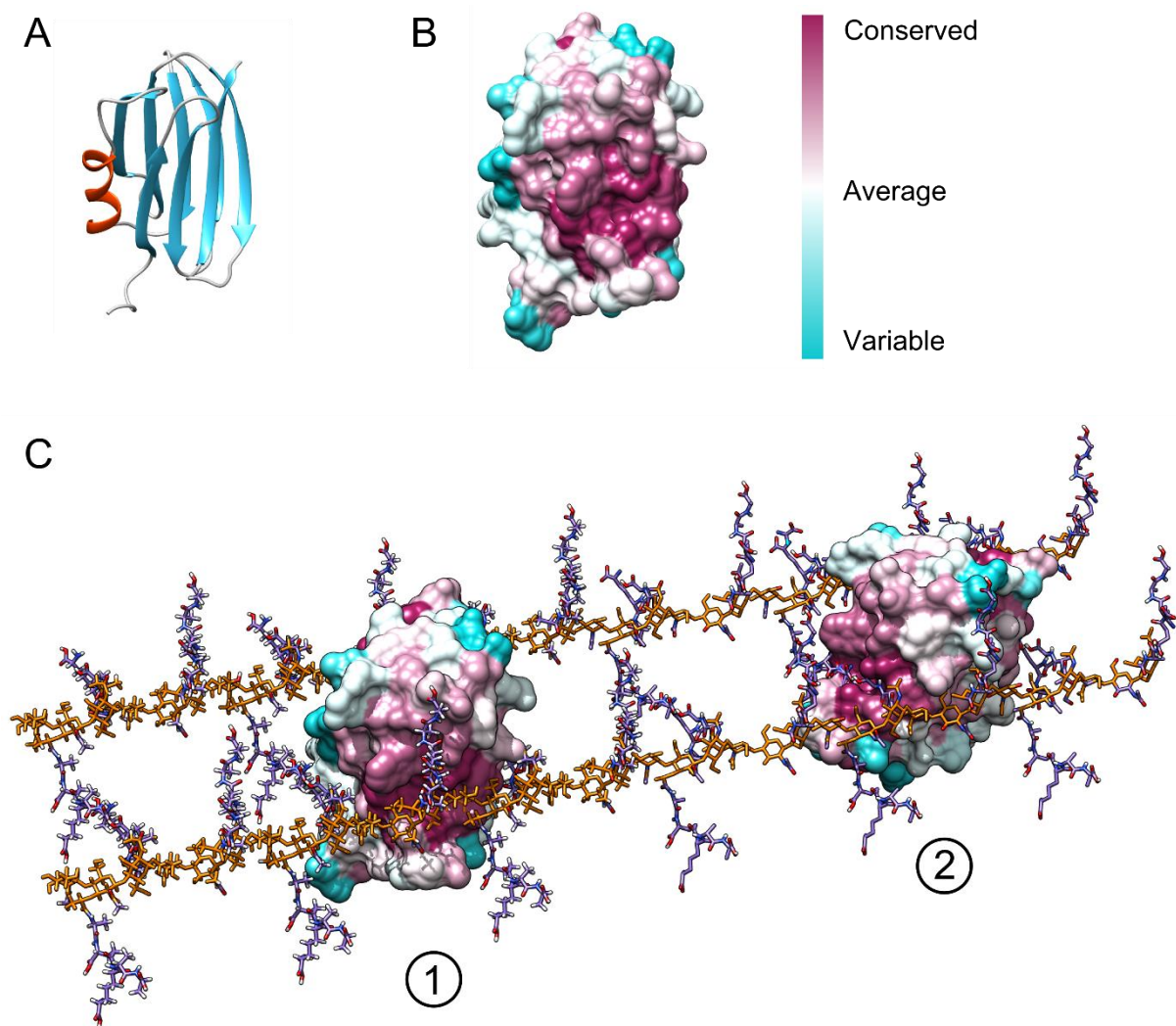


Figure 43. Model for the interaction of the AMIN domain of AmiC with peptidoglycan. A. Cartoon representation of the AMIN domain of AmiC. α helix and β strands are depicted in orange and blue respectively. B. Surface representation of the AMIN domain. Orientation of the protein is the same as represented in A. Conservation of amino-acids of AmiC related proteins is mapped onto the surface from highly conserved in purple to poorly conserved in blue. C. Proposed models for the peptidoglycan interaction of the AMIN domain. 1) Sugar moiety recognition 2) Peptide cross-link recognition. Disaccharides and peptides of the glycan chains are depicted in orange and purple respectively. The two AMIN domains are colored as in B.

Future experiments will focus on the analysis of the conserved residues on both surface of the AMIN domain and their potential involvement in the peptidoglycan binding. Site directed

mutagenesis will allow the production of AMIN domain variants which will be tested *in vivo* for the localization at the septum and *in vitro* for their peptidoglycan binding capacity. Interactions between the AMIN domain and peptidoglycan will also be studied by NMR to more precisely identify the AMIN domain residues involved and the peptidoglycan feature recognized.

AmiB is also known to be targeted to the cell division site via its N-terminal region (Peters et al., 2011). Secondary structure prediction attributes eight β -strands to this N-terminal targeting domain. However, sequence alignment with the AMIN domain of AmiC (25.8% identity) shows strong similarities only with the conserved amino-acids of the β -sheet2: four identical and three equivalent out of nine residues. For the β -sheet1, only one residue is strictly conserved and one is equivalent. Therefore, unlike the large majority of protein sharing the AMIN-amidase_3 architecture of AmiC, AmiB is characterized by relatively conserved residues on the β -sheet2 but lacks the conserved ones highlighted on the β -sheet1 of AmiC. To our knowledge, AmiB is not in any way deficient in localization at the septum compared to AmiC. The advantage of a symmetrical AMIN domain shared by most homologues of AmiC remains therefore unclear.

Model for the AmiC activation by the LytM factor NlpD

Our thermophoresis experiments provide evidence that a direct interaction occurs between AmiC and its cognate activator NlpD. However, our attempts to confirm the interaction by ITC and surface plasmon resonance (SPR) were unsuccessful so far. NlpD could directly compete with the AmiC active site for binding the inhibitory α -helix or recognize an adjacent area, inducing a conformational change of AmiC that would prevent the α -helix from obstructing the active site. For the latter case, a potential candidate is the conserved region of AmiC surrounding Pro365, which is relatively close to the catalytic site.

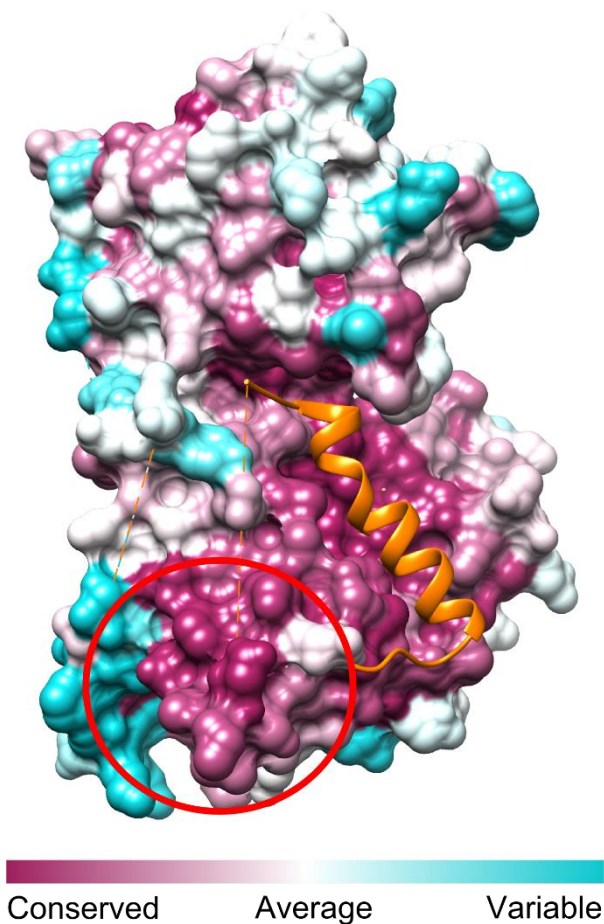


Figure 44. Surface representation of AmiC. The inhibitory helix $\alpha 5$ is depicted in orange. The region surrounding Pro365 is delimited by the red circle. Conservation of amino-acids of AmiC related proteins is mapped onto the surface from highly conserved in purple to poorly conserved in blue.

The septal localization of NlpD is dependent of FtsN and was shown to precede the recruitment of AmiC (Peters et al., 2011). However, the structural determinants involved in this division site targeting are still unknown. NlpD could require the participation of another septal component still unknown. Alternatively, in a similar fashion than the AMIN domain AmiC, the interaction between NlpD and the septal peptidoglycan could be direct via its two modular domains. The N-terminal LysM domain of NlpD, known to bind peptidoglycan (Buist et al., 2008) could be specialized in the recognition of the septal peptidoglycan architecture. The C-terminal LytM domain of NlpD could also directly interact with the septum. Recently, the LytM factor YebA involved in cell growth was found to cleave direct peptide cross-links present in the peptidoglycan (Singh et al., 2012). However, LytM factors NlpD and EnvC do not show activity against peptidoglycan due to a lack of critical residues chelating the catalytic zinc ion. But LytM domains of NlpD and EnvC could possess the structural determinants for the recognition of peptide cross-links. Thus, an attractive scenario would consist in the direct or indirect septal localization of NlpD and the peptide bridge targeting by its LytM domain. The following septal targeting of AmiC by its AMIN domain brings the catalytic site of AmiC in

the vicinity of the LytM domain of NlpD, allowing the amidase activation and the subsequent cleavage of the peptide cross-link (Figure 45).

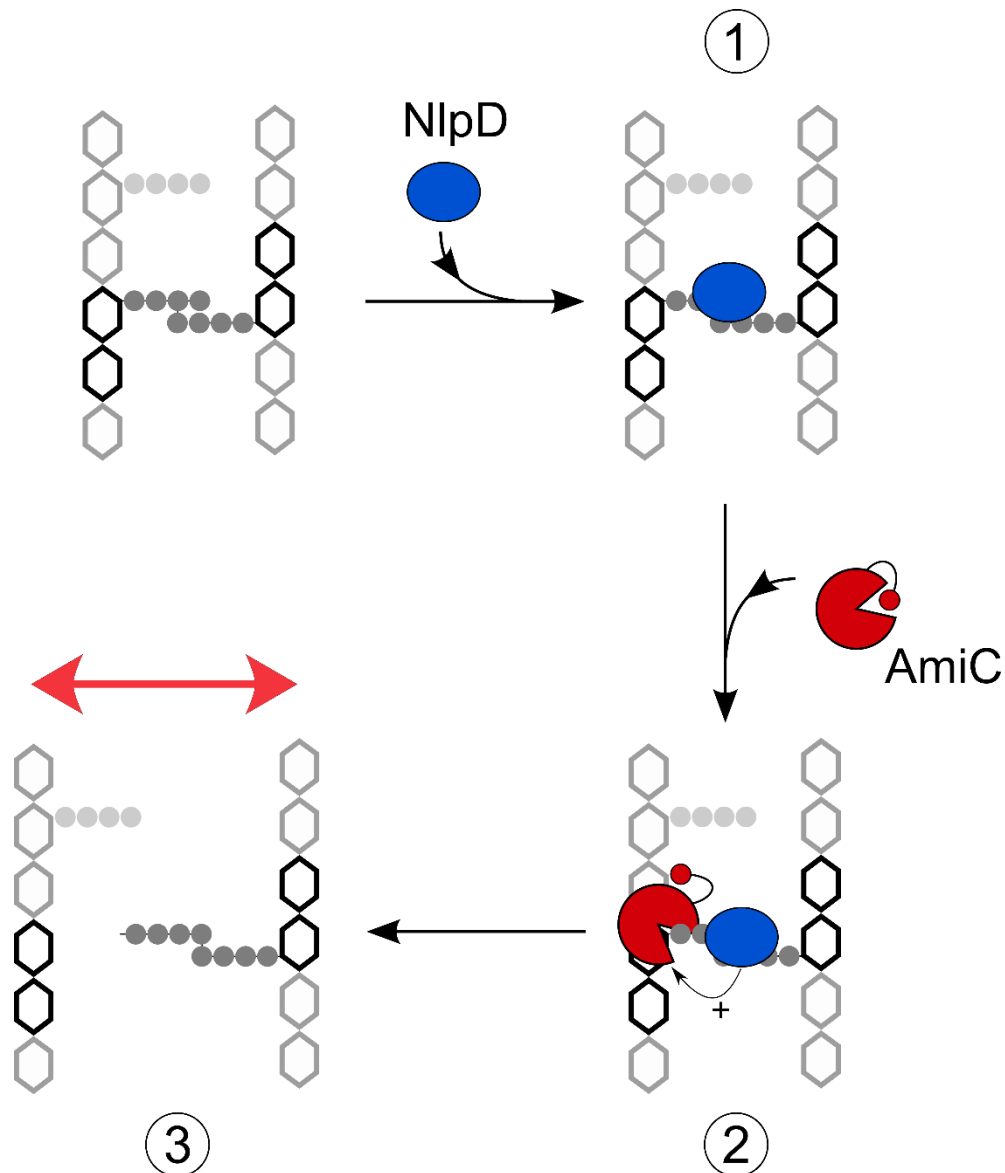


Figure 45. Hypothesis for the AmiC activation by the LytM factor NlpD. 1. Septal localization of NlpD and peptide cross-link targeting of the LytM domain 2. Septal localization of AmiC and activation by the LytM domain of NlpD. 3. Separation of the glycan chains. Sugars of glycan chains and tetra peptides are represented as black hexagons and grey circles respectively. NlpD and AmiC are depicted in blue and red respectively. For clarity, the LysM domain of NlpD and the AMIN domain of AmiC are not shown.

To support this model, the binding capacity of the LytM domain to the peptidoglycan should be assessed by pull down assay. The ITC experiments did not demonstrate any binding between the LytM domain and fragments of peptidoglycan (disaccharide tetrapeptide dimer or the cross-

link mimic peptide D-Glu-meso-DAP-D-Ala-meso-DAP-D-Glu). This raises the possibility of a specific peptidoglycan architecture recognition by the LytM domain. Localization studies with GFP variants of LysM and LytM domains of NlpD could give insight in the domain requirement for the septal localization of NlpD.

NlpD regulation?

A striking feature in the domain organization of NlpD is the presence of two large linkers of approximately a hundred residues in the N-terminal position and between the LysM and LytM domains. Apart from a possible activator still unknown, another level of regulation could therefore consist in a spatial and/or physical constraint of the LytM domain of NlpD dictated by the anchorage of this lipoprotein to the outer membrane and the length of the aforementioned linkers. This would lead to a restricted activation zone of AmiC around the constriction site determined by the proximity between peptidoglycan and the outer membrane. This mechanism seems in agreement with the membrane invagination that would allow a physical proximity of the LytM domain of NlpD with the newly synthesized peptidoglycan which has to be cleaved in order to release the future daughter cells.

This mechanism, along with the FtsE/X-dependent activation of the amidase activity, would take part in a hydrolysis machinery anchored in both cytoplasmic membrane and outer membrane responsible for a highly regulated cleavage of the septal peptidoglycan.

To test this model, the NlpD linkers could be engineered to generate length variants. Production of these NlpD variants in $\Delta nlpD$ cells would generate a chaining phenotype when the LytM domain cannot reach the septal peptidoglycan. Alternatively, longer linkers could induce a spatially unregulated activation of AmiC that could be detrimental for the bacterium.

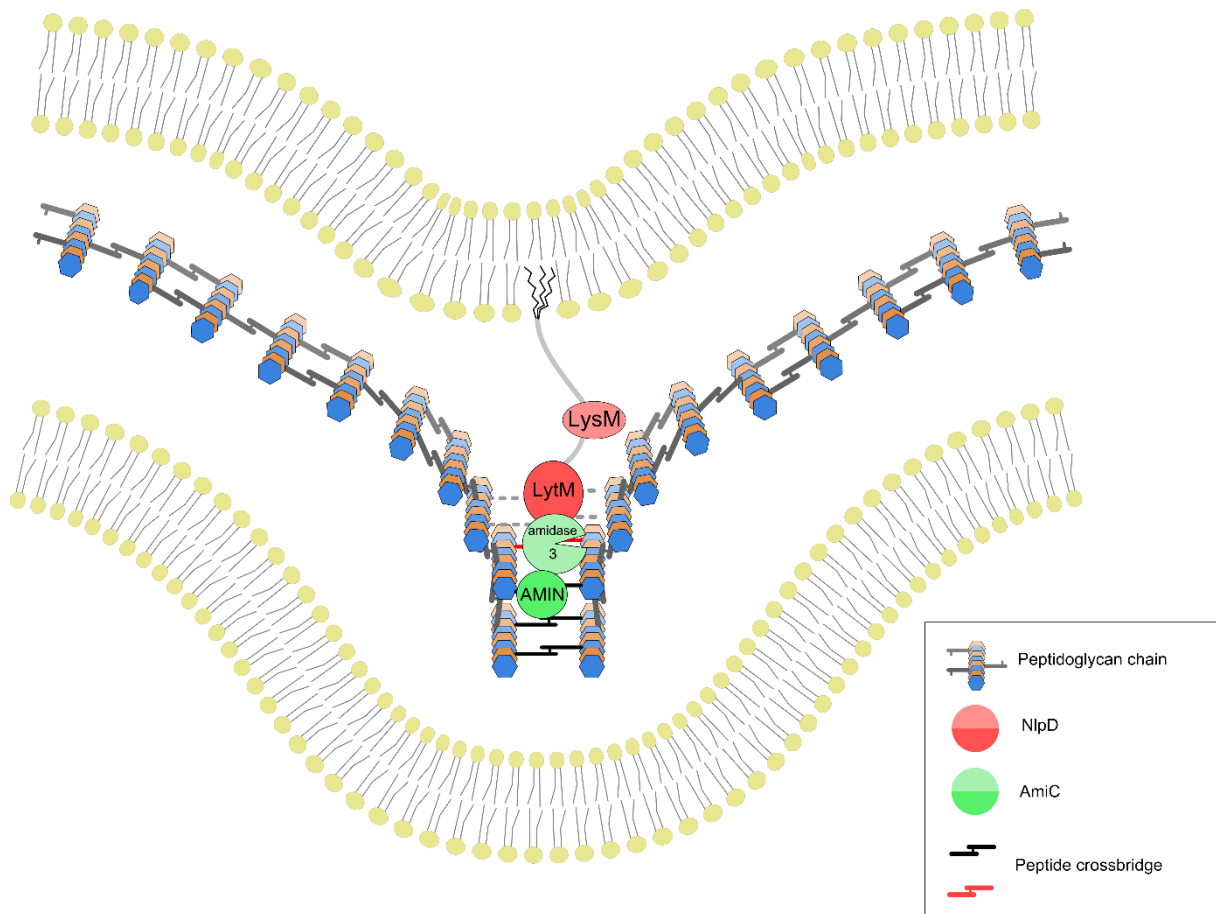


Figure 46. Model for the spatial organization of the AmiC/NlpD couple. Color code is explicated in the black box

Conclusion

The study of the mechanisms involved in bacterial division has been investigated for decades and great understanding has been gained but many questions remain unanswered. This thesis work tried to investigate the structural basis of the lipid II flippase FtsW, the septal amidase AmiC and its activator NlpD.

Recent advances in the understanding of septal peptidoglycan hydrolysis have revealed a high level of regulation in the activation of amidases involved in cell separation. The amidase_3 members AmiA and AmiB have been shown to be activated by the LytM factor EnvC, which is recruited by the ABC transporter-like FtsEX (Uehara et al., 2010, Yang et al., 2012). The latter is suggested to connect the FtsZ dynamics to the activation of amidases at the septum. Another amidase_3 member, AmiC, is regulated by the LytM factor NlpD. The structural basis of the amidase activity regulation by LytM factors is based on the conformational switch of an

inhibitory helix obstructing the active site of the septal amidases. Upon the release of this helix, this active site becomes available for the substrate (Yang et al., 2012).

The crystal structure of AmiC from *E. coli* presented in this work confirms the presence of the inhibitory helix in the active site. The AmiC variant lacking this helix exhibits by itself an activity comparable to that of the wild type AmiC activated by NlpD. Furthermore, the direct interaction between AmiC and NlpD has been detected by microscale thermophoresis with an apparent K_d of about 13 μM. The crystal structure of AmiC also reveals the β-sandwich fold of the AMIN domain, responsible for the septal targeting of AmiC to the division site. The two symmetrical four-stranded β-sheets exhibit highly conserved motifs on the two outer faces. Along with the peptidoglycan binding capacity of the AMIN domain, results obtained so far suggest that the AMIN domain could be involved in the recognition of the septal peptidoglycan architecture or a composition different than the lateral peptidoglycan. Future work will focus on the potential substrate specificity of the catalytic domain of AmiC with or without NlpD and the molecular details of the activation mechanism. The structural determinants for septal targeting and peptidoglycan binding of the AMIN domain of AmiC will be also investigated.

Production screenings of FtsW from different strains were realized and FstW from *E. coli* was purified. Production and purification screenings of other FtsWs will continue to obtain sufficient amounts of this challenging protein for structural investigation.

Information gathered in this work confirms the high level of regulation of the hydrolytic activity at the septum and gives a structural basis for a more precise molecular characterization of the division site targeting. Disruption or over-activation of these regulation mechanisms could represent a new strategy in the development of antibacterial compounds.

Annexes

Annexe 1:

Paper accepted in *Molecular Microbiology*

Rocaboy, M., R. Herman, E. Sauvage, H. Remaut, K. Moonens, M. Terrak, P. Charlier & F. Kerff, (2013) The crystal structure of the cell division amidase AmiC reveals the fold of the AMIN domain, a new peptidoglycan binding domain. *Mol Microbiol* **90**: 267-277.

The crystal structure of the cell division amidase AmiC reveals the fold of the AMIN domain, a new peptidoglycan binding domain

Mathieu Rocaboy,¹ Raphael Herman,¹ Eric Sauvage,¹ Han Remaut,² Kristof Moonens,² Mohammed Terrak,¹ Paulette Charlier^{1**} and Frederic Kerff^{1*}

¹Centre d'Ingénierie des Protéines, University of Liège, Liège, Belgium.

²VIB Laboratory of Structural and Molecular Microbiology, VUB, Brussels, Belgium.

Summary

Binary fission is the ultimate step of the prokaryotic cell cycle. In Gram-negative bacteria like *Escherichia coli*, this step implies the invagination of three biological layers (cytoplasmic membrane, peptidoglycan and outer membrane), biosynthesis of the new poles and eventually, daughter cells separation. The latter requires the coordinated action of the N-acetylmuramyl-L-alanine amidases AmiA/B/C and their LytM activators EnvC and NlpD to cleave the septal peptidoglycan. We present here the 2.5 Å crystal structure of AmiC which includes the first report of an AMIN domain structure, a β -sandwich of two symmetrical four-stranded β -sheets exposing highly conserved motifs on the two outer faces. We show that this N-terminal domain, involved in the localization of AmiC at the division site, is a new peptidoglycan-binding domain. The C-terminal catalytic domain shows an auto-inhibitory alpha helix obstructing the active site. AmiC lacking this helix exhibits by itself an activity comparable to that of the wild type AmiC activated by NlpD. We also demonstrate the interaction between AmiC and NlpD by microscale thermophoresis and confirm the importance of the active site blocking alpha helix in the regulation of the amidase activity.

Accepted 5 August, 2013. For correspondence. *E-mail fkerff@ulg.ac.be; Tel. (+32) 4366 36 20; Fax (+32) 4366 49 54; **E-mail paulette.charlier@ulg.ac.be; Tel. (+32) 4366 36 19; Fax (+32) 4366 49 54.

© 2013 John Wiley & Sons Ltd

Introduction

In *Escherichia coli*, cytokinesis involves the synthesis of new peptidoglycan material at midcell, which after maturation evolves to become the new poles of the daughter cells. Septal peptidoglycan synthesis is directed by a complex of essential and accessory proteins called the divisome and composed of cytoskeletal proteins, peptidoglycan synthases and peptidoglycan hydrolases with their cognate regulatory proteins. This division machinery includes at least 17 proteins: FtsZ, FtsA, ZipA, ZapA, ZapB and ZapC, FtsE, FtsX, FtsK, FtsQ, FtsL, FtsB, FtsW, FtsI (PBP3), PBP1B, FtsN, and AmiC (den Blaauwen *et al.*, 2008). Division is initiated by the polymerization of FtsZ into a ring at midcell underneath the cytoplasmic membrane and the association with the FtsA, ZipA, ZapA, ZapB, ZapC and ZapD proteins (Bi and Lutkenhaus, 1991; Hale and de Boer, 1997; Durand-Heredia *et al.*, 2011; 2012; Galli and Gerdes, 2012). The downstream components are then sequentially recruited, either as single molecules or as preformed subgroups (e.g. FtsQ-FtsB-FtsL and FtsW-PBP3) (Buddelmeijer and Beckwith, 2004; Goehring *et al.*, 2006; Fraipont *et al.*, 2011). PBP3 is a specific DD-transpeptidase essential for septal peptidoglycan synthesis during cell division (Spratt, 1975; Botta and Park, 1981; Weiss and Hilgenfeld, 1997). Its function is believed to be coordinated with that of the major bifunctional glycosyltransferase – transpeptidase peptidoglycan synthase PBP1b during cell division (Bertsche *et al.*, 2006). The function of PBP1b is controlled by the inner membrane and essential divisome protein FtsN, which has been shown to interact and stimulate the activity of PBP1b *in vitro* (Müller *et al.*, 2007) and by the outer membrane linked lipoprotein LpoB, which has also been found to interact with and stimulate the activity of PBP1b (Paradis-Bleau *et al.*, 2010; Typas *et al.*, 2010).

The resulting septal PG formed by the divisome is shared between two daughter cells and must be split to allow cell separation. This process depends on the periplasmic peptidoglycan amidases AmiA, AmiB and AmiC (amidase_3 family, PF01520) (Heidrich *et al.*, 2001). These proteins are Zn²⁺-metallo-enzymes which hydrolyse the amide bond between the stem peptide L-Ala and the

N-acetylmuramic acid (MurNAc). Inactivation of the *amiA*, *amiB* and *amiC* genes results in the formation of long chains of cells, a phenotype that is also observed to a different extent in *amiA* and *amiC* single mutants but not in the *amiB* single mutant (Heidrich *et al.*, 2001). AmiB and AmiC specifically localize to the division site, unlike AmiA, which shows dispersed localization in dividing cells (Bernhardt and de Boer, 2003; Peters *et al.*, 2011). The localization of AmiC to the septal ring is mediated by the non-catalytic N-terminal AMIN domain and requires FtsN (Bernhardt and de Boer, 2003). The activities of the three periplasmic N-acetylmuramyl-L-alanine amidases are regulated by two LytM domain containing proteins (NlpD and EnvC), which do not seem to possess any enzymatic activity (Uehara *et al.*, 2009; Peters *et al.*, 2013). Other LytM proteins with PG hydrolase activity have been identified in some Gram-negative as well as Gram-positive species such as *Staphylococcus aureus* (Collier, 2010; Möll *et al.*, 2010; Poggio *et al.*, 2010; Sycuro *et al.*, 2010). EnvC specifically activates AmiA and AmiB and NlpD specifically activates AmiC (Uehara *et al.*, 2010). Both EnvC and NlpD activators also localize to the division site (Bernhardt and de Boer, 2003; Uehara *et al.*, 2009). Unlike EnvC, AmiB and NlpD require FtsN for localization. A complex regulation mechanism involving proteins localization, peptidoglycan synthesis and degradation, and probably specific septal PG architecture is taking place during cell division (Peters *et al.*, 2011). The *E. coli* mutant lacking EnvC and NlpD forms long cell chains that resemble the triple amidases mutant, which confirms their essential roles in cell separation (Uehara *et al.*, 2009). The amidase activation by EnvC has been found to be regulated by the ATP-binding cassette (ABC) transporter-like complex FtsEX (Yang *et al.*, 2011). This shows that cell wall hydrolysis at the division site leading to cell separation is tightly regulated to prevent uncontrolled cell lysis. Further, the interaction of FtsE with FtsZ suggests a coordination between the hydrolase activity during cell division and Z-ring driven constriction (Corbin *et al.*, 2007).

Five structures of proteins belonging to the amidase_3 family have so far been solved. The activities of four of them appear to be unregulated: the bacteriophage PSA endolysin (Korndörfer *et al.*, 2006), the catalytic domain of the CwlV amidase from *Bacillus polymyxa* (PDB code 1JWQ), a putative amidase from *Neisseria meningitidis* (PDB code 3NCZ) and the catalytic domain of the CD27L endolysin targeting *Clostridium difficile* (Mayer *et al.*, 2011). The fifth structure is the catalytic domain of AmiB from *Bartonella henselae*. This amidase is characterized by the presence of an additional auto-inhibitory helix in the active site. The LytM domain responsible for the regulation of this protein thus needs to displace this helix for the enzyme to be fully active (Yang *et al.*, 2011).

Table 1. Crystallographic data and model refinement statistics.

Diffraction data statistics	
Space group	P2 ₁ 2 ₁ 2 ₁
a, b, c (Å)	59.03, 68.44, 90.58
Resolution range (Å)	49.6–2.5 (2.56–2.5)
Unique reflections	13 337 (1907)
Completeness (%)	99.9 (99.8)
Redundancy	12.7 (7.3)
R _{merge} (%) ^a	20.1 (100.5)
R _{rim} (%) ^b	5.7 (39.7)
Average I/σ	12.8 (2.2)
Refinement statistics	
Resolution range (Å)	90.58–2.5 (2.56–2.5)
R _{cryst} (%) ^c	17.6 (24.2)
R _{free} (%) ^d	23.1 (31.4)
RMS deviations	
Bond lengths (Å)	0.016
Bond angles (°)	1.625
Ramachandran analysis	
Favoured region (%)	95.9
Allowed region (%)	4.1
Outlier region (%)	0

a. $R_{merge} = \sum |I_i - \langle I \rangle| / \sum I_i$, where I_i is the intensity of the measured reflection and $\langle I \rangle$ is the mean intensity of all symmetry related reflections.

b. R_{rim} denotes the precision-indicating merging R factor (Weiss and Hilgenfeld, 1997).

c. $R_{work} = \sum |F_o - F_c| / \sum |F_o|$, where F_o denotes the observed structure factor amplitude, and F_c denotes the structure factor amplitude calculated from the model.

d. R_{free} is similar to R_{work} but calculated with randomly chosen reflections that are omitted from the refinement.

In this work, we present the crystal structure of the N-acetylmuramyl-L-alanine amidase AmiC at a 2.5 Å resolution, revealing the fold of the N-terminal AMIN domain, which consists of two perfectly superimposable four-stranded anti-parallel β-sheets with conserved outer faces. We present evidences that this domain interacts with the peptidoglycan. In the C-terminal catalytic domain, a member of the amidase_3 family, an alpha helix obstructs the active site. We demonstrate the role of this helix in the control of the AmiC activity and also show a direct interaction between AmiC and its activator NlpD. We confirm that the mechanism of activation of AmiC by NlpD consists in the displacement of the alpha helix that blocks the access to the AmiC active site.

Results

Structure of AmiC

Overall fold. The 2.5 Å resolution structure of AmiC was solved by molecular replacement for the catalytic domain and model building for the AMIN domain (see *Experimental procedures* for details). The R_{cryst} and R_{free} values after refinement are 17.6% and 23.1% respectively (Table 1). The final electron density map shows a clear density for the whole protein except for five disordered segments

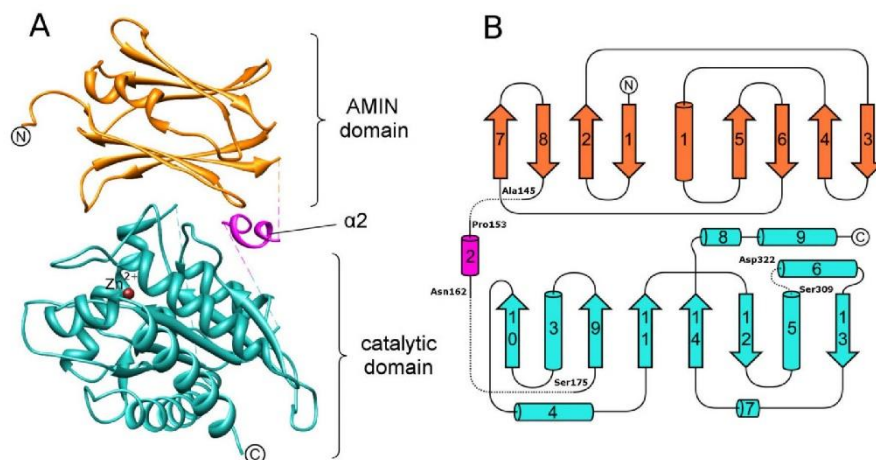


Fig. 1. Crystal structure of AmiC.

A. The AMIN domain, the linker and the catalytic domain are respectively shown in orange, violet and cyan.

B. Topology of AmiC. Stretches of missing residues are represented as dashed lines. Residues preceding and following the missing segments are labelled.

consisting of the first fifteen residues of the N-terminal purification tag, Asn146-Asp152, Lys163-Gln174, Lys310-Phe321 and the last nine residues at the C-terminus. AmiC is made of two structurally distinct domains linked by a flexible segment (Asn146-Gln160) containing the poorly defined $\alpha 2$ helix (Fig. 1). The N-terminal AMIN domain adopts an α -crystallin-like fold with two four-stranded anti-parallel β -sheets for which no structure has been reported so far. The C-terminal zinc-dependent catalytic domain (Ser175-Ala408) has an α/β fold with a six-stranded β -sheet flanked by α helices, and belongs to the amidase_3 family (Fig. 1) (Korndörfer *et al.*, 2006).

AMIN domain (Phe30-Ala145). One of the two β -sheets (β -sheet1) of the AMIN domain of AmiC is composed of strands $\beta 1$ -2-8-7 and the second one (β -sheet2) of strands $\beta 5$ -6-4-3 (Fig. 2B). An additional short α -helix ($\alpha 1$) located near the $\beta 1$ and $\beta 5$ strands closes one side of the β -sandwich. Four RxxxD/E motifs are present on strands $\beta 2$ (Arg49xxxGlu53), $\beta 4$ (Arg70xxxAsp74), $\beta 6$ (Arg112xxxGlu116) and $\beta 8$ (R137xxx-D141). These residues lie on the external face of the two central strands of each β -sheet (Fig. S1). Arg49 and Arg112 are involved in salt bridges with the aspartate of the two motifs located on the adjacent antiparallel strands (Asp141 and Asp74 respectively). This organization suggests that the repetition of the RxxxD/E motifs originates from the double duplication of a two-stranded ancestor encompassing one RxxxD/E motif on the second strand to form the AMIN

domain (de Souza *et al.*, 2008). Both interactions Arg49/Asp141 and Arg112/Asp74 could be important to stabilize a folding intermediate or the final scaffold of the domain.

A ConSurf analysis with AmiC related proteins (Ashkenazy *et al.*, 2010) reveals a patch of conserved residues on the outer face of both β -sheets (Fig. 2D). Moreover, the superposition of β -sheet1 and β -sheet2 (Fig. 2A and C) reveals a striking similarity between them [root mean square deviation (RMSD) of 0.64 Å on 25 residues]. On each face, two small residues are surrounded by five charged residues and two hydrophobic ones (Fig. 2C). ConSurf scores range from 9.8 to 9.9 for each of these residues except for Phe63 and Leu65 with scores of 7.6 and 8.7 respectively. These residues are strictly conserved between β -sheet1 and β -sheet2 except for the Thr51 that is replaced by the shape-equivalent Val114 in β -sheet2.

β -Sheet1 shares numerous interactions with the catalytic domain. In particular, Glu199 of the catalytic domain seems to play the role of electrostatic anchor by sharing multiple hydrogen bonds with the AMIN domain via amino acids that form a hydrophilic pocket (Arg40, Trp42, Thr51 and Arg137). Moreover, Arg49 which belongs to the RxxxE motif of strand $\beta 2$ interacts with the main chain carbonyl of Gly307 in the catalytic domain (Fig. S2). The AMIN domain also interacts with the C-terminus of helix $\alpha 5$ of the catalytic domain via hydrophobic interactions between Val131/Ala132/Phe134 and Leu304/Ile305 respectively. However, a PISA analysis (Krissinel and Henrick, 2007) of the inter-

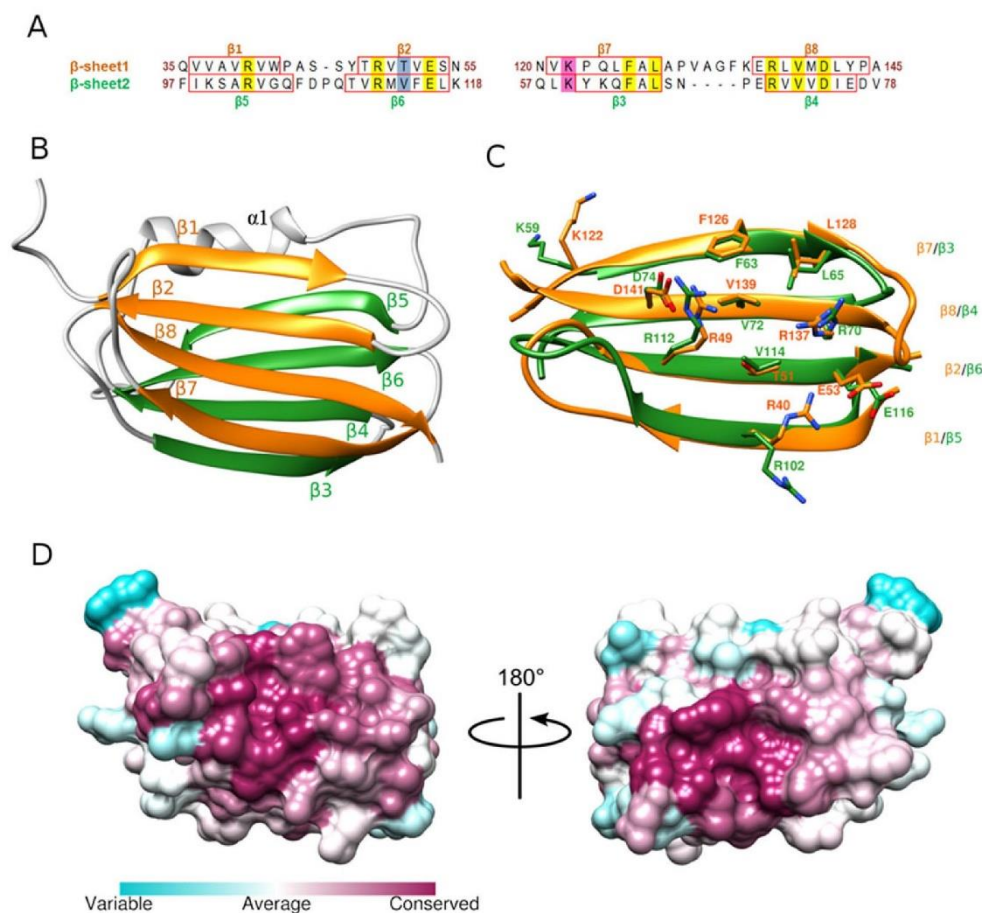


Fig. 2. AMIN domain of AmiC.

A. Sequence alignment of the two β -sheets composing the AMIN domain. β -strands are represented by red boxes. Surface residues conserved in the AMIN domains of amidases are highlighted: in yellow, for residues identical in β -sheet1 and β -sheet2 and in blue for residues of similar shape. Residues not conserved in AMIN domains but identical in the two β -sheets are represented in pink.

B. Cartoon representation of the AMIN domain. The β -sheet1 (strands β 1-2-8-7) and the β -sheet2 (strands β 3-4-6-5) are depicted in orange and green respectively. Coils and helix α 1 are shown in grey.

C. Superposition of the two β -sheets of the AMIN domain. The colour code is the same as in Fig. 2B. Amino-acids highlighted in Fig. 2A are represented as sticks (nitrogens and oxygens are shown in blue and red respectively).

D. Surface representation of the AMIN domain. Conservation of amino-acids of AmiC related proteins is mapped onto the surface from poorly conserved in blue to highly conserved in purple.

action surface between the AMIN and catalytic domains provides a Complex Significance Score of 0 and thus may indicate a crystal packing artefact rather than a specific binding. This suggests a relative flexibility of the AMIN domain that could expose both its conserved surfaces for a simultaneous interaction with two similar partners.

Catalytic domain (Ser175-Ala408). The catalytic domain of AmiC consists in a strongly twisted six-stranded β sheet flanked by six α -helices (Fig. 1). The overall fold is conserved when compared with the five solved structures of the amidase_3 family (Korndörfer *et al.*, 2006; Mayer *et al.*, 2011; Yang *et al.*, 2011). RMSDs between alpha carbons

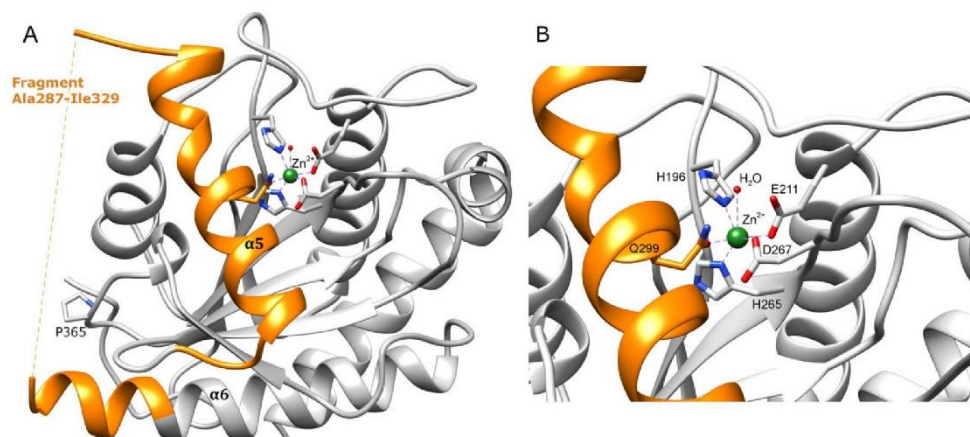


Fig. 3. Catalytic domain of AmiC.

A. Cartoon representation of the catalytic domain. The fragment removed to produce the mutant AmiCΔH5 (see in text) is depicted in orange. The catalytic zinc is shown in green.

B. Close-up on the catalytic site of AmiC. The catalytic zinc and the obstructing helix $\alpha 5$ are shown in green and orange respectively. The chelating residues are represented as sticks (nitrogens and oxygens are shown in blue and red respectively).

range from 0.8 Å (138 alpha carbons) with the N-acetylmuramyl-L-alanine amidase from *Bacillus polymyxa* (PDBID: 1JWQ) to 1.13 Å (85 alpha carbons) with the putative N-acetylmuramyl-L-alanine amidase from *Neisseria meningitidis* (PDBID: 3CZX). In the amidase_3 family, four residues involved in the catalytic activity are strictly conserved. Two histidines (His196 and His265) and one glutamate (Glu211) chelate the catalytic zinc ion (Fig. 3A and B). The fourth conserved residue (Glu373) is thought to be involved in the proton transfer during the catalysis in metallo-proteases (Christianson *et al.*, 1989). As observed in the amidase orthologue AmiB from *B. henselae* [PDBID: 3NE8 (Yang *et al.*, 2012)], the 43 amino-acid segment running from Ala287 to Ile329 contains the helix $\alpha 5$ (Thr290-Gly306) that obstructs the active site, and an extension to the helix $\alpha 6$ (Fig. 3A). Compared with the amidase_3 members with accessible active sites (PDB IDs: 1XOV, 3CZX and 1JWQ), this insertion induces slight conformational rearrangements in the loop connecting the strands $\beta 11$ and $\beta 12$. The most striking one is the position of Asp267 which is flipped in the direction of the catalytic site and coordinates the zinc ion (Fig. 3B) whereas in the other amidase_3 members, this aspartate is replaced by an asparagine oriented to the solvent. This conformation would be unfavourable in AmiC because of a steric hindrance with Leu295 present on helix $\alpha 5$. Zinc chelation by Asp267 could thus simply result from the blocking of the active site by helix $\alpha 5$ and this residue would not be involved in catalysis. Helix $\alpha 5$ also contains

a glutamine residue (Gln299) which chelates the zinc ion. Asn300 and Asp303 are highly conserved in the amidase_3 members exhibiting the additional segment. Asn300 is in close contact with the loop connecting strands $\beta 13$ and $\beta 14$, while Asp303 interacts with the main chain nitrogen of Leu246 located at the beginning of helix $\alpha 4$ (Fig. S3). Asn300, Asp303 as well as Ser302, which is not a conserved residue, appear to be important for the stabilization of the helix in the active site and the interactions that they share with the rest of the catalytic domain have to be disrupted during the activation process. Moreover, the displacement of the obstructing helix requires a relative flexibility of the whole additional segment. This is supported by the absence of interpretable density for the Lys310-Phe321 segment connecting the helices $\alpha 5$ and $\alpha 6$. The corresponding segment (Glu303-Thr308) is also missing in the crystal structure of AmiB from *B. henselae*.

Sequence conservation analysis highlights a proline in position 365 (Fig. 3A) surrounded by polar residues (Gln254, Asp322, Lys363 and Asp366). This highly conserved patch (ConSurf scores ranging from 9.8 to 9.9) is located at the beginning of helix $\alpha 6$, close to the flexible loop connected to the obstructing helix $\alpha 5$ and thus constitutes a potential interaction surface with the activator NlpD. Such an interaction could induce slight conformational changes, like the disruption of the hydrogen bonds shared by Asn300 (see above), and release the obstructing helix from the active site.

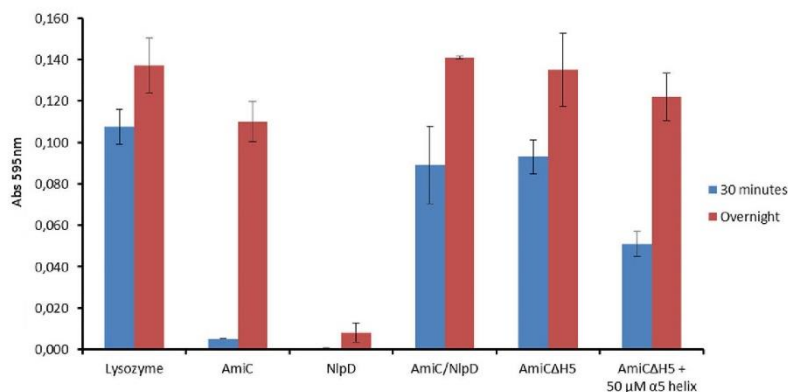


Fig. 4. Helix $\alpha 5$ of AmiC is involved in the activation mechanism by NlpD. The dye-release assay allows the following of the hydrolysis of RBB-labelled peptidoglycan. Each protein was used at $4 \mu\text{M}$ during 30 min (blue bars) or overnight (red bars). Lysozyme was used as positive control. AmiC Δ H5 is the AmiC mutant lacking the Ala287-Ile329 segment. The α -helix is the peptide mimicking the Thr288-Gly306 segment of AmiC. Error bars represent standard deviations from three independent measurements.

AmiC Δ H5 variant has maximal activity independent from NlpD

In order to characterize the activation mechanism of AmiC by the LytM factor NlpD, activity tests based on dye-release assay on Remazol Brilliant Blue (RBB)-labelled peptidoglycan were conducted (Fig. 4). Both proteins were purified and used at a $4 \mu\text{M}$ concentration and incubation times ranging from 30 min to nearly 15 h. The activation of AmiC by NlpD (Uehara *et al.*, 2010) was confirmed, as was the weak activity of AmiC for the shortest incubation time. NlpD did not show any significant activity by itself even for longer incubation times (overnight). Based on the structural data, we also produced and purified an AmiC mutant lacking the Ala287-Ile329 segment that includes helix $\alpha 5$ (AmiC Δ H5). This construct was designed on the basis of the available structures of amidase_3 members lacking this additional segment in order to maintain the overall fold of AmiC. The level of activity of AmiC Δ H5 against the RBB-labelled peptidoglycan is equivalent to that of AmiC activated by NlpD. Moreover, by adding a peptide mimicking helix $\alpha 5$ (Thr288-Gly306) at $50 \mu\text{M}$, the measured activity of AmiC Δ H5 was almost decreased by a factor 2. These results demonstrate that in the absence of helix $\alpha 5$, the AmiC Δ H5 variant becomes unregulated and exhibits maximal activity without activation by NlpD. *In vivo*, such uncontrolled hydrolase activity would have severe consequences for the integrity of the bacterium leading to cell lysis.

AmiC directly interacts with NlpD

In vitro activation of AmiC by NlpD strongly suggests a direct interaction between these two cell division com-

ponents. We tested the interaction by microscale thermophoresis, an immobilization-free technique that allows the monitoring of the displacement of molecules in a temperature gradient generated by an infrared laser. The behaviour of a particle in this gradient rests upon its mass, charge and solvation shell (Jerabek-Willemsen *et al.*, 2011). These properties are then altered when a binding partner is added to the system and titration series allow the determination of the binding affinity. Each protein was titrated against its potential partner and lysozyme was used as a negative control. In different experiments, each partner was labelled in turn with Dylight 650. Binding is detected for each titration involving the couple AmiC/NlpD and no binding is observed with lysozyme (Fig. 5). The apparent K_d values are $11.3 \pm 1.5 \mu\text{M}$ with labelled NlpD and $15.5 \pm 7.2 \mu\text{M}$ with labelled AmiC.

The AMIN domain of AmiC interacts with the peptidoglycan

The AMIN domain of AmiC is known to be necessary and sufficient for its proper localization to the division site (Bernhardt and de Boer, 2003). However, no binding partners have been identified so far. The interaction between the untagged AMIN domain of AmiC and the peptidoglycan was tested by pull-down experiments (Fig. 6). After two washing steps, a significant amount of the AMIN domain is released from the pelleted peptidoglycan in comparison with the control experiment without peptidoglycan. This assay clearly shows an interaction between the AMIN domain of AmiC and the peptidoglycan.

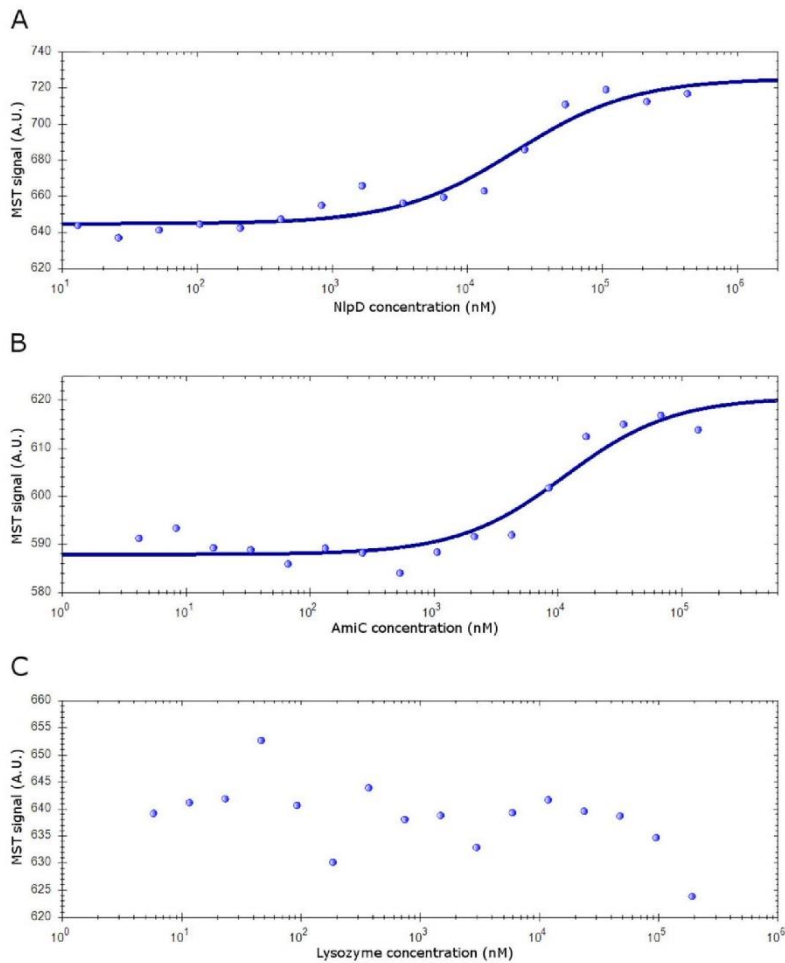


Fig. 5. AmiC directly interacts with NlpD. Microscale thermophoresis (MST) assays were realized with either AmiC labelled (A and C) or NlpD labelled (B) with Dylight 650. The negative control with lysozyme as binding partner did not exhibit the typical binding curve (C). Measures are represented by blue dots and fitted curves by blue lines.

Discussion

The final step of cellular division in *E. coli* consists in the splitting of one constricted cell into two daughter cells. This step requires the concerted action of three different N-acetylmuramyl-L-alanine amidases (AmiA/B/C) in order to cleave the septal peptidoglycan and release two independent cells. These enzymes have been recently shown to be regulated by LytM factors: EnvC activates AmiA/AmiB and NlpD activates AmiC (Uehara *et al.*, 2010).

The crystal structure of AmiC described in this paper highlights two structurally independent domains: the N-terminal AMIN domain and the C-terminal catalytic domain. The structure of the C-terminal amidase_3 domain clearly shows the obstruction of the active site by an α -helix confirming the observation made with the septal amidase AmiB from *B. henselae* (Yang *et al.*, 2012). This α -helix shares several contacts with the rest of the protein including a glutamine that chelates the catalytic zinc ion. The helix has to be displaced in order to accommodate the

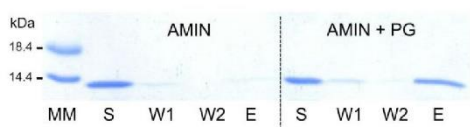


Fig. 6. The AMIN domain of AmiC interacts with the peptidoglycan (PG). 10 μ g of the purified AMIN domain were incubated with peptidoglycan for 2 h at 4°C in the binding buffer. The supernatant (S) was collected after centrifugation at 14 000 *g* during 20 min. The supernatants of two washes followed by centrifugation (W1 and W2) and the remaining pellet resuspended with 2% SDS (E) were analysed by SDS-PAGE. Molecular markers are present in the first lane (MM).

peptidoglycan. For AmiC, this conformational change has been shown to be induced by the LytM factor NlpD (Uehara *et al.*, 2010). Our thermophoresis experiments provide evidence that a direct interaction occurs between AmiC and its cognate activator NlpD. NlpD could directly compete with the AmiC active site for binding the inhibitory α -helix or recognize an adjacent area, inducing a conformation of AmiC that would prevent the α -helix from obstructing the active site. For the latter, a potential candidate is the conserved region of AmiC surrounding Pro365, which is relatively close to the catalytic site.

The addition of the synthetic form of the α 5 helix partially restores the inhibited form of the enzyme. *In vitro* AmiC exhibits a basal activity suggesting a competition between the auto-inhibitory helix and peptidoglycan, with a clear preference for the closed state. In the presence of NlpD, the equilibrium is displaced towards the open state and the active site becomes freely accessible to peptidoglycan.

Although the AMIN domain is packed onto the C-terminal domain in the crystal structure, the presence of a 30 amino acids linker suggests a high flexibility between these two domains. The PISA analysis and the high homology between the AMIN exposed surface and the AMIN surface in contact with the catalytic domain also argue in favour of a crystallographic artefact for the interaction between these two domains. Interestingly, in the outer membrane associated lipoprotein NlpD, a long linker also connects the LysM domain, which binds to the peptidoglycan, to the LytM domain, which activates AmiC. Therefore, the length of these two linkers could spatially regulate the interaction between the activator domain of NlpD and the catalytic domain of AmiC for a correct cell separation process.

In the N-terminal AMIN domain, conserved residues on both outer faces suggest two symmetric interaction regions. The two RxxxD/E motifs present on each face of the AMIN domain represent almost half of the conserved residues. Their conservation and the striking symmetry of this domain suggest the recognition of a repeated pattern like the building blocks of peptidoglycan or the simultane-

ous binding to two identical divisome components. We have tested two potential binding partners of the AMIN domain: FtsN because of its importance for the recruitment of AmiC at the division site, and the peptidoglycan. Our attempts to find an interaction between purified FtsN and the AMIN domain by different pull-down assays were unsuccessful (data not shown), but we were able to show that the AMIN domain directly interacts with the peptidoglycan. Because the AMIN domain is known to be sufficient for the localization of AmiC at the division site, it likely recognizes a specific characteristic of the septal peptidoglycan which remains, however, to be identified. Therefore, the AMIN domain seems to play the role of a septal peptidoglycan anchor that helps to localize the amidase_3 domain to the division site. The amidase activity of AmiC is thus spatially targeted by the AMIN domain and activated by the LytM domain of NlpD which also localizes to the division site.

AmiB is known to be targeted to the cell division site via its N-terminal region (Peters *et al.*, 2011). Secondary structure prediction attributes eight β -strands to this N-terminal targeting domain. However, sequence alignment with the AMIN domain of AmiC (25.8% identity) shows strong similarities only with the conserved amino-acids of the β -sheet2: four identical and three equivalent out of nine residues. For the β -sheet1, only one residue is strictly conserved and one is equivalent. Therefore, unlike the large majority of protein sharing the AMIN-amidase_3 architecture of AmiC, AmiB is characterized by relatively conserved residues on the β -sheet2 but lacks the conserved ones highlighted on the β -sheet1 of AmiC. To our knowledge, AmiB is not in any way deficient in localization at the septum compared with AmiC. The advantage of a symmetrical AMIN domain shared by most homologues of AmiC remains therefore unclear.

Conclusions

The AmiC structure highlights the importance of a helix obstructing the active site of this enzyme. We have shown that an AmiC variant lacking this helix is constitutively active and that the addition of a synthetic α 5 helix peptide restores the inhibited form of the enzyme. Together with the direct interaction between AmiC and NlpD *in vitro*, these results strongly suggest that the displacement of this helix by the cognate AmiC activator NlpD is the basis of the AmiC activation as proposed by Yang *et al.* (2012). The linker connecting the AMIN domain to the catalytic domain could facilitate the activation by NlpD and regulate its spatial localization between the outer membrane and the newly synthesized peptidoglycan layer. Finally, the peptidoglycan binding capacity of the AMIN domain along with its requirement for a proper localization of AmiC at the division site (Bernhardt and de Boer, 2003) argues for a specific recog-

nitiation of the septal peptidoglycan in order to properly position AmiC at the septum.

Experimental procedures

Cloning, overexpression and purification

Escherichia coli K12 genomic DNA was used for PCR amplification of *amiC* and *nlpD* genes with the following primers: 5'-GCGCATATGGGGCGCGATCGTCCGATTG-3'; 5'-CGCTCGAGTCATCCCCTTCTCGCCAGC-3' for *amiC* and 5'-GCGCATATGCTGTGACACTTCAAATCCACCGGCACC-3'; 5'-CGCTCGAGTTATCGTCTGCGCAAATAACGCAG-3' for *nlpD*. For AmiC, the amplified gene codes for a protein without its signal peptide (Gln35-Gly417). NlpD is also produced without its signal peptide (Ser27-Arg380). The gene coding for the AMIN domain (Gln35-Ala145) was amplified with the following primers: 5'-GCGCATATGTCAGGTCGTGGCGGTGCGC-3'; 5'-CGCTCGAGTTAGGCCGGATAGAGTCCATCACC-3'. PCR products have been cloned into pET28-MHL vector (SGC consortium) between NdeI and XhoI sites allowing the expression of the proteins with a 6xHis Tag followed by a TEV cleavage site at the N-terminal position. The gene coding for AmiC lacking residues Ala287 to Ile329 (called AmiC Δ H5) was synthesized *de novo* (Geneart GmbH, Regensburg, Germany) and cloned into pET28-MHL between NdeI and XhoI. After cleavage of the 6xHis Tag with the TEV protease, all the proteins produced with the pET28-MHL contain three additional N-terminal amino acids (Gly-His-Met).

Transformed C43 (DE3) cells were grown in TB medium supplemented with kanamycin (50 μ g ml⁻¹) until the OD₆₀₀ reached 0.8. The culture was then induced with 0.5 mM IPTG for 3 h at 28°C. The cells were harvested by centrifugation (4000 g, 20 min, 4°C) and the pellet was resuspended in the lysis buffer (30 mM Tris/HCl pH 7.5, 300 mM NaCl, 10% Glycerol, 2 mM MgSO₄, 1.5 U ml⁻¹ benzonase) before disruption using an Emulsiflex C3 homogenizer. The lysate was spun down at 40 000 g for 30 min and the supernatant was filtered through a 0.22 μ m membrane (Millex-GP, Millipore) before purification.

The sample was loaded onto a HisTrap column (GE Healthcare) equilibrated with buffer A (30 mM Tris-HCl pH 7.5, 300 mM NaCl, 10% Glycerol). The column was washed with Buffer A containing 50 mM Imidazole and the proteins were eluted with increasing concentration of imidazole in buffer A: between 50 and 100 mM for NlpD and between 150 and 200 mM for AmiC and the AMIN domain. AmiC Δ H5 was isolated by batch purification with Ni-NTA agarose gel (GE Healthcare) and eluted at 250–300 mM imidazole in buffer A. After SDS-PAGE analysis pure fractions were pooled and dialysed overnight against buffer A, frozen with liquid nitrogen and stored at -80°C at approximately 30 μ M. For interaction and activity tests, His-tags were removed by an overnight incubation at 4°C with the TEV-protease. The cleaved tags, the uncleaved protein and the His-tagged TEV-protease were removed by a second passage on a HisTrap column (GE Healthcare).

Crystallization and data collection

His-tagged AmiC was concentrated to 13 mg ml⁻¹ and crystallized using the hanging-drop vapour diffusion method. 1 μ l

of protein was mixed with 1 μ l of precipitant buffer (20% PEG 8000, 0.1 M CABS pH 12, 20 mM CoCl₂) and crystals grew at room temperature. The crystals were transferred into a cryoprotectant solution containing 50% glycerol before flash-freezing in a liquid nitrogen bath. Diffraction data were collected at the European Synchrotron Radiation Source Facility FIP-BM30a beamline (Grenoble).

Data processing

Data were integrated and scaled with Mosflm (Leslie and Powell, 2007) and Scala from the CCP4 software package (1994). A first model of the catalytic domain of AmiC was determined by molecular replacement using the structure of AmiB from *B. henselae* as a search model (PDB ID: 3ne8). Five poly-alanine β -strands of the N-terminal AMIN domain were built in the electron density and subjected to a DALI search. The most structurally related structure, the chaperone Hsp26, was used as a template to build seven poly-alanine β -strands of the AMIN domain. This partial model was provided to the software ARP/wARP (Morris *et al.*, 2003) to build and assign the whole domain. Helix α 2 was solved by fitting the Leu140-Leu144 (LLALL) segment in the electron density and, although the density was less clear for the residues, the helix could be completed from Pro139 to Asn148.

Structure analysis

The ConSurf server was used to analyse the amino acid conservation on the surface of AmiC (<http://consurf.tau.ac.il/>) (Ashkenazy *et al.*, 2010). The homologous sequences were selected using three iterations of CSI-Blast within the UNIREF-90 database and the 150 most representative sequences were used to generate conservation scores (Table S1). The PISA server provided an analysis of the interface between N and C-terminal domains (http://www.ebi.ac.uk/msd-srv/prot_int/pistart.html) (Krissinel and Henrick, 2007). The different figures were generated with Chimera (Pettersen *et al.*, 2004).

Preparation of peptidoglycan sacculi and labelling with Remazol Brilliant Blue

Peptidoglycan sacculi were prepared from MC1061 cells as described earlier (Glauner *et al.*, 1988). The RBB-labelled peptidoglycan was prepared as described (Uehara *et al.*, 2009). The sacculi were incubated overnight with 20 mM RBB (Sigma) in 0.25 M NaOH at 37°C. The next morning, the sample was neutralized by addition of HCl before centrifugation (16 000 g, 20 min, room temperature). The pelleted sacculi were then washed with MilliQ water until no more soluble RBB was detected after centrifugation. The labelled sacculi were finally resuspended in water with 0.02% sodium azide and stored at 4°C.

Activity tests with RBB-labelled peptidoglycan

For activity tests, 10 μ l of the RBB-PG were incubated with 4 μ M of AmiC and/or NlpD (without His tag) in 30 mM Tris/HCl buffer pH 7.5, 300 mM NaCl and 10% glycerol (100 μ l total) for 30 min to 15 h (overnight) in a total volume of 100 μ l. The

samples were centrifuged for 10 min at 14 000 *g* and the absorbance of the supernatant was measured at 595 nm (Tecan Infinite 200 PRO microplate reader, Tecan Austria GmbH, Austria). Reported results were standardized with a negative control consisting of 10 μ l of RBB-PG and 90 μ l of the aforementioned buffer. Lysozyme was used as a positive control at a 4 μ M concentration. The peptide corresponding to the α 5 helix (Thr288-Gly306) was synthesized by Genscript (NJ, USA).

Peptidoglycan-binding assay

The pull down experiments were carried out with the untagged AMIN domain. 10 μ g of protein was incubated 2 h either with or without peptidoglycan in the binding buffer (30 mM Tris pH 6.8, 50 mM NaCl, 10 mM MgCl₂) in a total volume of 100 μ l. The samples were centrifuged for 20 min at 14 000 *g*. The pellets were washed twice in 150 μ l of binding buffer and then resuspended in 40 μ l of SDS 2% and incubated for 1 h. The supernatants of the binding step, the washing steps and the resuspended pellet were analysed by SDS-PAGE.

Microscale thermophoresis

Interactions between freshly prepared AmiC and NlpD (without 6x His Tags) were measured using microscale thermophoresis (Jerabek-Willemsen *et al.*, 2011) with a Monolith NT.115 (NanoTemper Technologies GmbH, Munich, Germany). Each protein was in turn labelled with DyLight 650 (Thermo Scientific) and mixed with sixteen twofold serial dilutions of the other unlabelled protein starting from 272 μ M for AmiC and 426 μ M for NlpD. The final buffer contained 50 mM Tris-HCl pH 7.5, 150 mM NaCl, 10 mM MgCl₂, 0.05 % Tween-20 and measurement were performed in hydrophilic capillaries with 100% LED power and 80% IR-laser power. NanoTemper Analysis 1.2.101 software was used for the fitting of the data and determination of the apparent *K*_d values. The experiments were performed three times for each combination.

Accession code

Atomic coordinates and experimental structure factors for AmiC have been deposited in the Protein Data Bank under the accession code 4BIN.

Acknowledgements

We thank Jean-Marie Frère for critical reading of the manuscript. We also thank the staff of beamline BM30a at ESRF for assistance in X-ray data collection. This work was supported in part by the European Commission Sixth Framework Program grants LSMH-CT-EUR-INTAFAR 2004-512138, by the Belgian Program on Interuniversity Poles of Attraction initiated by the Belgian State, Prime Minister's Office, Science Policy programming (IAP no. P6/19 and P7/44), by the Fonds de la Recherche Scientifique (IISN 4.4509.09, IISN 4.4503.11) and the University of Liège (Fonds spéciaux,

Crédit classique). M. R. is recipient of a FRIA (Fonds de la Recherche pour l'Industrie et l'Agriculture) fellowship (F.R.S.-FNRS, Brussels, Belgium). F. K. and M. T. are research associates of the FRS-FNRS.

References

- Ashkenazy, H., Erez, E., Martz, E., Pupko, T., and Ben-Tal, N. (2010) ConSurf 2010: calculating evolutionary conservation in sequence and structure of proteins and nucleic acids. *Nucleic Acids Res* **38**: W529–W533.
- Bernhardt, T.G., and De Boer, P.A.J. (2003) The *Escherichia coli* amidase AmiC is a periplasmic septal ring component exported via the twin-arginine transport pathway. *Mol Microbiol* **48**: 1171–1182.
- Bertsche, U., Kast, T., Wolf, B., Fraipont, C., Aarsman, M.E.G., Kannenberg, K., *et al.* (2006) Interaction between two murein (peptidoglycan) synthases, PBP3 and PBP1B, in *Escherichia coli*. *Mol Microbiol* **61**: 675–690.
- Bi, E.F., and Lutkenhaus, J. (1991) FtsZ ring structure associated with division in *Escherichia coli*. *Nature* **354**: 161–164.
- Botta, G.A., and Park, J.T. (1981) Evidence for involvement of penicillin-binding protein 3 in murein synthesis during septation but not during cell elongation. *J Bacteriol* **145**: 333–340.
- Buddelmeijer, N., and Beckwith, J. (2004) A complex of the *Escherichia coli* cell division proteins FtsL, FtsB and FtsQ forms independently of its localization to the septal region. *Mol Microbiol* **52**: 1315–1327.
- Christianson, D.W., Mangani, S., Shoham, G., and Lipscomb, W.N. (1989) Binding of D-phenylalanine and D-tyrosine to carboxypeptidase A. *J Biol Chem* **264**: 12849–12853.
- Collier, J. (2010) A new factor stimulating peptidoglycan hydrolysis to separate daughter cells in *Caulobacter crescentus*. *Mol Microbiol* **77**: 11–14.
- Corbin, B.D., Wang, Y., Beuria, T.K., and Margolin, W. (2007) Interaction between cell division proteins FtsE and FtsZ. *J Bacteriol* **189**: 3026–3035.
- De Souza, R.F., Anantharaman, V., De Souza, S.J., Aravind, L., and Gueiros-Filho, F.J. (2008) AMIN domains have a predicted role in localization of diverse periplasmic protein complexes. *Bioinformatics* **24**: 2423–2426.
- Den Blaauwen, T., De Pedro, M.A., Nguyen-Distèche, M., and Ayala, J.A. (2008) Morphogenesis of rod-shaped sacculi. *FEMS Microbiol Rev* **32**: 321–344.
- Durand-Heredia, J., Rivkin, E., Fan, G., Morales, J., and Janakiraman, A. (2012) Identification of ZapD as a cell division factor that promotes the assembly of FtsZ in *Escherichia coli*. *J Bacteriol* **194**: 3189–3198.
- Durand-Heredia, J.M., Yu, H.H., De Carlo, S., Lesser, C.F., and Janakiraman, A. (2011) Identification and characterization of ZapC, a stabilizer of the FtsZ ring in *Escherichia coli*. *J Bacteriol* **193**: 1405–1413.
- Fraipont, C., Alexeeva, S., Wolf, B., Van Der Ploeg, R., Schloesser, M., Den Blaauwen, T., and Nguyen-Distèche, M. (2011) The integral membrane FtsW protein and peptidoglycan synthase PBP3 form a subcomplex in *Escherichia coli*. *Microbiology* **157**: 251–259.
- Galli, E., and Gerdes, K. (2012) FtsZ-ZapA-ZapB interactome of *Escherichia coli*. *J Bacteriol* **194**: 292–302.

- Glauner, B., Höltje, J.V., and Schwarz, U. (1988) The composition of the murein of *Escherichia coli*. *J Biol Chem* **263**: 10088–10095.
- Goehring, N.W., Gonzalez, M.D., and Beckwith, J. (2006) Premature targeting of cell division proteins to midcell reveals hierarchies of protein interactions involved in division assembly. *Mol Microbiol* **61**: 33–45.
- Hale, C.A., and De Boer, P.A.J. (1997) Direct binding of FtsZ to ZipA, an essential component of the septal ring structure that mediates cell division in *E. coli*. *Cell* **88**: 175–185.
- Heidrich, C., Templin, M.F., Ursinus, A., Merdanovic, M., Berger, J., Schwarz, H., et al. (2001) Involvement of N-acetylmuramyl-L-alanine amidases in cell separation and antibiotic-induced autolysis of *Escherichia coli*. *Mol Microbiol* **41**: 167–178.
- Jerabek-Willemsen, M., Wienken, C.J., Braun, D., Baaske, P., and Dühr, S. (2011) Molecular interaction studies using microscale thermophoresis. *Assay Drug Dev Technol* **9**: 342–353.
- Korndörfer, I.P., Danzer, J., Schmelcher, M., Zimmer, M., Skerra, A., and Loessner, M.J. (2006) The crystal structure of the bacteriophage PSA endolysin reveals a unique fold responsible for specific recognition of *Listeria* cell walls. *J Mol Biol* **364**: 678–689.
- Krissinel, E., and Henrick, K. (2007) Inference of macromolecular assemblies from crystalline state. *J Mol Biol* **372**: 774–797.
- Leslie, A.G.W., and Powell, H.R. (2007) Processing diffraction data with mosflm. In *Evolving Methods for Macromolecular Crystallography*. Read, R.J., and Sussman, J.L. (eds). Dordrecht: Springer Netherlands, pp. 41–51.
- Mayer, M.J., Garefalaki, V., Spoerl, R., Narbad, A., and Meijers, R. (2011) Structure-based modification of a *Clostridium difficile*-targeting endolysin affects activity and host range. *J Bacteriol* **193**: 5477–5486.
- Möll, A., Schlimpert, S., Briegel, A., Jensen, G.J., and Thanbichler, M. (2010) DipM, a new factor required for peptidoglycan remodelling during cell division in *Caulobacter crescentus*. *Mol Microbiol* **77**: 90–107.
- Morris, R.J., Perrakis, A., and Lamzin, V.S. (2003) ARP/wARP and automatic interpretation of protein electron density maps. *Methods Enzymol* **374**: 229–244.
- Müller, P., Ewers, C., Bertsche, U., Anstett, M., Kallis, T., Breukink, E., et al. (2007) The essential cell division protein FtsN interacts with the murein (peptidoglycan) synthase PBP1B in *Escherichia coli*. *J Biol Chem* **282**: 36394–36402.
- Paradis-Bleau, C., Markovski, M., Uehara, T., Lupoli, T.J., Walker, S., Kahne, D.E., and Bernhardt, T.G. (2010) Lipoprotein cofactors located in the outer membrane activate bacterial cell wall polymerases. *Cell* **143**: 1110–1120.
- Peters, N.T., Dinh, T., and Bernhardt, T.G. (2011) A fail-safe mechanism in the septal ring assembly pathway generated by the sequential recruitment of cell separation amidases and their activators. *J Bacteriol* **193**: 4973–4983.
- Peters, N.T., Morlot, C., Yang, D.C., Uehara, T., Vernet, T., and Bernhardt, T.G. (2013) Structure-function analysis of the LytM domain of EnvC, an activator of cell wall remodelling at the *Escherichia coli* division site. *Mol Microbiol* **89**: 690–701.
- Pettersen, E.F., Goddard, T.D., Huang, C.C., Couch, G.S., Greenblatt, D.M., Meng, E.C., and Ferrin, T.E. (2004) UCSF Chimera – a visualization system for exploratory research and analysis. *J Comput Chem* **25**: 1605–1612.
- Poggio, S., Takacs, C.N., Vollmer, W., and Jacobs-Wagner, C. (2010) A protein critical for cell constriction in the Gram-negative bacterium *Caulobacter crescentus* localizes at the division site through its peptidoglycan-binding LysM domains. *Mol Microbiol* **77**: 74–89.
- Spratt, B.G. (1975) Distinct penicillin binding proteins involved in the division, elongation, and shape of *Escherichia coli* K12. *Proc Natl Acad Sci USA* **72**: 2999–3003.
- Sycuro, L.K., Pincus, Z., Gutierrez, K.D., Biboy, J., Stern, C.A., Vollmer, W., and Salama, N.R. (2010) Peptidoglycan crosslinking relaxation promotes *Helicobacter pylori*'s helical shape and stomach colonization. *Cell* **141**: 822–833.
- Typas, A., Banzhaf, M., Van Den Berg Van Sapareoa, B., Verheul, J., Biboy, J., Nichols, R.J., et al. (2010) Regulation of peptidoglycan synthesis by outer-membrane proteins. *Cell* **143**: 1097–1109.
- Uehara, T., Dinh, T., and Bernhardt, T.G. (2009) LytM-domain factors are required for daughter cell separation and rapid ampicillin-induced lysis in *Escherichia coli*. *J Bacteriol* **191**: 5094–5107.
- Uehara, T., Parzych, K.R., Dinh, T., and Bernhardt, T.G. (2010) Daughter cell separation is controlled by cytokinetic ring-activated cell wall hydrolysis. *EMBO J* **29**: 1412–1422.
- Weiss, M.S., and Hilgenfeld, R. (1997) On the use of the merging R factor as a quality indicator for X-ray data. *J Appl Crystallogr* **30**: 203–205.
- Yang, D.C., Peters, N.T., Parzych, K.R., Uehara, T., Markovski, M., and Bernhardt, T.G. (2011) An ATP-binding cassette transporter-like complex governs cell-wall hydrolysis at the bacterial cytokinetic ring. *Proc Natl Acad Sci USA* **108**: 18209–18210.
- Yang, D.C., Tan, K., Joachimiak, A., and Bernhardt, T.G. (2012) A conformational switch controls cell wall-remodelling enzymes required for bacterial cell division. *Mol Microbiol* **85**: 768–781.

Supporting information

Additional supporting information may be found in the online version of this article at the publisher's web-site.

Annexe 2:

List of protein sequences related to AmiC used for the amino-acid conservation analysis with Consurf

UniRef90_P63884_30_408 N-acetylmuramoyl-L-alanine amidase AmiC n=454 Tax=Enterobacteriaceae RepID=AMIC_ECOL6
UniRef90_G9Z3C8_55_433 N-acetylmuramoyl-L-alanine amidase n=1 Tax=Yokenella regensburgei ATCC 43003 RepID=G9Z3C8_9ENTR
UniRef90_H5V0D0_30_411 N-acetylmuramoyl-L-alanine amidase AmiC n=1 Tax=Escherichia hermannii NBRC 105704 RepID=H5V0D0_ESCHE
UniRef90_H3LSY8_67_433 N-acetylmuramoyl-L-alanine amidase AmiC n=3 Tax=Klebsiella oxytoca RepID=H3LSY8_KLEOX
UniRef90_I2EF79_30_408 N-acetylmuramoyl-L-alanine amidase AmiC n=4 Tax=Cronobacter RepID=I2EF79_ENTSA
UniRef90_E5YIN6_30_408 N-acetylmuramoyl-L-alanine amidase n=2 Tax=Enterobacteriaceae RepID=E5YIN6_9ENTR
UniRef90_D4BWR1_30_407 N-acetylmuramoyl-L-alanine amidase AmiC n=5 Tax=Providencia RepID=D4BWR1_PRORE
UniRef90_C7BKK1_30_407 N-acetylmuramoyl-L-alanine amidase n=2 Tax=Photorhabdus RepID=C7BKK1_PHOAA
UniRef90_Q8CZY4_36_414 N-acetylmuramoyl-L-alanine amidase AmiC n=26 Tax=Yersinia RepID=Q8CZY4_YERPE
UniRef90_I2B5Y2_30_405 N-acetylmuramoyl-L-alanine amidase AmiC n=1 Tax=Escherichia blattae DSM 4481 RepID=I2B5Y2_ESCBL
UniRef90_D4F2D6_30_412 N-acetylmuramoyl-L-alanine amidase AmiC n=4 Tax=Edwardsiella RepID=D4F2D6_EDWTA
UniRef90_C4UJ47_30_408 N-acetylmuramoyl-L-alanine amidase AmiC n=1 Tax=Yersinia ruckeri ATCC 29473 RepID=C4UJ47_YERRU
UniRef90_D4E2A8_30_410 N-acetylmuramoyl-L-alanine amidase n=7 Tax=Serratia RepID=D4E2A8_SEROD
UniRef90_F4MUX5_30_407 N-acetylmuramoyl-L-alanine amidase AmiC n=12 Tax=Yersinia RepID=F4MUX5_YEREN
UniRef90_C6DAG2_30_409 N-acetylmuramoyl-L-alanine amidase n=5 Tax=Pectobacterium RepID=C6DAG2_PECCP
UniRef90_H8NMM7_30_408 N-acetylmuramoyl-L-alanine amidase n=3 Tax=Rahnella RepID=H8NMM7_RAHAQ
UniRef90_D3VCM3_30_406 N-acetylmuramoyl-L-alanine amidase n=1 Tax=Xenorhabdus nematophila ATCC 19061 RepID=D3VCM3_XENNA
UniRef90_D3V592_31_406 N-acetylmuramoyl-L-alanine amidase n=1 Tax=Xenorhabdus bovienii SS-2004 RepID=D3V592_XENBS
UniRef90_C6CHQ3_30_408 N-acetylmuramoyl-L-alanine amidase n=3 Tax=Dickeya RepID=C6CHQ3_DICZE
UniRef90_G7LRP5_30_408 Cell wall hydrolase/autolysin n=1 Tax=Brenneria sp. EniD312 RepID=G7LRP5_9ENTR
UniRef90_C2LKY0_30_409 N-acetylmuramoyl-L-alanine amidase AmiC n=3 Tax=Proteus RepID=C2LKY0_PROMI
UniRef90_G2IZF0_30_402 N-acetylmuramoyl-L-alanine amidase AmiC n=2 Tax=Pseudogulbenkiania RepID=G2IZF0_PSEUL
UniRef90_E6WGD9_30_406 Cell wall hydrolase/autolysin n=1 Tax=Pantoea sp. At-9b RepID=E6WGD9_PANSA
UniRef90_Q7NRF9_22_391 Probable N-acetylmuramoyl-L-alanine amidase n=1

Tax=Chromobacterium violaceum ATCC 12472 RepID=Q7NRF9_CHRVO
UniRef90_I0QSH7_30_412 N-acetylmuramoyl-L-alanine amidase n=1 Tax=Serratia sp. M24T3 RepID=I0QSH7_9ENTR
UniRef90_D8MW97_29_408 N-acetylmuramoyl-L-alanine amidase n=1 Tax=Erwinia billingiae Eb661 RepID=D8MW97_ERWBE
UniRef90_C6CC19_30_409 N-acetylmuramoyl-L-alanine amidase n=1 Tax=Dickeya dadantii Ech703 RepID=C6CC19_DICDC
UniRef90_D2U282_33_407 N-acetylmuramoyl-L-alanine amidase n=1 Tax=Arsenophonus nasoniae RepID=D2U282_9ENTR
UniRef90_D0FVE6_29_406 N-acetylmuramoyl-L-alanine amidase n=7 Tax=Erwinia RepID=D0FVE6_ERWPE
UniRef90_A6SV57_40_423 N-acetylmuramoyl-L-alanine amidase n=2 Tax=Oxalobacteraceae RepID=A6SV57_JANMA
UniRef90_Q2NRI9_36_411 N-acetylmuramoyl-L-alanine amidase n=1 Tax=Sodalis glossinidius str. 'morsitans' RepID=Q2NRI9_SODGM
UniRef90_E1SCT8_30_404 N-acetylmuramoyl-L-alanine amidase n=4 Tax=Pantoea RepID=E1SCT8_PANVC
UniRef90_G7UGD1_30_405 N-acetylmuramoyl-L-alanine amidase AmiC n=4 Tax=Pantoea RepID=G7UGD1_PANAN
UniRef90_C1DBT6_29_403 Probable N-acetylmuramoyl-L-alanine amidase n=1 Tax=Laribacter hongkongensis HLHK9 RepID=C1DBT6_LARHH
UniRef90_G0ADD1_40_438 N-acetylmuramoyl-L-alanine amidase AmiC n=1 Tax=Collimonas fungivorans Ter331 RepID=G0ADD1_COLFT
UniRef90_D8J019_40_442 N-acetylmuramoyl-L-alanine amidase protein n=2 Tax=Herbaspirillum RepID=D8J019_HERSS
UniRef90_C3XBA4_34_428 N-acetylmuramoyl-L-alanine amidase n=1 Tax=Oxalobacter formigenes OXCC13 RepID=C3XBA4_OXAFO
UniRef90_Q1H1I8_30_430 N-acetylmuramoyl-L-alanine amidase n=1 Tax=Methylobacillus flagellatus KT RepID=Q1H1I8_METFK
UniRef90_E5UHS6_34_408 N-acetylmuramoyl-L-alanine amidase amiC n=3 Tax=Neisseria RepID=E5UHS6_NEIMU
UniRef90_E7RXW3_82_462 N-acetylmuramoyl-L-alanine amidase n=1 Tax=Lautropia mirabilis ATCC 51599 RepID=E7RXW3_9BURK
UniRef90_G4CT34_30_417 N-acetylmuramoyl-L-alanine amidase n=1 Tax=Neisseria wadsworthii 9715 RepID=G4CT34_9NEIS
UniRef90_F1W4X7_25_425 N-acetylmuramoyl-L-alanine amidase n=1 Tax=Oxalobacteraceae bacterium IMCC9480 RepID=F1W4X7_9BURK
UniRef90_C3X533_34_424 N-acetylmuramoyl-L-alanine amidase n=1 Tax=Oxalobacter formigenes HOxBL5 RepID=C3X533_OXAFO
UniRef90_UPI0000E87E6E_23_399 N-acetylmuramoyl-L-alanine amidase n=1 Tax=Methylophilales bacterium HTCC2181 RepID=UPI0000E87E6E
UniRef90_C6M7L8_36_410 N-acetylmuramoyl-L-alanine amidase AmiC n=5 Tax=Neisseria RepID=C6M7L8_NEISI
UniRef90_D5CR30_21_417 N-acetylmuramoyl-L-alanine amidase n=1 Tax=Sideroxydans lithotrophicus ES-1 RepID=D5CR30_SIDLE
UniRef90_Q9K0V3_35_409 N-acetylmuramoyl-L-alanine amidase AmiC n=48 Tax=Neisseria RepID=AMIC_NEIMB
UniRef90_G4CKS8_33_419 N-acetylmuramoyl-L-alanine amidase n=1 Tax=Neisseria shayegani 871 RepID=G4CKS8_9NEIS
UniRef90_D6KY56_48_420 N-acetylmuramoyl-L-alanine amidase AmiC n=1 Tax=Simonsiella muelleri ATCC 29453 RepID=D6KY56_9NEIS

UniRef90_D9SDS3_31_410 N-acetylmuramoyl-L-alanine amidase n=1 Tax=Gallionella capsiferriformans ES-2 RepID=D9SDS3_GALCS
UniRef90_H0PYZ1_44_446 N-acetylmuramoyl-L-alanine amidase n=1 Tax=Azoarcus sp. KH32C RepID=H0PYZ1_9RHOO
UniRef90_UPI000248F995_44_434 N-acetylmuramoyl-L-alanine amidase n=1 Tax=Advenella kashmirensis WT001 RepID=UPI000248F995
UniRef90_G2DIV8_34_419 N-acetylmuramoyl-L-alanine amidase n=2 Tax=Neisseria weaveri RepID=G2DIV8_9NEIS
UniRef90_F5RHM0_40_448 N-acetylmuramoyl-L-alanine amidase n=1 Tax=Methyloversatilis universalis FAM5 RepID=F5RHM0_9RHOO
UniRef90_G8QLB5_42_441 N-acetylmuramoyl-L-alanine amidase n=1 Tax=Dechlorosoma suillum PS RepID=G8QLB5_AZOSU
UniRef90_Q47BK2_39_433 Cell wall hydrolase/autolysin n=1 Tax=Dechloromonas aromatica RCB RepID=Q47BK2_DECAR
UniRef90_Q3SIQ3_37_404 N-acetylmuramoyl-L-alanine amidase n=1 Tax=Thiobacillus denitrificans ATCC 25259 RepID=Q3SIQ3_THIDA
UniRef90_F4GUF6_21_423 Putative uncharacterized protein n=1 Tax=Pusillimonas sp. T7-7 RepID=F4GUF6_PUSST
UniRef90_A9I7Y8_43_445 AmiC protein n=1 Tax=Bordetella petrii DSM 12804 RepID=A9I7Y8_BORPD
UniRef90_A6GSM0_29_437 N-Acetylmuramoyl-L-alanine amidase n=1 Tax=Limnobacter sp. MED105 RepID=A6GSM0_9BURK
UniRef90_B1XVL5_40_441 N-acetylmuramoyl-L-alanine amidase n=2 Tax=Polynucleobacter necessarius RepID=B1XVL5_POLNS
UniRef90_E8UE27_92_503 N-acetylmuramoyl-L-alanine amidase n=1 Tax=Taylorella equigenitalis MCE9 RepID=E8UE27_TAYEM
UniRef90_D7N403_51_428 N-acetylmuramoyl-L-alanine amidase AmiC n=1 Tax=Neisseria sp. oral taxon 014 str. F0314 RepID=D7N403_9NEIS
UniRef90_Q0AEV4_31_421 N-acetylmuramoyl-L-alanine amidase n=1 Tax=Nitrosomonas eutropha C91 RepID=Q0AEV4_NITEC
UniRef90_C0DSH8_28_404 Putative uncharacterized protein n=1 Tax=Eikenella corrodens ATCC 23834 RepID=C0DSH8_EIKCO
UniRef90_E3HHL8_44_448 N-acetylmuramoyl-L-alanine amidase n=5 Tax=Achromobacter RepID=E3HHL8_ACHXA
UniRef90_F2BF22_33_421 N-acetylmuramoyl-L-alanine amidase n=1 Tax=Neisseria bacilliformis ATCC BAA-1200 RepID=F2BF22_9NEIS
UniRef90_F2N197_28_402 N-acetylmuramoyl-L-alanine amidase n=4 Tax=Pseudomonas stutzeri RepID=F2N197_PSEU6
UniRef90_Q82WLS_34_421 Cell wall hydrolase/autolysin n=1 Tax=Nitrosomonas europaea ATCC 19718 RepID=Q82WLS_NITEU
UniRef90_A1K4V5_54_446 Conserved hypothetical N-acetylmuramoyl-L-alanine amidase n=1 Tax=Azoarcus sp. BH72 RepID=A1K4V5_AZOSB
UniRef90_Q2SBB8_18_371 N-acetylmuramoyl-L-alanine amidase n=1 Tax=Hahella chejuensis KCTC 2396 RepID=Q2SBB8_HAHCH
UniRef90_A6VD60_39_412 N-acetylmuramoyl-L-alanine amidase n=17 Tax=Pseudomonas RepID=A6VD60_PSEA7
UniRef90_Q2Y600_53_442 N-acetylmuramoyl-L-alanine amidase n=1 Tax=Nitrosospira multiformis ATCC 25196 RepID=Q2Y600_NITMU
UniRef90_Q5P219_54_431 N-acetylmuramoyl-L-alanine amidase, AMIC protein n=1 Tax=Aromatoleum aromaticum EbN1 RepID=Q5P219_AROAE
UniRef90_G6YNU4_26_382 N-acetylmuramoyl-L-alanine amidase n=2 Tax=Marinobacter

RepID=G6YNU4_9ALTE
UniRef90_F3KEM8_23_376 N-acetylmuramoyl-L-alanine amidase n=1 Tax=gamma proteobacterium IMCC2047 RepID=F3KEM8_9GAMM
UniRef90_B8KW61_32_391 N-acetylmuramoyl-L-alanine amidase AmiC n=1 Tax=gamma proteobacterium NOR51-B RepID=B8KW61_9GAMM
UniRef90_C7RVF1_38_437 N-acetylmuramoyl-L-alanine amidase n=1 Tax=Candidatus Accumulibacter phosphatis clade IIA str. UW-1 RepID=C7RVF1_ACCPU
UniRef90_G4QBK5_107_516 N-acetylmuramoyl-L-alanine amidase n=1 Tax=Taylorella asinigenitalis MCE3 RepID=G4QBK5_TAYAM
UniRef90_F3LI84_35_407 N-acetylmuramoyl-L-alanine amidase n=1 Tax=gamma proteobacterium IMCC1989 RepID=F3LI84_9GAMM
UniRef90_H8WBE0_20_374 N-acetylmuramoyl-L-alanine amidase II, murein hydrolase n=2 Tax=Marinobacter hydrocarbonoclasticus RepID=H8WBE0_MARHY
UniRef90_A6F3J8_14_367 N-acetylmuramoyl-L-alanine amidase n=1 Tax=Marinobacter algicola DG893 RepID=A6F3J8_9ALTE
UniRef90_B1JAD7_23_401 N-acetylmuramoyl-L-alanine amidase n=8 Tax=Pseudomonas RepID=B1JAD7_PSEPW
UniRef90_F4L9T5_1_401 N-acetylmuramoyl-L-alanine amidase n=4 Tax=Bordetella RepID=F4L9T5_BORPC
UniRef90_UPI00025577DA_25_374 N-acetylmuramoyl-L-alanine amidase n=1 Tax=Marinobacterium stanieri S30 RepID=UPI00025577DA
UniRef90_Q2KX09_9_406 N-acetylmuramoyl-L-alanine amidase (Fragment) n=1 Tax=Bordetella avium 197N RepID=Q2KX09_BORA1
UniRef90_H3NVI2_26_381 N-acetylmuramoyl-L-alanine amidase n=1 Tax=gamma proteobacterium HIMB55 RepID=H3NVI2_9GAMM
UniRef90_F5Y3P0_27_429 Candidate N-acetylmuramoyl-L-alanine amidase amiC n=1 Tax=Ramlibacter tataouinensis TTB310 RepID=F5Y3P0_RAMTT
UniRef90_A3JF37_29_387 N-acetylmuramoyl-L-alanine amidase n=1 Tax=Marinobacter sp. ELB17 RepID=A3JF37_9ALTE
UniRef90_D7HU21_23_396 N-acetylmuramoyl-L-alanine amidase AmiB n=22 Tax=Pseudomonas syringae group RepID=D7HU21_PSESS
UniRef90_E6QSM4_33_442 N-acetylmuramoyl-L-alanine amidase n=1 Tax=mine drainage metagenome RepID=E6QSM4_9ZZZZ
UniRef90_Q2BIN9_23_377 N-acetylmuramoyl-L-alanine amidase n=1 Tax=Neptuniibacter caesariensis RepID=Q2BIN9_9GAMM
UniRef90_I2BRA2_25_382 N-acetylmuramoyl-L-alanine amidase n=3 Tax=Pseudomonas fluorescens RepID=I2BRA2_PSEFL
UniRef90_F3LRY7_28_437 N-acetylmuramoyl-L-alanine amidase n=2 Tax=Rubrivivax RepID=F3LRY7_9BURK
UniRef90_D5C1A7_30_389 N-acetylmuramoyl-L-alanine amidase n=1 Tax=Nitrosococcus halophilus Nc4 RepID=D5C1A7_NITHN
UniRef90_C1DLP9_24_399 N-acetylmuramoyl-L-alanine amidase n=1 Tax=Azotobacter vinelandii DJ RepID=C1DLP9_AZOV D
UniRef90_Q1N270_27_383 N-acetylmuramoyl-L-alanine amidase n=1 Tax=Bermanella marisrubri RepID=Q1N270_9GAMM
UniRef90_B6BTT5_26_399 N-acetylmuramoyl-L-alanine amidase, amic protein n=1 Tax=beta proteobacterium KB13 RepID=B6BTT5_9PROT
UniRef90_H0JEH4_43_415 N-acetylmuramoyl-L-alanine amidase n=1 Tax=Pseudomonas psychrotolerans L19 RepID=H0JEH4_9PSED
UniRef90_Q3K4B1_16_369 Putative N-acetylmuramoyl-L-alanine amidase n=1 Tax=Pseudomonas fluorescens Pf0-1 RepID=Q3K4B1_PSEPF

UniRef90_F3BE66_26_382 N-acetylmuramoyl-L-alanine amidase n=10 Tax=Alteromonadales RepID=F3BE66_PSEHA
UniRef90_A8FRD2_27_378 N-acetylmuramoyl-L-alanine amidase n=1 Tax=Shewanella sediminis HAW-EB3 RepID=A8FRD2_SHESH
UniRef90_F8GHD2_48_472 Cell wall hydrolase/autolysin n=1 Tax=Nitrosomonas sp. Is79A3 RepID=F8GHD2_NITSI
UniRef90_A0Z0Q3_32_381 N-acetylmuramoyl-L-alanine amidase n=1 Tax=marine gamma proteobacterium HTCC2080 RepID=A0Z0Q3_9GAMM
UniRef90_B1KHV1_28_377 N-acetylmuramoyl-L-alanine amidase n=1 Tax=Shewanella woodyi ATCC 51908 RepID=B1KHV1_SHEWM
UniRef90_A3L195_23_379 N-acetylmuramoyl-L-alanine amidase n=15 Tax=Pseudomonas RepID=A3L195_PSEAI
UniRef90_Q21H99_23_374 N-acetylmuramoyl-L-alanine amidase n=1 Tax=Saccharophagus degradans 2-40 RepID=Q21H99_SACD2
UniRef90_Q4K3E9_25_385 N-acetylmuramoyl-L-alanine amidase n=1 Tax=Pseudomonas fluorescens Pf-5 RepID=Q4K3E9_PSEF5
UniRef90_B5JUV9_25_376 N-acetylmuramoyl-L-alanine amidase n=1 Tax=gamma proteobacterium HTCC5015 RepID=B5JUV9_9GAMM
UniRef90_G2DD63_48_400 Protein hfq n=2 Tax=sulfur-oxidizing symbionts RepID=G2DD63_9GAMM
UniRef90_C4ZKL8_65_450 N-acetylmuramoyl-L-alanine amidase n=1 Tax=Thauera sp. MZ1T RepID=C4ZKL8_THASP
UniRef90_F6AJX2_31_404 Cell wall hydrolase/autolysin n=1 Tax=Pseudomonas fulva 12-X RepID=F6AJX2_PSEF1
UniRef90_A8H8G9_28_378 N-acetylmuramoyl-L-alanine amidase n=2 Tax=Shewanella RepID=A8H8G9_SHEPA
UniRef90_B8CIX2_28_377 N-acetylmuramoyl-L-alanine amidase n=1 Tax=Shewanella piezotolerans WP3 RepID=B8CIX2_SHEPW
UniRef90_F9U177_21_374 Cell wall hydrolase/autolysin n=1 Tax=Marichromatium purpuratum 984 RepID=F9U177_MARPU
UniRef90_UPI00025575EA_23_396 N-acetylmuramoyl-L-alanine amidase n=1 Tax=Pseudomonas sp. S9 RepID=UPI00025575EA
UniRef90_F4DNH7_31_400 N-acetylmuramoyl-L-alanine amidase n=2 Tax=Pseudomonas mendocina RepID=F4DNH7_PSEMN
UniRef90_A0KSR4_28_386 Cell wall hydrolase/autolysin n=3 Tax=Shewanella RepID=A0KSR4_SHESA
UniRef90_Q1YRZ0_10_359 N-acetylmuramoyl-L-alanine amidase n=1 Tax=gamma proteobacterium HTCC2207 RepID=Q1YRZ0_9GAMM
UniRef90_F9UFS4_24_387 Cell wall hydrolase/autolysin n=1 Tax=Thiocapsa marina 5811 RepID=F9UFS4_9GAMM
UniRef90_G8Q3Z0_28_400 N-acetylmuramoyl-L-alanine amidase n=4 Tax=Pseudomonas RepID=G8Q3Z0_PSEFL
UniRef90_H3KCC3_28_432 N-acetylmuramoyl-L-alanine amidase n=1 Tax=Sutterella parvirubra YIT 11816 RepID=H3KCC3_9BURK
UniRef90_A9D1D7_27_378 N-acetylmuramoyl-L-alanine amidase n=1 Tax=Shewanella benthica KT99 RepID=A9D1D7_9GAMM
UniRef90_Q8EJ71_28_387 N-acetylmuramoyl-L-alanine amidase n=1 Tax=Shewanella oneidensis MR-1 RepID=Q8EJ71_SHEON
UniRef90_F3L1V6_22_368 N-acetylmuramoyl-L-alanine amidase n=1 Tax=gamma proteobacterium IMCC3088 RepID=F3L1V6_9GAMM
UniRef90_H8Z513_22_388 N-acetylmuramoyl-L-alanine amidase n=1 Tax=Thiorhodovibrio sp.

970 RepID=H8Z513_9GAMM
UniRef90_Q12J92_28_388 N-acetylmuramoyl-L-alanine amidase n=1 Tax=Shewanella denitrificans OS217 RepID=Q12J92_SHEDO
UniRef90_A1RFR4_24_387 N-acetylmuramoyl-L-alanine amidase n=3 Tax=Shewanella RepID=A1RFR4_SHESW
UniRef90_A4C8M6_26_388 N-acetylmuramoyl-L-alanine amidase II, murein hydrolase n=1 Tax=Pseudoalteromonas tunicata D2 RepID=A4C8M6_9GAMM
UniRef90_D4ZFK4_28_379 N-acetylmuramoyl-L-alanine amidase n=1 Tax=Shewanella violacea DSS12 RepID=D4ZFK4_SHEVD
UniRef90_D8KAV7_18_406 N-acetylmuramoyl-L-alanine amidase n=1 Tax=Nitrosococcus watsonii C-113 RepID=D8KAV7_NITWC
UniRef90_B3PDC4_12_392 N-acetylmuramoyl-L-alanine amidase n=1 Tax=Cellvibrio japonicus Ueda107 RepID=B3PDC4_CELJU
UniRef90_A4BEB1_20_379 N-acetylmuramoyl-L-alanine amidase n=1 Tax=Reinekea blandensis MED297 RepID=A4BEB1_9GAMM
UniRef90_A2SHE6_28_443 N-acetylmuramoyl-L-alanine amidase n=1 Tax=Methylbium petroleiphilum PM1 RepID=A2SHE6_METPP
UniRef90_I2JIZ7_22_370 N-acetylmuramoyl-L-alanine amidase n=1 Tax=gamma proteobacterium BDW918 RepID=I2JIZ7_9GAMM
UniRef90_D716T1_30_390 N-acetylmuramoyl-L-alanine amidase AmiC n=22 Tax=Pseudomonas syringae group RepID=D716T1_PSESS
UniRef90_A4A6K8_26_376 N-acetylmuramoyl-L-alanine amidase n=1 Tax=Congregibacter litoralis KT71 RepID=A4A6K8_9GAMM
UniRef90_A3QAD7_28_377 N-acetylmuramoyl-L-alanine amidase n=1 Tax=Shewanella loihica PV-4 RepID=A3QAD7_SHELP
UniRef90_H0J3Y5_31_423 N-acetylmuramoyl-L-alanine amidase n=1 Tax=Halomonas sp. GFAJ-1 RepID=H0J3Y5_9GAMM
UniRef90_B7RW29_24_370 N-acetylmuramoyl-L-alanine amidase domain protein n=2 Tax=Bacteria RepID=B7RW29_9GAMM
UniRef90_G0AQA5_28_386 Cell wall hydrolase/autolysin n=9 Tax=Shewanella baltica RepID=G0AQA5_9GAMM
UniRef90_C3KDW0_23_398 N-acetylmuramoyl-L-alanine amidase n=3 Tax=Pseudomonas fluorescens RepID=C3KDW0_PSEFS
UniRef90_A0Y808_31_378 N-acetylmuramoyl-L-alanine amidase n=1 Tax=marine gamma proteobacterium HTCC2143 RepID=A0Y808_9GAMM
UniRef90_E1V681_28_414 N-acetylmuramoyl-L-alanine amidase n=1 Tax=Halomonas elongata DSM 2581 RepID=E1V681_HALED
UniRef90_B8KNJ5_17_367 N-acetylmuramoyl-L-alanine amidase n=1 Tax=gamma proteobacterium NOR5-3 RepID=B8KNJ5_9GAMM
UniRef90_Q0AB63_25_389 N-acetylmuramoyl-L-alanine amidase n=1 Tax=Alkalilimnicola ehrlichii MLHE-1 RepID=Q0AB63_ALHEH
UniRef90_E8U234_35_457 Cell wall hydrolase/autolysin n=2 Tax=Alicyclophilus denitrificans RepID=E8U234_ALIDB
UniRef90_I1XLL6_20_405 N-acetylmuramoyl-L-alanine amidase n=1 Tax=Methylophaga sp. JAM1 RepID=I1XLL6_9GAMM
UniRef90_C5BRI0_33_384 Putative N-acetylmuramoyl-L-alanine amidase n=1 Tax=Teredinibacter turnerae T7901 RepID=C5BRI0_TERTT

References

- Aarsman, M.E.G., A. Piette, C. Fraipont, T.M.F. Vinkenvleugel, M. Nguyen-Distèche & T. den Blaauwen, (2005) Maturation of the Escherichia coli divisome occurs in two steps. *Molecular Microbiology* **55**: 1631-1645.
- Akerlund, T., B. Gullbrand & K. Nordstrom, (2002) Effects of the Min system on nucleoid segregation in Escherichia coli. *Microbiology* **148**: 3213-3222.
- Alexeeva, S., T.W.J. Gadella, J. Verheul, G.S. Verhoeven & T. den Blaauwen, (2010) Direct interactions of early and late assembling division proteins in Escherichia coli cells resolved by FRET. *Molecular Microbiology* **77**: 384-398.
- Amano, K., H. Hayashi, Y. Araki & E. Ito, (1977) The action of lysozyme on peptidoglycan with N-unsubstituted glucosamine residues. Isolation of glycan fragments and their susceptibility to lysozyme. *European journal of biochemistry / FEBS* **76**: 299-307.
- Arends, S.J.R., K. Williams, R.J. Scott, S. Rolong, D.L. Popham & D.S. Weiss, (2010) Discovery and characterization of three new Escherichia coli septal ring proteins that contain a SPOR domain: DamX, DedD, and RlpA. *J Bacteriol* **192**: 242-255.
- Ashkenazy, H., E. Erez, E. Martz, T. Pupko & N. Ben-Tal, (2010) ConSurf 2010: calculating evolutionary conservation in sequence and structure of proteins and nucleic acids. *Nucl. Acids Res.* **38**: W529-W533.
- Aussel, L., F.X. Barre, M. Aroyo, A. Stasiak, A.Z. Stasiak & D. Sherratt, (2002) FtsK Is a DNA motor protein that activates chromosome dimer resolution by switching the catalytic state of the XerC and XerD recombinases. *Cell* **108**: 195-205.
- Ayala, J.A., T. Garrido, M.A. de Pedro & M. Vicente, (1994) *Molecular biology of bacterial septation*. Elsevier Science, Amsterdam, The Netherlands.
- Beeby, M., J.C. Gumbart, B. Roux & G.J. Jensen, (2013) Architecture and assembly of the Gram-positive cell wall. *Mol Microbiol* **88**: 664-672.
- Beech, P.L., T. Nheu, T. Schultz, S. Herbert, T. Lithgow, P.R. Gilson & G.I. McFadden, (2000) Mitochondrial FtsZ in a chromophyte alga. *Science* **287**: 1276-1279.
- Bernard, E., T. Rolain, P. Courtin, A. Guillot, P. Langella, P. Hols & M.P. Chapot-Chartier, (2011) Characterization of O-acetylation of N-acetylglucosamine: a novel structural variation of bacterial peptidoglycan. *J Biol Chem* **286**: 23950-23958.
- Bernhardt, T.G. & P.A. de Boer, (2005) SlmA, a nucleoid-associated, FtsZ binding protein required for blocking septal ring assembly over Chromosomes in E. coli. *Molecular cell* **18**: 555-564.
- Bernhardt, T.G. & P.A.J. de Boer, (2003) The Escherichia coli amidase AmiC is a periplasmic septal ring component exported via the twin-arginine transport pathway. *Molecular Microbiology* **48**: 1171-1182.
- Bertsche, U., E. Breukink, T. Kast & W. Vollmer, (2005) In vitro murein peptidoglycan synthesis by dimers of the bifunctional transglycosylase-transpeptidase PBP1B from Escherichia coli. *J Biol Chem* **280**: 38096-38101.
- Bertsche, U., T. Kast, B. Wolf, C. Fraipont, M.E.G. Aarsman, K. Kannenberg, M. von Rechenberg, M. Nguyen-Distèche, T. den Blaauwen, J.-V. Höltje & W. Vollmer, (2006) Interaction between two murein (peptidoglycan) synthases, PBP3 and PBP1B, in Escherichia coli. *Molecular Microbiology* **61**: 675-690.
- Bi, E. & J. Lutkenhaus, (1993) Cell division inhibitors SulA and MinCD prevent formation of the FtsZ ring. *J Bacteriol* **175**: 1118-1125.
- Bi, E.F. & J. Lutkenhaus, (1991) FtsZ ring structure associated with division in Escherichia coli. *Nature* **354**: 161-164.
- Bisicchia, P., D. Noone, E. Lioliou, A. Howell, S. Quigley, T. Jensen, H. Jarmer & K.M. Devine, (2007) The essential YycFG two-component system controls cell wall metabolism in Bacillus subtilis. *Mol Microbiol* **65**: 180-200.
- Bouhss, A., S. Dementin, C. Parquet, D. Mengin-Lecreulx, J.A. Bertrand, D. Le Beller, O. Dideberg, J. van Heijenoort & D. Blanot, (1999) Role of the ortholog and paralog amino acid invariants in the

- active site of the UDP-MurNAc-L-alanine:D-glutamate ligase (MurD). *Biochemistry* **38**: 12240-12247.
- Bouhss, A., D. Mengin-Lecreux, D. Blanot, J. van Heijenoort & C. Parquet, (1997) Invariant amino acids in the Mur peptide synthetases of bacterial peptidoglycan synthesis and their modification by site-directed mutagenesis in the UDP-MurNAc:L-alanine ligase from *Escherichia coli*. *Biochemistry* **36**: 11556-11563.
- Bouhss, A., A.E. Trunkfield, T.D.H. Bugg & D. Mengin-Lecreux, (2008) The biosynthesis of peptidoglycan lipid-linked intermediates. *FEMS Microbiol. Rev* **32**: 208-233.
- Browder, H.P., W.A. Zygmunt, J.R. Young & P.A. Tavormina, (1965) LYSOSTAPHIN: ENZYMATIC MODE OF ACTION. *Biochemical and biophysical research communications* **19**: 383-389.
- Brown, E.D., E.I. Vivas, C.T. Walsh & R. Kolter, (1995) MurA (MurZ), the enzyme that catalyzes the first committed step in peptidoglycan biosynthesis, is essential in *Escherichia coli*. *J Bacteriol* **177**: 4194-4197.
- Brumfitt, W., A.C. Wardlaw & J.T. Park, (1958) Development of lysozyme-resistance in *Micrococcus lysodieticus* and its association with an increased O-acetyl content of the cell wall. *Nature* **181**: 1783-1784.
- Buddelmeijer, N. & J. Beckwith, (2004) A complex of the *Escherichia coli* cell division proteins FtsL, FtsB and FtsQ forms independently of its localization to the septal region. *Molecular microbiology* **52**: 1315-1327.
- Buist, G., A. Steen, J. Kok & O.P. Kuipers, (2008) LysM, a widely distributed protein motif for binding to (peptido)glycans. *Molecular microbiology* **68**: 838-847.
- Busiek, K.K., J.M. Eraso, Y. Wang & W. Margolin, (2012) The early divisome protein FtsA interacts directly through its 1c subdomain with the cytoplasmic domain of the late divisome protein FtsN. *J Bacteriol* **194**: 1989-2000.
- Carr, S., C.N. Penfold, V. Bamford, R. James & A.M. Hemmings, (2000) The structure of TolB, an essential component of the tol-dependent translocation system, and its protein-protein interaction with the translocation domain of colicin E9. *Structure* **8**: 57-66.
- Cascales, E., A. Bernadac, M. Gavioli, J.C. Lazzaroni & R. Lloubes, (2002) Pal lipoprotein of *Escherichia coli* plays a major role in outer membrane integrity. *J Bacteriol* **184**: 754-759.
- Cascales, E., M. Gavioli, J.N. Sturgis & R. Lloubes, (2000) Proton motive force drives the interaction of the inner membrane TolA and outer membrane pal proteins in *Escherichia coli*. *Mol Microbiol* **38**: 904-915.
- Cascales, E., R. Lloubes & J.N. Sturgis, (2001) The TolQ-TolR proteins energize TolA and share homologies with the flagellar motor proteins MotA-MotB. *Mol Microbiol* **42**: 795-807.
- Chen, J.C., M. Minev & J. Beckwith, (2002) Analysis of ftsQ mutant alleles in *Escherichia coli*: complementation, septal localization, and recruitment of downstream cell division proteins. *J Bacteriol* **184**: 695-705.
- Chen, Y. & H.P. Erickson, (2005) Rapid in vitro assembly dynamics and subunit turnover of FtsZ demonstrated by fluorescence resonance energy transfer. *J Biol Chem* **280**: 22549-22554.
- Chen, Y. & H.P. Erickson, (2009) FtsZ filament dynamics at steady state: subunit exchange with and without nucleotide hydrolysis. *Biochemistry* **48**: 6664-6673.
- Chen, Y., S.L. Milam & H.P. Erickson, (2012) Sula inhibits assembly of FtsZ by a simple sequestration mechanism. *Biochemistry* **51**: 3100-3109.
- Cohen, D.N., Y.Y. Sham, G.D. Haugstad, Y. Xiang, M.G. Rossmann, D.L. Anderson & D.L. Popham, (2009) Shared catalysis in virus entry and bacterial cell wall depolymerization. *J Mol Biol* **387**: 607-618.
- Corbin, B.D., B. Geissler, M. Sadasivam & W. Margolin, (2004) Z-ring-independent interaction between a subdomain of FtsA and late septation proteins as revealed by a polar recruitment assay. *J Bacteriol* **186**: 7736-7744.
- Corbin, B.D., Y. Wang, T.K. Beuria & W. Margolin, (2007) Interaction Between Cell Division Proteins FtsE and FtsZ. *J Bacteriol* **189**: 3026-3035.

- D'Ulisse, V., M. Fagioli, P. Ghelardini & L. Paolozzi, (2007) Three functional subdomains of the Escherichia coli FtsQ protein are involved in its interaction with the other division proteins. *Microbiology* **153**: 124-138.
- Dajkovic, A., G. Lan, S.X. Sun, D. Wirtz & J. Lutkenhaus, (2008) MinC spatially controls bacterial cytokinesis by antagonizing the scaffolding function of FtsZ. *Current biology : CB* **18**: 235-244.
- Datta, P., A. Dasgupta, A.K. Singh, P. Mukherjee, M. Kundu & J. Basu, (2006) Interaction between FtsW and penicillin-binding protein 3 (PBP3) directs PBP3 to mid-cell, controls cell septation and mediates the formation of a trimeric complex involving FtsZ, FtsW and PBP3 in mycobacteria. *Mol Microbiol* **62**: 1655-1673.
- Davis, M.A. & S.J. Austin, (1988) Recognition of the P1 plasmid centromere analog involves binding of the ParB protein and is modified by a specific host factor. *EMBO J* **7**: 1881-1888.
- de Boer, P.A., (2010) Advances in understanding E. coli cell fission. *Current opinion in microbiology* **13**: 730-737.
- de Souza, R.F., V. Anantharaman, S.J. de Souza, L. Aravind & F.J. Gueiros-Filho, (2008) AMIN domains have a predicted role in localization of diverse periplasmic protein complexes. *Bioinformatics* **24**: 2423-2426.
- den Blaauwen, T., (2013) Prokaryotic cell division: flexible and diverse. *Current opinion in microbiology*.
- den Blaauwen, T., M.E. Aarsman, N.O. Vischer & N. Nanninga, (2003) Penicillin-binding protein PBP2 of Escherichia coli localizes preferentially in the lateral wall and at mid-cell in comparison with the old cell pole. *Mol Microbiol* **47**: 539-547.
- Dewar, S.J., K.J. Begg & W.D. Donachie, (1992) Inhibition of cell division initiation by an imbalance in the ratio of FtsA to FtsZ. *J Bacteriol* **174**: 6314-6316.
- Di Lallo, G., M. Fagioli, D. Barionovi, P. Ghelardini & L. Paolozzi, (2003) Use of a two-hybrid assay to study the assembly of a complex multicomponent protein machinery: bacterial septosome differentiation. *Microbiology* **149**: 3353-3359.
- Di Ventura, B., B. Knecht, H. Andreas, W.J. Godinez, M. Fritsche, K. Rohr, W. Nickel, D.W. Heermann & V. Sourjik, (2013) Chromosome segregation by the Escherichia coli Min system. *Molecular systems biology* **9**: 686.
- Din, N., E.M. Quardokus, M.J. Sackett & Y.V. Brun, (1998) Dominant C-terminal deletions of FtsZ that affect its ability to localize in Caulobacter and its interaction with FtsA. *Mol Microbiol* **27**: 1051-1063.
- Dmitriev, B.A., F.V. Toukach, K.J. Schaper, O. Holst, E.T. Rietschel & S. Ehlers, (2003) Tertiary structure of bacterial murein: the scaffold model. *J Bacteriol* **185**: 3458-3468.
- Dorazi, R. & S.J. Dewar, (2000) Membrane topology of the N-terminus of the Escherichia coli FtsK division protein. *FEBS Lett* **478**: 13-18.
- Doublet, S., (2007) Production of selenomethionyl proteins in prokaryotic and eukaryotic expression systems. *Methods Mol Biol* **363**: 91-108.
- Dubarry, N. & F.X. Barre, (2010) Fully efficient chromosome dimer resolution in Escherichia coli cells lacking the integral membrane domain of FtsK. *EMBO J* **29**: 597-605.
- Dubarry, N., C. Possoz & F.X. Barre, (2010) Multiple regions along the Escherichia coli FtsK protein are implicated in cell division. *Mol Microbiol* **78**: 1088-1100.
- Duncan, T.R., A. Yahashiri, S.J. Arends, D.L. Popham & D.S. Weiss, (2013) The Cell Division Protein FtsN: Identification of SPOR Domain Amino Acids Important for Septal Localization, Peptidoglycan-binding, and a Disulfide Bond. *J Bacteriol*.
- Durand-Heredia, J., E. Rivkin, G. Fan, J. Morales & A. Janakiraman, (2012) Identification of ZapD as a cell division factor that promotes the assembly of FtsZ in Escherichia coli. *J Bacteriol* **194**: 3189-3198.
- Durand-Heredia, J.M., H.H. Yu, S. De Carlo, C.F. Lesser & A. Janakiraman, (2011) Identification and characterization of ZapC, a stabilizer of the FtsZ ring in Escherichia coli. *J Bacteriol* **193**: 1405-1413.

- Ebersbach, G., E. Galli, J. Moller-Jensen, J. Lowe & K. Gerdes, (2008) Novel coiled-coil cell division factor ZapB stimulates Z ring assembly and cell division. *Mol Microbiol* **68**: 720-735.
- Egan, A.J.F. & W. Vollmer, (2013) The physiology of bacterial cell division. *Annals of the New York Academy of Sciences* **1277**: 8-28.
- Erickson, H.P., (2009) Modeling the physics of FtsZ assembly and force generation. *Proc Natl Acad Sci U S A* **106**: 9238-9243.
- Erickson, H.P., D.E. Anderson & M. Osawa, (2010) FtsZ in bacterial cytokinesis: cytoskeleton and force generator all in one. *Microbiol Mol Biol Rev* **74**: 504-528.
- Eswaramoorthy, P., M.L. Erb, J.A. Gregory, J. Silverman, K. Pogliano, J. Pogliano & K.S. Ramamurthi, (2011) Cellular architecture mediates DivIVA ultrastructure and regulates min activity in *Bacillus subtilis*. *mBio* **2**.
- Eveland, S.S., D.L. Pompliano & M.S. Anderson, (1997) Conditionally lethal *Escherichia coli* murein mutants contain point defects that map to regions conserved among murein and folyl poly-gamma-glutamate ligases: identification of a ligase superfamily. *Biochemistry* **36**: 6223-6229.
- Fay, A. & J. Dworkin, (2009) *Bacillus subtilis* homologs of MviN (MurJ), the putative *Escherichia coli* lipid II flippase, are not essential for growth. *J Bacteriol* **191**: 6020-6028.
- Fay, A., P. Meyer & J. Dworkin, (2010) Interactions between late-acting proteins required for peptidoglycan synthesis during sporulation. *J. Mol. Biol* **399**: 547-561.
- Firczuk, M., A. Mucha & M. Bochtler, (2005) Crystal structures of active LytM. *J Mol Biol* **354**: 578-590.
- Fraipont, C., S. Alexeeva, B. Wolf, R. van der Ploeg, M. Schloesser, T. den Blaauwen & M. Nguyen-Distèche, (2011) The integral membrane FtsW protein and peptidoglycan synthase PBP3 form a subcomplex in *Escherichia coli*. *Microbiology (Reading, Engl.)* **157**: 251-259.
- Fu, G., T. Huang, J. Buss, C. Coltharp, Z. Hensel & J. Xiao, (2010) In vivo structure of the *E. coli* FtsZ-ring revealed by photoactivated localization microscopy (PALM). *PLoS One* **5**: e12682.
- Fu, X., Y.L. Shih, Y. Zhang & L.I. Rothfield, (2001) The MinE ring required for proper placement of the division site is a mobile structure that changes its cellular location during the *Escherichia coli* division cycle. *Proc Natl Acad Sci U S A* **98**: 980-985.
- Galli, E. & K. Gerdes, (2010) Spatial resolution of two bacterial cell division proteins: ZapA recruits ZapB to the inner face of the Z-ring. *Mol Microbiol* **76**: 1514-1526.
- Galli, E. & K. Gerdes, (2012) FtsZ-ZapA-ZapB interactome of *Escherichia coli*. *J Bacteriol* **194**: 292-302.
- Gamba, P., J.W. Veening, N.J. Saunders, L.W. Hamoen & R.A. Daniel, (2009) Two-step assembly dynamics of the *Bacillus subtilis* divisome. *J Bacteriol* **191**: 4186-4194.
- Gan, L., S. Chen & G.J. Jensen, (2008) Molecular organization of Gram-negative peptidoglycan. *Proc Natl Acad Sci U S A* **105**: 18953-18957.
- Garti-Levi, S., R. Hazan, J. Kain, M. Fujita & S. Ben-Yehuda, (2008) The FtsEX ABC transporter directs cellular differentiation in *Bacillus subtilis*. *Mol Microbiol* **69**: 1018-1028.
- Geissler, B. & W. Margolin, (2005) Evidence for functional overlap among multiple bacterial cell division proteins: compensating for the loss of FtsK. *Mol Microbiol* **58**: 596-612.
- Gérard, P., T. Vernet & A. Zapun, (2002) Membrane topology of the *Streptococcus pneumoniae* FtsW division protein. *J Bacteriol* **184**: 1925-1931.
- Gerding, M.A., B. Liu, F.O. Bendezu, C.A. Hale, T.G. Bernhardt & P.A. de Boer, (2009) Self-enhanced accumulation of FtsN at Division Sites and Roles for Other Proteins with a SPOR domain (DamX, DedD, and RlpA) in *Escherichia coli* cell constriction. *J Bacteriol* **191**: 7383-7401.
- Gerding, M.A., Y. Ogata, N.D. Pecora, H. Niki & P.A. de Boer, (2007) The trans-envelope Tol-Pal complex is part of the cell division machinery and required for proper outer-membrane invagination during cell constriction in *E. coli*. *Mol Microbiol* **63**: 1008-1025.
- Ghosh, A.S., C. Chowdhury & D.E. Nelson, (2008) Physiological functions of D-alanine carboxypeptidases in *Escherichia coli*. *Trends Microbiol* **16**: 309-317.
- Ghuysen, J.M., (1968) Use of bacteriolytic enzymes in determination of wall structure and their role in cell metabolism. *Bacteriological reviews* **32**: 425-464.

- Glauner, B., J.V. Höltje & U. Schwarz, (1988) The composition of the murein of *Escherichia coli*. *J. Biol. Chem* **263**: 10088-10095.
- Godlewska, R., K. Wisniewska, Z. Pietras & E.K. Jagusztyn-Krynicka, (2009) Peptidoglycan-associated lipoprotein (Pal) of Gram-negative bacteria: function, structure, role in pathogenesis and potential application in immunoprophylaxis. *FEMS Microbiol Lett* **298**: 1-11.
- Goffin, C., C. Fraipont, J. Ayala, M. Terrak, M. Nguyen-Disteche & J.M. Ghuysen, (1996) The non-penicillin-binding module of the tripartite penicillin-binding protein 3 of *Escherichia coli* is required for folding and/or stability of the penicillin-binding module and the membrane-anchoring module confers cell septation activity on the folded structure. *J Bacteriol* **178**: 5402-5409.
- Goley, E.D., N.A. Dye, J.N. Werner, Z. Gitai & L. Shapiro, (2010) Imaging-based identification of a critical regulator of FtsZ protofilament curvature in *Caulobacter*. *Molecular cell* **39**: 975-987.
- Goley, E.D., Y.C. Yeh, S.H. Hong, M.J. Fero, E. Abeliuk, H.H. McAdams & L. Shapiro, (2011) Assembly of the *Caulobacter* cell division machine. *Mol Microbiol* **80**: 1680-1698.
- Gonzalez, M.D. & J. Beckwith, (2009) Divisome under construction: distinct domains of the small membrane protein FtsB are necessary for interaction with multiple cell division proteins. *J Bacteriol* **191**: 2815-2825.
- Grenga, L., G. Guglielmi, S. Melino, P. Ghelardini & L. Paolozzi, (2010) FtsQ interaction mutants: a way to identify new antibacterial targets. *New biotechnology* **27**: 870-881.
- Grenga, L., G. Luzi, L. Paolozzi & P. Ghelardini, (2008) The *Escherichia coli* FtsK functional domains involved in its interaction with its divisome protein partners. *FEMS Microbiol Lett* **287**: 163-167.
- Gueiros-Filho, F.J. & R. Losick, (2002) A widely conserved bacterial cell division protein that promotes assembly of the tubulin-like protein FtsZ. *Genes Dev* **16**: 2544-2556.
- Gundogdu, M.E., Y. Kawai, N. Pavlendova, N. Ogasawara, J. Errington, D.J. Scheffers & L.W. Hamoen, (2011) Large ring polymers align FtsZ polymers for normal septum formation. *EMBO J* **30**: 617-626.
- Guzman, L.M., D. Belin, M.J. Carson & J. Beckwith, (1995) Tight regulation, modulation, and high-level expression by vectors containing the arabinose PBAD promoter. *J Bacteriol* **177**: 4121-4130.
- Hale, C.A. & P.A. de Boer, (1999) Recruitment of ZipA to the septal ring of *Escherichia coli* is dependent on FtsZ and independent of FtsA. *J Bacteriol* **181**: 167-176.
- Hale, C.A. & P.A. de Boer, (2002) ZipA is required for recruitment of FtsK, FtsQ, FtsL, and FtsN to the septal ring in *Escherichia coli*. *J Bacteriol* **184**: 2552-2556.
- Hale, C.A., D. Shiomi, B. Liu, T.G. Bernhardt, W. Margolin, H. Niki & P.A. de Boer, (2011) Identification of *Escherichia coli* ZapC (YcbW) as a component of the division apparatus that binds and bundles FtsZ polymers. *J Bacteriol* **193**: 1393-1404.
- Hamoen, L.W., J.C. Meile, W. de Jong, P. Noirot & J. Errington, (2006) SepF, a novel FtsZ-interacting protein required for a late step in cell division. *Mol Microbiol* **59**: 989-999.
- Haney, S.A., E. Glasfeld, C. Hale, D. Keeney, Z. He & P. de Boer, (2001) Genetic analysis of the *Escherichia coli* FtsZ.ZipA interaction in the yeast two-hybrid system. Characterization of FtsZ residues essential for the interactions with ZipA and with FtsA. *J Biol Chem* **276**: 11980-11987.
- Hashimoto, M., S. Ooiwa & J. Sekiguchi, (2012) Synthetic lethality of the lytE cwLO genotype in *Bacillus subtilis* is caused by lack of D,L-endopeptidase activity at the lateral cell wall. *J Bacteriol* **194**: 796-803.
- Hayashi, K., (1975) A rapid determination of sodium dodecyl sulfate with methylene blue. *Anal. Biochem.* **67**: 503-506.
- Hayhurst, E.J., L. Kailas, J.K. Hobbs & S.J. Foster, (2008) Cell wall peptidoglycan architecture in *Bacillus subtilis*. *PNAS* **105**: 14603-14608.
- Heidrich, C., M.F. Templin, A. Ursinus, M. Merdanovic, J. Berger, H. Schwarz, M.A. de Pedro & J.V. Höltje, (2001) Involvement of N-acetylmuramyl-L-alanine amidases in cell separation and antibiotic-induced autolysis of *Escherichia coli*. *Molecular Microbiology* **41**: 167-178.

- Heidrich, C., A. Ursinus, J. Berger, H. Schwarz & J.V. Holtje, (2002) Effects of multiple deletions of murein hydrolases on viability, septum cleavage, and sensitivity to large toxic molecules in *Escherichia coli*. *J Bacteriol* **184**: 6093-6099.
- Holtje, J.V., (1998) Growth of the stress-bearing and shape-maintaining murein sacculus of *Escherichia coli*. *Microbiol Mol Biol Rev* **62**: 181-203.
- Holtje, J.V., U. Kopp, A. Ursinus & B. Wiedemann, (1994) The negative regulator of beta-lactamase induction AmpD is a N-acetyl-anhydromuramyl-L-alanine amidase. *FEMS Microbiol Lett* **122**: 159-164.
- Holtje, J.V., D. Mirelman, N. Sharon & U. Schwarz, (1975) Novel type of murein transglycosylase in *Escherichia coli*. *J Bacteriol* **124**: 1067-1076.
- Horger, I., E. Velasco, J. Mingorance, G. Rivas, P. Tarazona & M. Velez, (2008) Langevin computer simulations of bacterial protein filaments and the force-generating mechanism during cell division. *Physical review. E, Statistical, nonlinear, and soft matter physics* **77**: 011902.
- Hu, Z., E.P. Gogol & J. Lutkenhaus, (2002) Dynamic assembly of MinD on phospholipid vesicles regulated by ATP and MinE. *Proc Natl Acad Sci U S A* **99**: 6761-6766.
- Hu, Z. & J. Lutkenhaus, (1999) Topological regulation of cell division in *Escherichia coli* involves rapid pole to pole oscillation of the division inhibitor MinC under the control of MinD and MinE. *Mol Microbiol* **34**: 82-90.
- Hu, Z. & J. Lutkenhaus, (2000) Analysis of MinC Reveals Two Independent Domains Involved in Interaction with MinD and FtsZ. *J Bacteriol* **182**: 3965-3971.
- Huang, K.H., J. Durand-Heredia & A. Janakiraman, (2013) FtsZ ring stability: of bundles, tubules, crosslinks, and curves. *J Bacteriol* **195**: 1859-1868.
- Huecas, S. & J.M. Andreu, (2004) Polymerization of nucleotide-free, GDP- and GTP-bound cell division protein FtsZ: GDP makes the difference. *FEBS Lett* **569**: 43-48.
- Ichikawa, J.K., C. Li, J. Fu & S. Clarke, (1994) A gene at 59 minutes on the *Escherichia coli* chromosome encodes a lipoprotein with unusual amino acid repeat sequences. *J Bacteriol* **176**: 1630-1638.
- Ikeda, M., T. Sato, M. Wachi, H.K. Jung, F. Ishino, Y. Kobayashi & M. Matsuhashi, (1989) Structural similarity among *Escherichia coli* FtsW and RodA proteins and *Bacillus subtilis* SpoVE protein, which function in cell division, cell elongation, and spore formation, respectively. *J Bacteriol* **171**: 6375-6378.
- Jacobs, C., L.J. Huang, E. Bartowsky, S. Normark & J.T. Park, (1994) Bacterial cell wall recycling provides cytosolic muropeptides as effectors for beta-lactamase induction. *EMBO J* **13**: 4684-4694.
- Jerabek-Willemsen, M., C.J. Wienken, D. Braun, P. Baaske & S. Duhr, (2011) Molecular interaction studies using microscale thermophoresis. *Assay Drug Dev Technol* **9**: 342-353.
- Karimova, G., N. Dautin & D. Ladant, (2005) Interaction network among *Escherichia coli* membrane proteins involved in cell division as revealed by bacterial two-hybrid analysis. *J Bacteriol* **187**: 2233-2243.
- Karimova, G., C. Robichon & D. Ladant, (2009) Characterization of YmgF, a 72-residue inner membrane protein that associates with the *Escherichia coli* cell division machinery. *J Bacteriol* **191**: 333-346.
- Kerff, F., S. Petrella, F. Mercier, E. Sauvage, R. Herman, A. Pennartz, A. Zervosen, A. Luxen, J.-M. Frère, B. Joris & P. Charlier, (2010) Specific structural features of the N-acetylmuramoyl-L-alanine amidase AmiD from *Escherichia coli* and mechanistic implications for enzymes of this family. *J. Mol. Biol* **397**: 249-259.
- Kiekebusch, D., K.A. Michie, L.O. Essen, J. Lowe & M. Thanbichler, (2012) Localized dimerization and nucleoid binding drive gradient formation by the bacterial cell division inhibitor MipZ. *Molecular cell* **46**: 245-259.
- Krissinel, E. & K. Henrick, (2007) Inference of macromolecular assemblies from crystalline state. *J. Mol. Biol* **372**: 774-797.
- Lan, G., B.R. Daniels, T.M. Dobrowsky, D. Wirtz & S.X. Sun, (2009) Condensation of FtsZ filaments can drive bacterial cell division. *Proc Natl Acad Sci U S A* **106**: 121-126.

- Lange, R. & R. Hengge-Aronis, (1994) The *nlpD* gene is located in an operon with *rpoS* on the *Escherichia coli* chromosome and encodes a novel lipoprotein with a potential function in cell wall formation. *Molecular Microbiology* **13**: 733-743.
- Lara, B. & J.A. Ayala, (2002) Topological characterization of the essential *Escherichia coli* cell division protein FtsW. *FEMS Microbiology Letters* **216**: 23-32.
- Lavollay, M., M. Arthur, M. Fourgeaud, L. Dubost, A. Marie, N. Veziris, D. Blanot, L. Gutmann & J.L. Mainardi, (2008) The peptidoglycan of stationary-phase *Mycobacterium tuberculosis* predominantly contains cross-links generated by L,D-transpeptidation. *J Bacteriol* **190**: 4360-4366.
- Lenarcic, R., S. Halbedel, L. Visser, M. Shaw, L.J. Wu, J. Errington, D. Marenduzzo & L.W. Hamoen, (2009) Localisation of DivIVA by targeting to negatively curved membranes. *EMBO J* **28**: 2272-2282.
- Leslie, A.G.W. & H.R. Powell, (2007) Processing diffraction data with mosflm. In: *Evolving Methods for Macromolecular Crystallography*. R.J. Read & J.L. Sussman (eds). Springer Netherlands, pp. 41-51.
- Li, Y., J. Hsin, L. Zhao, Y. Cheng, W. Shang, K.C. Huang, H.W. Wang & S. Ye, (2013) FtsZ protofilaments use a hinge-opening mechanism for constrictive force generation. *Science* **341**: 392-395.
- Li, Z., M.J. Trimble, Y.V. Brun & G.J. Jensen, (2007) The structure of FtsZ filaments in vivo suggests a force-generating role in cell division. *EMBO J* **26**: 4694-4708.
- Lloubes, R., E. Cascales, A. Walburger, E. Bouveret, C. Lazdunski, A. Bernadac & L. Journet, (2001) The Tol-Pal proteins of the *Escherichia coli* cell envelope: an energized system required for outer membrane integrity? *Research in microbiology* **152**: 523-529.
- Low, H.H., M.C. Moncrieffe & J. Lowe, (2004) The crystal structure of ZapA and its modulation of FtsZ polymerisation. *J Mol Biol* **341**: 839-852.
- Lowe, J. & L.A. Amos, (1998) Crystal structure of the bacterial cell-division protein FtsZ. *Nature* **391**: 203-206.
- Lu, C., M. Reedy & H.P. Erickson, (2000) Straight and curved conformations of FtsZ are regulated by GTP hydrolysis. *J Bacteriol* **182**: 164-170.
- Ma, X. & W. Margolin, (1999) Genetic and functional analyses of the conserved C-terminal core domain of *Escherichia coli* FtsZ. *J Bacteriol* **181**: 7531-7544.
- Maggi, S., O. Massidda, G. Luzi, D. Fadda, L. Paolozzi & P. Ghelardini, (2008) Division protein interaction web: identification of a phylogenetically conserved common interactome between *Streptococcus pneumoniae* and *Escherichia coli*. *Microbiology* **154**: 3042-3052.
- Magnet, S., L. Dubost, A. Marie, M. Arthur & L. Gutmann, (2008) Identification of the L,d-Transpeptidases for Peptidoglycan Cross-Linking in *Escherichia coli*. *J Bacteriol* **190**: 4782-4785.
- Mainardi, J.L., M. Fourgeaud, J.E. Hugonnet, L. Dubost, J.P. Brouard, J. Ouazzani, L.B. Rice, L. Gutmann & M. Arthur, (2005) A novel peptidoglycan cross-linking enzyme for a beta-lactam-resistant transpeptidation pathway. *J Biol Chem* **280**: 38146-38152.
- Mainardi, J.L., R. Legrand, M. Arthur, B. Schoot, J. van Heijenoort & L. Gutmann, (2000) Novel mechanism of beta-lactam resistance due to bypass of DD-transpeptidation in *Enterococcus faecium*. *J Biol Chem* **275**: 16490-16496.
- Massey, T.H., C.P. Mercogliano, J. Yates, D.J. Sherratt & J. Lowe, (2006) Double-stranded DNA translocation: structure and mechanism of hexameric FtsK. *Molecular cell* **23**: 457-469.
- Massidda, O., L. Novakova & W. Vollmer, (2013) From models to pathogens: how much have we learned about *Streptococcus pneumoniae* cell division? *Environ Microbiol*.
- Matias, V.R.F. & T.J. Beveridge, (2005) Cryo-electron microscopy reveals native polymeric cell wall structure in *Bacillus subtilis* 168 and the existence of a periplasmic space. *Molecular Microbiology* **56**: 240-251.
- Matsui, T., J. Yamane, N. Mogi, H. Yamaguchi, H. Takemoto, M. Yao & I. Tanaka, (2012) Structural reorganization of the bacterial cell-division protein FtsZ from *Staphylococcus aureus*. *Acta Crystallogr D Biol Crystallogr* **68**: 1175-1188.

- Meury, J. & G. Devilliers, (1999) Impairment of cell division in *tolA* mutants of *Escherichia coli* at low and high medium osmolarities. *Biology of the cell / under the auspices of the European Cell Biology Organization* **91**: 67-75.
- Mohammadi, T., V. van Dam, R. Sijbrandi, T. Vernet, A. Zapun, A. Bouhss, M. Diepeveen-de Bruin, M. Nguyen-Distèche, B. de Kruijff & E. Breukink, (2011) Identification of FtsW as a transporter of lipid-linked cell wall precursors across the membrane. *EMBO J* **30**: 1425-1432.
- Möll, A. & M. Thanbichler, (2009) FtsN-like proteins are conserved components of the cell division machinery in proteobacteria. *Molecular microbiology* **72**: 1037-1053.
- Morris, R.J., A. Perrakis & V.S. Lamzin, (2003) ARP/wARP and automatic interpretation of protein electron density maps. *Meth. Enzymol.* **374**: 229-244.
- Mosyak, L., Y. Zhang, E. Glasfeld, S. Haney, M. Stahl, J. Seehra & W.S. Somers, (2000) The bacterial cell-division protein ZipA and its interaction with an FtsZ fragment revealed by X-ray crystallography. *EMBO J* **19**: 3179-3191.
- Moy, F.J., E. Glasfeld, L. Mosyak & R. Powers, (2000) Solution structure of ZipA, a crucial component of *Escherichia coli* cell division. *Biochemistry* **39**: 9146-9156.
- Müller, P., C. Ewers, U. Bertsche, M. Anstett, T. Kallis, E. Breukink, C. Fraipont, M. Terrak, M. Nguyen-Distèche & W. Vollmer, (2007) The Essential Cell Division Protein FtsN Interacts with the Murein (Peptidoglycan) Synthase PBP1B in *Escherichia coli*. *Journal of Biological Chemistry* **282**: 36394-36402.
- Natale, P., M. Pazos & M. Vicente, (2013) The *Escherichia coli* divisome: born to divide. *Environ Microbiol.*
- Niki, H., Y. Yamaichi & S. Hiraga, (2000) Dynamic organization of chromosomal DNA in *Escherichia coli*. *Genes Dev* **14**: 212-223.
- Oliva, M.A., D. Trambaiolo & J. Lowe, (2007) Structural insights into the conformational variability of FtsZ. *J Mol Biol* **373**: 1229-1242.
- Osawa, M., D.E. Anderson & H.P. Erickson, (2008) Reconstitution of contractile FtsZ rings in liposomes. *Science* **320**: 792-794.
- Paradis-Bleau, C., M. Markovski, T. Uehara, T.J. Lupoli, S. Walker, D.E. Kahne & T.G. Bernhardt, (2010) Lipoprotein Cofactors Located in the Outer Membrane Activate Bacterial Cell Wall Polymerases. *Cell* **143**: 1110-1120.
- Pares, S., N. Mouz, Y. Petillot, R. Hakenbeck & O. Dideberg, (1996) X-ray structure of *Streptococcus pneumoniae* PBP2x, a primary penicillin target enzyme. *Nature structural biology* **3**: 284-289.
- Pastoret, S., C. Fraipont, T. den Blaauwen, B. Wolf, M.E. Aarsman, A. Piette, A. Thomas, R. Brasseur & M. Nguyen-Distèche, (2004) Functional analysis of the cell division protein FtsW of *Escherichia coli*. *J Bacteriol* **186**: 8370-8379.
- Peters, N.T., T. Dinh & T.G. Bernhardt, (2011) A fail-safe mechanism in the septal ring assembly pathway generated by the sequential recruitment of cell separation amidases and their activators. *J Bacteriol* **193**: 4973-4983.
- Peters, N.T., C. Morlot, D.C. Yang, T. Uehara, T. Vernet & T.G. Bernhardt, (2013) Structure-function analysis of the LytM domain of EnvC, an activator of cell wall remodelling at the *Escherichia coli* division site. *Mol Microbiol.*
- Pettersen, E.F., T.D. Goddard, C.C. Huang, G.S. Couch, D.M. Greenblatt, E.C. Meng & T.E. Ferrin, (2004) UCSF Chimera--a visualization system for exploratory research and analysis. *J Comput Chem* **25**: 1605-1612.
- Pichoff, S. & J. Lutkenhaus, (2002) Unique and overlapping roles for ZipA and FtsA in septal ring assembly in *Escherichia coli*. *EMBO J* **21**: 685-693.
- Pichoff, S. & J. Lutkenhaus, (2005) Tethering the Z ring to the membrane through a conserved membrane targeting sequence in FtsA. *Molecular Microbiology* **55**: 1722-1734.
- Piette, A., C. Fraipont, T. Den Blaauwen, M.E. Aarsman, S. Pastoret & M. Nguyen-Distèche, (2004) Structural determinants required to target penicillin-binding protein 3 to the septum of *Escherichia coli*. *J Bacteriol* **186**: 6110-6117.

- Popham, D.L., (2013) Visualizing the production and arrangement of peptidoglycan in Gram-positive cells. *Mol Microbiol* **88**: 645-649.
- Potluri, L.P., M.A. de Pedro & K.D. Young, (2012) Escherichia coli low-molecular-weight penicillin-binding proteins help orient septal FtsZ, and their absence leads to asymmetric cell division and branching. *Mol Microbiol* **84**: 203-224.
- Priyadarshini, R., D.L. Popham & K.D. Young, (2006) Daughter Cell Separation by Penicillin-Binding Proteins and Peptidoglycan Amidases in Escherichia coli. *J Bacteriol* **188**: 5345-5355.
- Rajagopalan, M., E. Maloney, J. Dziadek, M. Poplawska, H. Lofton, A. Chauhan & M.V. Madiraju, (2005) Genetic evidence that mycobacterial FtsZ and FtsW proteins interact, and colocalize to the division site in Mycobacterium smegmatis. *FEMS Microbiol Lett* **250**: 9-17.
- Raskin, D.M. & P.A. de Boer, (1999) Rapid pole-to-pole oscillation of a protein required for directing division to the middle of Escherichia coli. *Proc Natl Acad Sci U S A* **96**: 4971-4976.
- Rath, A., M. Glibowicka, V.G. Nadeau, G. Chen & C.M. Deber, (2009) Detergent binding explains anomalous SDS-PAGE migration of membrane proteins. *Proc Natl Acad Sci U S A* **106**: 1760-1765.
- RayChaudhuri, D., (1999) ZipA is a MAP-Tau homolog and is essential for structural integrity of the cytokinetic FtsZ ring during bacterial cell division. *EMBO J* **18**: 2372-2383.
- Rico, A.I., M. Garcia-Ovalle, J. Mingorance & M. Vicente, (2004) Role of two essential domains of Escherichia coli FtsA in localization and progression of the division ring. *Mol Microbiol* **53**: 1359-1371.
- Rico, A.I., M. García-Ovalle, P. Palacios, M. Casanova & M. Vicente, (2010) Role of Escherichia coli FtsN protein in the assembly and stability of the cell division ring. *Molecular Microbiology* **76**: 760-771.
- Robichon, C., G. Karimova, J. Beckwith & D. Ladant, (2011) Role of leucine zipper motifs in association of the Escherichia coli cell division proteins FtsL and FtsB. *J Bacteriol* **193**: 4988-4992.
- Romberg, L. & P.A. Levin, (2003) Assembly dynamics of the bacterial cell division protein FTSZ: poised at the edge of stability. *Annual review of microbiology* **57**: 125-154.
- Romeis, T. & J.V. Holtje, (1994) Specific interaction of penicillin-binding proteins 3 and 7/8 with soluble lytic transglycosylase in Escherichia coli. *J Biol Chem* **269**: 21603-21607.
- Ruiz, N., (2008) Bioinformatics identification of MurJ (MviN) as the peptidoglycan lipid II flippase in Escherichia coli. *Proc Natl Acad Sci U S A* **105**: 15553-15557.
- Sauvage, E., F. Kerff, M. Terrak, J.A. Ayala & P. Charlier, (2008) The penicillin-binding proteins: structure and role in peptidoglycan biosynthesis. *FEMS Microbiol Rev* **32**: 234-258.
- Schleifer, K.H. & O. Kandler, (1972) Peptidoglycan types of bacterial cell walls and their taxonomic implications. *Bacteriological reviews* **36**: 407-477.
- Schmidt, K.L., N.D. Peterson, R.J. Kustus, M.C. Wissel, B. Graham, G.J. Phillips & D.S. Weiss, (2004) A predicted ABC transporter, FtsEX, is needed for cell division in Escherichia coli. *J Bacteriol* **186**: 785-793.
- Sham, L.T., S.M. Barendt, K.E. Kopecky & M.E. Winkler, (2011) Essential PcsB putative peptidoglycan hydrolase interacts with the essential FtsXSpn cell division protein in Streptococcus pneumoniae D39. *Proc Natl Acad Sci U S A* **108**: E1061-1069.
- Sham, L.T., K.R. Jensen, K.E. Bruce & M.E. Winkler, (2013) Involvement of FtsE ATPase and FtsX extracellular loops 1 and 2 in FtsEX-PcsB complex function in cell division of Streptococcus pneumoniae D39. *mBio* **4**.
- Sham, L.T., H.C. Tsui, A.D. Land, S.M. Barendt & M.E. Winkler, (2012) Recent advances in pneumococcal peptidoglycan biosynthesis suggest new vaccine and antimicrobial targets. *Current opinion in microbiology* **15**: 194-203.
- Shiomi, D. & W. Margolin, (2007) The C-terminal domain of MinC inhibits assembly of the Z ring in Escherichia coli. *J Bacteriol* **189**: 236-243.

- Singh, S.K., L. SaiSree, R.N. Amrutha & M. Reddy, (2012) Three redundant murein endopeptidases catalyse an essential cleavage step in peptidoglycan synthesis of *Escherichia coli* K12. *Mol Microbiol* **86**: 1036-1051.
- Sung, M.T., Y.T. Lai, C.Y. Huang, L.Y. Chou, H.W. Shih, W.C. Cheng, C.H. Wong & C. Ma, (2009) Crystal structure of the membrane-bound bifunctional transglycosylase PBP1b from *Escherichia coli*. *Proc Natl Acad Sci U S A* **106**: 8824-8829.
- Szwedziak, P., Q. Wang, S.M. Freund & J. Lowe, (2012) FtsA forms actin-like protofilaments. *EMBO J* **31**: 2249-2260.
- Takahara, M., H. Takahashi, S. Matsunaga, S. Miyagishima, H. Takano, A. Sakai, S. Kawano & T. Kuroiwa, (2000) A putative mitochondrial ftsZ gene is present in the unicellular primitive red alga *Cyanidioschyzon merolae*. *Molecular & general genetics : MGG* **264**: 452-460.
- Taku, A., K.G. Gunetileke & R.A. Anwar, (1970) Biosynthesis of Uridine Diphospho-N-acetylmuramic Acid : III. PURIFICATION AND PROPERTIES OF URIDINE DIPHOSPHO-N-ACETYLENOLPYRUVYL-GLUCOSAMINE REDUCTASE. *Journal of Biological Chemistry* **245**: 5012-5016.
- Teleha, M.A., A.C. Miller & R.A. Larsen, (2013) Overexpression of the *Escherichia coli* TolQ protein leads to a null-FtsN-like division phenotype. *MicrobiologyOpen* **2**: 618-632.
- Thanbichler, M., (2010) Synchronization of chromosome dynamics and cell division in bacteria. *Cold Spring Harb Perspect Biol* **2**: a000331.
- Tocheva, E.I., J. Lopez-Garrido, H.V. Hughes, J. Fredlund, E. Kuru, M.S. Vannieuwenhze, Y.V. Brun, K. Pogliano & G.J. Jensen, (2013) Peptidoglycan transformations during *Bacillus subtilis* sporulation. *Mol Microbiol* **88**: 673-686.
- Tonthat, N.K., S.T. Arold, B.F. Pickering, M.W. Van Dyke, S. Liang, Y. Lu, T.K. Beuria, W. Margolin & M.A. Schumacher, (2011) Molecular mechanism by which the nucleoid occlusion factor, SlmA, keeps cytokinesis in check. *EMBO J* **30**: 154-164.
- Tonthat, N.K., S.L. Milam, N. Chinnam, T. Whitfill, W. Margolin & M.A. Schumacher, (2013) SlmA forms a higher-order structure on DNA that inhibits cytokinetic Z-ring formation over the nucleoid. *Proc Natl Acad Sci U S A* **110**: 10586-10591.
- Trueba, F.J., (1982) On the precision and accuracy achieved by *Escherichia coli* cells at fission about their middle. *Archives of microbiology* **131**: 55-59.
- Tullman-Ercek, D., M.P. DeLisa, Y. Kawarasaki, P. Iranpour, B. Ribnicky, T. Palmer & G. Georgiou, (2007) Export pathway selectivity of *Escherichia coli* twin arginine translocation signal peptides. *J. Biol. Chem* **282**: 8309-8316.
- Typas, A., M. Banzhaf, B. van den Berg van Saparoea, J. Verheul, J. Biboy, R.J. Nichols, M. Zietek, K. Beilharz, K. Kannenberg, M. von Rechenberg, E. Breukink, T. den Blaauwen, C.A. Gross & W. Vollmer, (2010) Regulation of Peptidoglycan Synthesis by Outer-Membrane Proteins. *Cell* **143**: 1097-1109.
- Uehara, T., T. Dinh & T.G. Bernhardt, (2009) LytM-domain factors are required for daughter cell separation and rapid ampicillin-induced lysis in *Escherichia coli*. *J Bacteriol* **191**: 5094-5107.
- Uehara, T., K.R. Parzych, T. Dinh & T.G. Bernhardt, (2010) Daughter cell separation is controlled by cytokinetic ring-activated cell wall hydrolysis. *EMBO J* **29**: 1412-1422.
- Ursinus, A., F. van den Ent, S. Brechtel, M. de Pedro, J.-V. Höltje, J. Löwe & W. Vollmer, (2004) Murein (peptidoglycan) binding property of the essential cell division protein FtsN from *Escherichia coli*. *J Bacteriol* **186**: 6728-6737.
- van den Ent, F., T.M. Vinkenvleugel, A. Ind, P. West, D. Veprintsev, N. Nanninga, T. den Blaauwen & J. Lowe, (2008) Structural and mutational analysis of the cell division protein FtsQ. *Mol Microbiol* **68**: 110-123.
- van der Ploeg, R., J. Verheul, N.O. Vischer, S. Alexeeva, E. Hoogendoorn, M. Postma, M. Banzhaf, W. Vollmer & T. den Blaauwen, (2013) Colocalization and interaction between elongasome and divisome during a preparative cell division phase in *Escherichia coli*. *Mol Microbiol* **87**: 1074-1087.

- van Teeffelen, S., S. Wang, L. Furchtgott, K.C. Huang, N.S. Wingreen, J.W. Shaevitz & Z. Gitai, (2011) The bacterial actin MreB rotates, and rotation depends on cell-wall assembly. *Proc Natl Acad Sci U S A* **108**: 15822-15827.
- Vera, L., B. Czarny, D. Georgiadis, V. Dive & E.A. Stura, (2011) Practical Use of Glycerol in Protein Crystallization. *Crystal Growth & Design* **11**: 2755-2762.
- Villanelo, F., A. Ordenes, J. Brunet, R. Lagos & O. Monasterio, (2011) A model for the Escherichia coli FtsB/FtsL/FtsQ cell division complex. *BMC structural biology* **11**: 28.
- Viollier, P.H., M. Thanbichler, P.T. McGrath, L. West, M. Meewan, H.H. McAdams & L. Shapiro, (2004) Rapid and sequential movement of individual chromosomal loci to specific subcellular locations during bacterial DNA replication. *Proc Natl Acad Sci U S A* **101**: 9257-9262.
- Vollmer, W., (2008) Structural variation in the glycan strands of bacterial peptidoglycan. *FEMS Microbiol Rev* **32**: 287-306.
- Vollmer, W., B. Joris, P. Charlier & S. Foster, (2008) Bacterial peptidoglycan (murein) hydrolases. *FEMS Microbiol Rev* **32**: 259-286.
- Vollmer, W., M. von Rechenberg & J.V. Holtje, (1999) Demonstration of molecular interactions between the murein polymerase PBP1B, the lytic transglycosylase MltA, and the scaffolding protein MipA of Escherichia coli. *J Biol Chem* **274**: 6726-6734.
- Weiss, D.S., J.C. Chen, J.M. Ghigo, D. Boyd & J. Beckwith, (1999) Localization of FtsI (PBP3) to the septal ring requires its membrane anchor, the Z ring, FtsA, FtsQ, and FtsL. *J Bacteriol* **181**: 508-520.
- Weiss, D.S., K. Pogliano, M. Carson, L.M. Guzman, C. Fraipont, M. Nguyen-Distèche, R. Losick & J. Beckwith, (1997) Localization of the Escherichia coli cell division protein FtsI (PBP3) to the division site and cell pole. *Molecular microbiology* **25**: 671-681.
- Williams, K.B., A. Yahashiri, S.J. Arends, D.L. Popham, C.A. Fowler & D.S. Weiss, (2013) Nuclear magnetic resonance solution structure of the peptidoglycan-binding SPOR domain from Escherichia coli DamX: insights into septal localization. *Biochemistry* **52**: 627-639.
- Wissel, M.C. & D.S. Weiss, (2004) Genetic analysis of the cell division protein FtsI (PBP3): amino acid substitutions that impair septal localization of FtsI and recruitment of FtsN. *J Bacteriol* **186**: 490-502.
- Wu, L.J. & J. Errington, (2004) Coordination of cell division and chromosome segregation by a nucleoid occlusion protein in Bacillus subtilis. *Cell* **117**: 915-925.
- Wu, L.J., S. Ishikawa, Y. Kawai, T. Oshima, N. Ogasawara & J. Errington, (2009) Noc protein binds to specific DNA sequences to coordinate cell division with chromosome segregation. *EMBO J* **28**: 1940-1952.
- Yang, D.C., N.T. Peters, K.R. Parzych, T. Uehara, M. Markovski & T.G. Bernhardt, (2011) An ATP-Binding Cassette Transporter-Like Complex Governs Cell-Wall Hydrolysis at the Bacterial Cytokinetic Ring. *PNAS* **108**: 18209-18210.
- Yang, D.C., K. Tan, A. Joachimiak & T.G. Bernhardt, (2012) A conformational switch controls cell wall-remodelling enzymes required for bacterial cell division. *Molecular microbiology* **85**: 768-781.
- Yang, J.C., F. Van Den Ent, D. Neuhaus, J. Brevier & J. Lowe, (2004) Solution structure and domain architecture of the divisome protein FtsN. *Mol Microbiol* **52**: 651-660.
- Yu, X.C. & W. Margolin, (1999) FtsZ ring clusters in min and partition mutants: role of both the Min system and the nucleoid in regulating FtsZ ring localization. *Mol Microbiol* **32**: 315-326.
- Yu, X.C., A.H. Tran, Q. Sun & W. Margolin, (1998) Localization of cell division protein FtsK to the Escherichia coli septum and identification of a potential N-terminal targeting domain. *J Bacteriol* **180**: 1296-1304.
- Zemell, R.I. & R.A. Anwar, (1975) Pyruvate-uridine diphospho-N-acetylglucosamine transferase. Purification to homogeneity and feedback inhibition. *J Biol Chem* **250**: 3185-3192.
- Zhang, X.Y., E.L. Goemaere, R. Thome, M. Gavioli, E. Cascales & R. Lloubes, (2009) Mapping the interactions between escherichia coli tol subunits: rotation of the TolR transmembrane helix. *J Biol Chem* **284**: 4275-4282.

Zoll, S., B. Patzold, M. Schlag, F. Gotz, H. Kalbacher & T. Stehle, (2010) Structural basis of cell wall cleavage by a staphylococcal autolysin. *PLoS pathogens* **6**: e1000807.